POLITECNICO DI MILANO

Scuola di Ingegneria Industriale e dell'Informazione

Dipartimento di Scienze e Tecnologie Aerospaziali

Corso di Laurea Magistrale in Ingegneria Spaziale

Ground Beacons to Enhance Lunar Landing Autonomous Navigation Architectures

Relatore: Prof. Michèle LAVAGNA

Correlatore: Dr. Ing. Stephan THEIL

Tesi di Laurea di:

Leonardo BORA Matr. 796807

Anno Accademico 2013-2014

A Fabrizia e Raffaele

Aknowledgements/Ringraziamenti

Desidero ringraziare i cari e gli amici, con particolare riferimento ai miei genitori, per avermi sostenuto in questi anni di studi e per aver in qualche modo contribuito a far nascere in me la voglia di intraprendere questo percorso, aspro ma intenso e appassionante.
Ringrazio Evym per avermi sopportato in questi anni ed essermi stata vicina anche quando sparivo per giorni interi, o ero sentimentalmente assente, per i momenti di gioia che mi ha regalato finora e per quelli che ci auguro verranno.
Vorrei ringraziare la professoressa Michèle Lavagna per avermi fatto appassionare tramite le sue lezioni ai temi trattati in questo lavoro e tutti i professori incontrati prima e durante il percorso di studi universitari, per avermi trasmesso parte del loro sapere ed esperienza.
Infine ci tengo a ringraziare i miei compagni del corso di ingegneria spaziale del Polimi con i quali ho condiviso l'avventura che mi ha condotto sino a questo punto e che spero ci condurrà in un futuro denso e felice, come ci meritiamo.

A special thank to the people in the GNC Department of DLR Institute of Space Systems in Bremen, in particular to my co-supervisor Dr. Stephan Theil, Federico, Guilherme and Marco, for their precious help in the development of this work and for having shared their knowledge with me.

Leonardo Bora

Contents

List of Figures

List of Tables

Abstract

Current and future landing missions are relying on a combination of inertial and optical sensor measurements to accomplish the navigation task. The present thesis work carried out at *DLR Institute of Space Systems*, is mainly focused on the conceptual definition and analyses of possible configurations for a ground based infrastructure aiding the on-board navigation system in a lunar landing scenario. From aircraft navigation legacy, range, range-rate and bearing measurements from beacons on ground have been devised and fused together with the optical and inertial ones provided by the on-board navigation system: an error state Extended Kalman Filter (eEKF) is used for the scope. Different configurations of this on-ground navigation infrastructures, changing number of beacons and combination of the new measurements have been tested through Monte Carlo analyses; the navigation performance has been evaluated through appropriately defined cost parameters. The results obtained are very good and promising, even in presence of just one beacon placed near the landing site providing range and range-rate. The results open the door to further development of the research in the field of ground-based navigation for planetary landing, quite unexplored at the time being, but very interesting in the light of future extraterrestrial settlements.

Keywords: navigation, navigation system, beacon navigation, Extended Kalman Filter, lunar landing.

Riassunto

Al giorno d'oggi e nell'immediato futuro le missioni di esplorazione fanno affidamento su una combinazione di misure inerziali e da sensori ottici, per la navigazione in fase di atterraggio. Questo lavoro di tesi sviluppato all'Istituto di Sistemi Spaziali del DLR è principalmente focalizzato sullo studio concettuale e la successiva analisi numerica di possibili configurazioni per una infrastruttura a terra che aiuti il sistema di navigazione a bordo del lander, avendo come riferimento una missione di allunaggio. Prendendo come esempio i sistemi di navigazione usati in ambiente aeronautico, si è pensato di fornire al sistema di navigazione presente a bordo del lander misure di range, range-rate e bearing, fornite da beacons disposti a terra; queste misure poi vengono processate dal filtro di navigazione, un error-state Extended Kalman Filter (eEKF), insieme alle altre misure ottiche e inerziali effettuate dal sistema a bordo. Sono state effettuate delle analisi di Monte Carlo su varie configurazioni, cambiando numero di beacons e combinazioni di misure; la performance di navigazione è poi stata valutata per mezzo di opportune funzioni costo. I risultati ottenuti sono positivi e promettenti, anche in presenza di un unico beacon che fornisca misure di range e range-rate, posizionato vicino al sito di atterraggio. Questi risultati aprono la porta ad ulteriori sviluppi sul tema della navigazione assistita da un'infrastruttura a terra per atterraggi planetari, un campo di ricerca al momento poco sondato, ma molto interessante dal punto di vista della possibile presenza di future basi extraterrestri.

Parole chiave: navigazione, sistema di navigazione, navigazione con beacon, Extended Kalman Filter, allunaggio.

CHAPTER 1

Introduction

Since the beginning of human space activity, safe and soft landing on an extraterrestrial planet has been a central objective to be pursued for space exploration.
Starting from the first landings on the Moon which had generally precision above 1 km, today improvements in the navigation architecture and filters have made it possible to decrease both the final accuracy and the mass of the dedicated payload.

1.1 A Human Base On The Moon

The neverending need of mankind for exploration will make it possible to have the first extraterrestrial human base in the nearest future. Our satellite is definitely the best candidate for this big step and there are many reasons which make it desirable to locate an establishment there:

- recent studies have revealed the probable presence of volatiles trapped in permanently shadowed craters in the lunar South pole, which could make ISRU possible [1];
- it has been highlighted the existence of peak of lights located in the South pole , which could serve as possible source for an hypothetical lunar power station [2];
- trapped in the surface of the Moon there is Helium-3, a possible fuel for future nuclear fusion power stations, brought there in billions of years

by solar wind, whose presence was already discovered during Apollo missions [3];

- the Moon would be a very good "trampoline" for future space exploration exploiting low energy transfers [4];

This is partly why space agencies around the world have already started to think and define the possible architectures of a lunar base.

1.2 Thesis Objectives And Structure

The GNC Systems Department at the Institute of Space Systems in DLR and Politecnico di Milano Department of Aerospace Science and Technology, are working on navigation technologies for lunar, planetary and asteroid exploration. Current and future landing missions are relying on a combination of inertial and optical sensor measurements to determine the current flight state with respect to the target body and the desired landing site. As soon as an infrastructure at the landing site exists, the requirements as well as conditions change for vehicles landing close to this existing infrastructure.

The aim of the research is to investigate the options for ground based infrastructure supporting the on-board navigation system, to analyze the impact on achievable navigation accuracy, and to propose a way of demonstrating the developed concept on ground with off-the-shelf (OTS) hardware.

The present work will be subdivided in the following steps:

- brief survey of existing navigation architectures and filters for optical navigation for planetary landing vehicles;
- survey of existing applications for navigation support with ground infrastructure;
- development of a navigation system architecture to complement the on-board navigation system with ground based support infrastructure including trade-offs;
- integration of ground based navigation support in the existing on-board navigation architecture and filter;
- analyses and discussion of simulation results;
- proposal of demonstration ways to verify the concept on ground.

CHAPTER 2

State Of The Art

This chapter is focused on a brief review of state of art navigation architectures capable of performing soft landing, followed by a review of key examples of use of ground stations for navigation, with some already proposed studies about possible implementation for lunar landing or surface exploration.

2.1 Navigation Architectures And Filters

Nowadays, existing or proposed navigation architectures for performing soft landing are all based on a combination of inertial measurements and relative measurements. The trend is to have measurements from multiple sensors and to fuse them using Extended Kalman Filters (EKF), which allow good noise and bias reduction [5].

2.1.1 SINPLEX

SINPLEX (Small Integrated Navigator for Planetary EXploration) is an autonomous navigation architecture developed in Europe under the coordination of DLR, which aims at reducing the mass of current navigation architectures without loss of accuracy [6, 7]. It can work in multiple scenarios such as planetary and asteroid landing, or objects rendez-vouz. It is based on a combination of sensors:

- Inertial Measurement Unit (IMU);

- Star Tracker (ST);
- Navigation Camera (NavCam);
- Laser Altimeter (LA).

The state is estimated with a combination of strap-down integration and delayed error state Extended Kalman Filter (eEKF) [8]. In the case of lunar landing the camera enables Crater Navigation (CN) until a limit altitude is reached, when feature tracking (FT) is activated [9]. The order of precision obtainable is below 100 m at 1-σ.

2.1.2 ALHAT

ALHAT (Autonomous Landing Hazard Avoidance Technology) is an autonomous navigation architecture under development at NASA, whose objective is to develop capability to safely land near a desired target regardless of lighting conditions, and with limited a priori knowledge of the terrain and surface features at or near the landing site [10]. The set of sensor includes:

- IMU;
- ST;
- 3D Flash Lidar;
- Altimeter;
- Doppler Velocimeter.

2.2 Radiometric Navigation

Radiometric navigation is extensively used on Earth, especially in the aviation field. There are many kinds of electromagnetic signals and modulation techniques that could be used and measurements on them that could be made, which are specific for the different existing navigation services. However, basically the information that radiometric navigation provides to the user can be divided into the following three main categories:

- range measurement;
- range rate measurement;
- bearing measurement.

In the following there is a brief overview of existing or existed navigation architectures on Earth, mainly in the aeronautic field, which are possible starting points for a lunar ground based navigation architecture. Eventually there is also a brief overview of literature concerning the use of ground base infrastructure for lunar landing assistance.

2.2.1 Radar

Radar is, in the most general way, a technique based on measuring the echo of a signal reflected by a reflector. The measurement of the elapsed time between the transmission of the signal and the reception of the reflected one (time-of-arrival, TOA) is proportional to the distance of the reflector. The measure of the frequency shift (one or two-way Doppler) is instead related to the relative velocity along the line of sight (LOS). The frequencies that are used are in the spectrum of the UHF and SHF in order to have sharp beams. The power used is relatively high, otherwise it could be hard to distinguish the reflected signal from noise.
Since level of power is directly connected to the dimension and therefore mass of the system, radar does not seem the best option in an optic of mass and power reduction for the design of the ground based infrastructure, although just one ground station (emitter) would be already enough for measuring both range, range rate and bearing.

2.2.2 ADF

Automatic direction finder is based on the detection of the direction of the incoming signal generated by a ground beacon. It has been one of the first techniques used in aviation. The radio wave (in the MF band) is received by a sense (non directional) antenna and a loop (directional) antenna on the airplane. Originally the determination of the bearing was manually operated by the crew with a radio-goniometer, i.e. a radio receiver integrated with compass, sense and loop antenna; the minimum signal intensity from the loop antenna was obtained when it was aligned with the radio wave. Nowadays implemented system got rid of rotating mechanism thanks to the use of loop antennas made of rose of coils. The simplicity of this system guarantees it to be still in use, although much better positioning techniques have been developed so far.

2.2.3 VOR-DME

VOR (VHF omni-directional range) is a short-range navigation system that enables the determination of the bearing of the aircraft with respect to the north. The ground station provides one reference-phase signal and a variable-phase one (which acts like a directional signal): the difference in phase among the two is dependent on the radial position of the user. It can be also possible to measure the 2D position of the user when at least two beacons are used. Usually VOR is coupled with a DME (distance measuring equipment) which evaluates the distance through elapsed time between a signal emitted by the user and re-sent by the ground station after a prescribed delay. With the implementation of a VOR-DME like technique, it could be possible to fully localize the incoming lander in polar coordinates, with the use of a single beacon. Precision of this system for Earth application is relatively poor, although being dependent on the distance from beacon.
It could be imagined that the accuracy would increase in a lunar scenario thanks to the absence of atmosphere, which absorbs and deviates the electromagnetic wave, depending on the frequency.

2.2.4 LORAN-C

Another class of navigation system is the one which provides the difference among the distance from two ground stations, therefore placing the receiver (user) in an hyperbolic pattern. For this reason this class is called hyperbolic navigation systems. The one still in use in aviation as back-up for GPS is LORAN-C, which is also the one capable of better accuracy with respect to the others (DECCA, OMEGA). This system is based on couple of ground stations, one master and one slave. The master emits an omni-directional pulse in the LF band. When the slave receives it, after a fixed delay, it emits a pulse itself. The user, measuring the elapsed time since reception of the two signals (TDOA) can determine the hyperbolic pattern in which it could lie. At least two couples, i.e. a master and two slaves are needed to recover the position on a plane. The propagation mechanism is based on ionospheric waveguide, enabled by the low frequency of the signals. This allows the signals to have a wide coverage, also much far beyond the horizon.
The same could not be applied in a lunar scenario, where the propagation shall be the direct one, therefore reducing the range. The fact of needing at least 3 GS to have the position, together with the quite low accuracy experienced on Earth, does not make it the most favorable system to take as reference for this work.

2.2.5 GPS

Global positioning system is a service provided by USAF which enables a 3D position detection. It makes use of signals in the UHF band, modulated by a pseudorandom noise (PRN) code (spread-spectrum technique). This modulation, thanks to the high process gain, guarantees good narrow-band noise rejection, therefore allowing very low radiated spectral densities (i.e. more compact systems). The GPS makes use of a network of 24 telecommunication satellites (the space segment) and of some GS's which track and upload them with their ephemerides. The user (receiver) receives a signal emitted by a satellite through which he is able to compute the pseudorange and to know the position of the satellite through the ephemerides, information contained in the signal. The pseudorange is affected by errors in the elapsed time measurement which are related to the fact that the user's clock has a level of accuracy not comparable to the atomic clocks on board of the satellites. This bias, which is the same for all pseudorange measurements, can be recovered when 4 satellites are used to determine the position. The accuracy is much better with respect to the aforementioned navigation techniques.
The extension of a similar system on the Moon would require a dedicated constellation of satellites around the planet, which is out of the scope of this study, being focused on ground base infrastructure usage in the navigation of a lander. However, the study of GPS results interesting for the possibility of using similar methods to detect distance, i.e. based on spread-spectrum systems, that allows low levels of power, as already said. If coupled with a Doppler measure it is possible to obtain pseudorange and range rate using one beacon.

2.2.6 Indoor Geolocation

Due to signal attenuation caused by construction materials GPS cannot be used to locate an user inside a building. That is why there exist in the market many geolocation techniques capable of working indoor [11] They are pretty all based on trilateration like GPS, using nodes of known position to locate the user after having determined the range from them. Some of these systems, beside the aforementioned possible ways of determining range, make use of the measure of the received signal strength (RSS) to locate the user. Others are based on angle of arrival (AOA) determination. Some existing systems claim very good accuracy also below 1 m.
The interest on these technologies is mainly the fact that they are off-the-shelf equipment that could be used for a possible set-up on ground, e.g. in order to test the output of this work.

2.2.7 Lunar Application Of Radiometrics In Literature

There have been studies about the evaluation or design of possible Moon based navigation architectures. Many of these studies are about the necessity of locating a user on the surface of the Moon during an extra-vehicular-activity (EVA), which could be the case if a lunar base is established (see e.g. [12, 13, 14].
In recent years NASA, for its lunar base architecture design, has proposed a navigation architecture based on lunar relay satellites (LRS) and lunar communication terminals (LCT), which combined would provide 1 and 2 way range and Doppler measurement to the lander. The LCT's alone would instead provide 1-way S-band Doppler and range. It is also proposed the use of atomic clocks to drive the radiometric measurements [15].
[16, 17] have recently studied the obtainable performance of a lander navigation aided by radiometrics (beacon-relative), where the lander transponds signals from available radiometric assets, i.e. LRS or LCT, receiving range and range rate information from them. These measurements are inserted in a EKF together with other navigation measurements coming from IMU, star camera, velocimeter and altimeter, which is the basic sensor suite of ALHAT. That study has evaluated performance of the navigation accuracy through linear covariance analyses, when on-board system is supported by a single surface beacon: the result shows that surface beacons provide the best radiometric measure if they are not located directly under the path of the lander as it approaches the landing site. A well placed beacon could support with accuracy below 10 m at 3-σ the final phases of landing, while it is not possible to assist all landing phases with similar accuracy, i.e. powered descent is better supported by a beacon placed well up-range with respect to landing site. With the aim of improving landing accuracy in final phases, the best placement was found to be at about 2 km both up-range with respect to the landing site and off-track with respect to the lander footprint. A beacon directly placed on the landing site is not the best configuration according to their study.

2.2.8 Conclusion

As far as an infrastructure will be present of the Moon the natural consequence is to make use of a beacon placed there to get measurements that, filtered together with others, would possibly increase the accuracy level of current on-board navigation architecture or decrease their weight, since, for example, some on-board sensors could be discarded.
Having a look on the current Earth's applications, one of the most limiting

factors in their accuracy (schematically represented in figure 2.1) is the presence of the atmosphere; therefore it can be imagined that an equivalent or similar architecture used on the Moon would give a better accuracy. On the other way round some wide-range applications like LORAN would not work on Moon due to lack of atmosphere. The applications on Moon shall rely on direct propagation being therefore the coverage limited to the horizon.
In general a Doppler measurement, especially when 2-way, reveals to be more accurate than a range evaluation, which is affected by errors in TOA determination: the use of atomic clocks could surely improve the range calculations. On the Moon all problems related to frequency allocation or atmospheric disturbance (as said) are not present, therefore it is in principle possible to select whichever frequency. The use of UHF or SHF would be preferable, leading to more compact antennas.
It is important then to notice that many of the aforementioned application requires maintenance that could be difficult or impossible to manage in an extraterrestrial scenario.

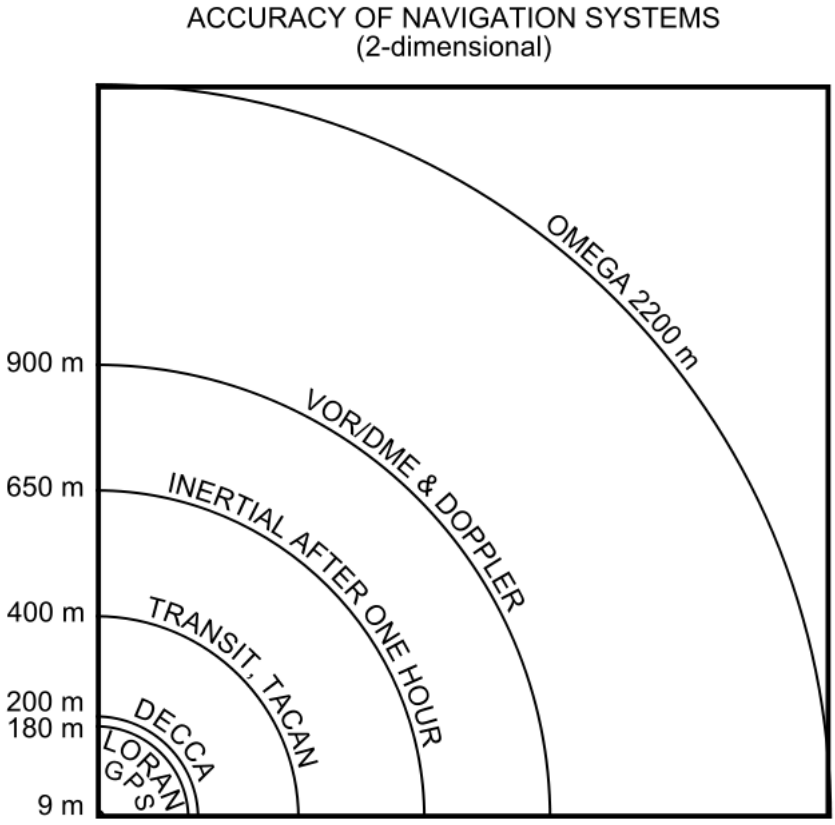

Figure 2.1: Accuracy of radiometric navigation applications on Earth

CHAPTER 3

Ground Based Navigation System Architecture

This chapter presents the selection and discussion of the navigation system architecture to complement the on-board navigation system with ground based infrastructure, coupling radiometric measurements with the ones provided in the existing navigation system (i.e. SINPLEX).
The number of quantities that it is possible to measure (i.e. range, range-rate, bearing etc...), coupled with the fact that there exist many alternatives to sense them through radiometric measurements (as seen in section 2.2), leads to a vast field of possible navigation architectures. Moreover, depending on the type of measurements chosen, the number of ground stations can not be defined a priori.
In principle, from a general point of view, a ground base infrastructure could support alone the lander navigation if something like the GPS is developed; or it could only provide partial information, e.g. a relative velocity or a distance from a known station. This gives a feeling of the difficulty of following an unconstrained philosophy for the architecture selection process.
There is therefore the need to put appropriate constraints in the architecture definition, useful to build a preliminary list of candidate solutions to make analyses and trade-offs.

3.1 GBNS High Level Requirements

In order to set these constraints it is necessary to state some high level requirements for the navigation systems in development, considering the on-

board segment and ground segment parts of the same system, which is the ground based navigation system (GBNS).
In table 3.1 the list of the self-imposed high level requirements is reported. The second column contains the importance of the requirement, where M and NH stand respectively for mandatory and nice to have.

Table 3.1: GBNS high level requirements

ID	Imp.	Requirement
GBNS-1	M	The GBNS shall provide navigation support for an accurate landing of the lander on the desired landing site
GBNS-2	NH	The GBNS should provide navigation support for the lander starting from the PD
GBNS-3	M	The number of the GS's shall be minimized
GBNS-4	M	The dispersion of the GS's shall be minimized
GBNS-5	NH	The GBNS should take redundancies into account
GBNS-6	M	The GBNS shall not constrain the S/C attitude
GBNS-7	M	The mass and size of the GBNS related components shall be minimized
GBNS-8	NH	The ground segment should be capable also of vehicles navigation for surface operations
GBNS-9	M	The GBNS shall avoid rotating mechanisms

GBNS-3/4 are related to the fact that at the time being no such an infrastructure exists on the surface of the Moon. In order to have the system operational, a first mission should be carried out to bring the necessary GS's there and dislocate them as needed. Therefore the higher the number of beacons and the more distant one another have to be placed, the more the mission gets difficult and expensive.
GBNS-6 is imposed since the lander attitude is already constrained by thrust profile and other navigation sensor in the existing architecture, like the ST and the NC. It has been decided not to set any requirement at this stage on the kind of measurements, since this will be part of the trade-off.
No specific requirement is set on the accuracy because it is one objective of this work to investigate on the level of accuracy achievable. It is in any case expected it to be better or comparable to current state of the art landing navigation system achievable performances.
The kind of signals and modulation techniques or radiometrics in general, although fundamental for the design and for example strictly correlated to

GBNS-6, will be not taken into account in the analyses carried out in this work; as soon as the design process has driven to the choice of which quantities to be measured and the configuration of the beacons, the radiometrics could be considered, also with the aim of proposing an experimental setup to test the feasibility on ground with OTS equipment.

3.2 Preliminary Architecture Proposals

In this section architecture candidates are proposed, and the first filtering is mainly based on the experience of Earth's radionavigation applications. The aim is to have a pool of alternatives to be further analyzed, through simulations.

3.2.1 Single Beacon

There are some reasons why the single beacon architecture is of interests, e.g.:

- the first robotic mission to set the lunar base would not need rovers, hoppers or multiple landers to displace the extra beacons;
- the single beacon could be larger and therefore have more power or redundancies in the hardware, at same level of launch mass and volume of this hypothetical mission;
- it is possible to unambiguously locate a lander on a 2D space if appropriate measurements are taken, as some airplane navigation systems show. Drawbacks would be the lack of redundancy and 3D positioning and the difficulty or impossibility of supporting all phases of landing operations.

Starting from the subdivision of the possible measurements made in section 2.2 on the base of current applications on Earth, there are 7 possible alternatives, addressed in table 3.2.

It is possible to notice that only 1-E, 1-F and 1-G, if coupled with an altitude measurement, would give enough information for an unambiguous positioning in space.
A solution like 1-E would be conceptually working like the VOR-DME: the predictable accuracy in bearing determination of this is around $\pm$ 1.4 deg, and, being independent on the range, the position determination improves when near the beacon. The beacon could be placed right in the ground base, or near it.

Table 3.2: Combination of measurements for a single beacon

ID	Measurements
1-A	Range
1-B	Range-Rate
1-C	Bearing
1-D	Range + Range-Rate
1-E	Range + Bearing
1-F	Range-rate + Bearing
1-G	Range + Range-Rate + Bearing

In practice, a range determination is more inaccurate than a Doppler one, being affected by errors in TOA determinations, therefore it could be reasonable to constrain the GBNS to have range-rate measurements whenever range is sensed, since this would not add much complexity. For this 1-A would be not considered, while a second candidate could be an extension of VOR-DME, obtained adding a Doppler measurement (1-G in table 3.2).
It is also interesting the evaluation of case 1-D since the results could be compared with what obtained by D. Christensen and D. Geller [16, 17].
At that stage it could be also interesting to compare the performance of the multiple measurements solutions with the single measurements (i.e. 1-A, 1-B and 1-C) since once the measurement and dynamic models for the added variables are available, it is mostly a matter of simulation time.
Therefore all candidates listed in table 3.2 are valid at this stage, since a priori it is really difficult to decide which is the best solution: it could for example come out that a simple Doppler measurement alone is already sufficient to improve the current on-board navigation system, either in terms of landing accuracy or mass.

3.2.2 Two Beacons

A navigation architecture relying on two beacons would have some advantages with respect to the single beacon, for example:

- it could be possible to place the two beacons in such a way to support all phases of the powered landing;
- an improved accuracy could be expected, having one extra measurement;

- the GBNS would withstand a failure in one beacon, with a degradation of accuracy;
- 3D positioning is possible, with the appropriate set of measurement (for example 2 VOR-DME like systems would allow this).

The main drawback is the need of a dedicated vehicle to locate the second beacon, which could be very difficult, also considering the morphology of the lunar surface, especially in the South pole area, the most probable site for the lunar base.
It has been decided that all beacons in the architecture enable the same set of measurements. In fact it has been considered that there is no logic to have, for example, a measure of range from one beacon and range-rate from another. Moreover, this choice is also driven by the fact that allowing mixed measurements would make the number of combinations to explode.
With the constraint expressed above the cases to analyze would be the same of table 3.2, just considering two identical beacons.

3.2.3 Three or More Beacons

The same advantages as well as disadvantages of the two beacons configurations apply in this case. Three beacons enable trilateration, i.e. a range measurement from each beacon would permit unambiguous positioning in space; as GPS teaches this information would be affected by error due to time bias and therefore a 4^{th} beacon is needed to correct the error.
Maybe, in a not too distant future, the lunar base could have 3 or 4 beacons available, since they are also useful, for instance, for Earth communication, orbiters tracking and localization of a user on the surface. With this perspective it is of interest to check for the performance of a GPS-like navigation system, with 3 and 4 beacons. For what stated in 3.2.1 it would be reasonable to dispose also Doppler measurements from these beacons.
This study will not investigate on architectures based on more than four beacons.

3.2.4 Options Summary and Selection

Many possible configurations have been found and discussed up to this point. It must be considered the fact that each configuration in table 3.3 would require many simulations (Monte-Carlo analyses).
Moreover, there are N added DOF's, being N the number of beacons, that represent the possible locations of the beacons on ground. It is therefore

necessary to further filter out configurations in the list, in order to concentrate on fewer GBNS architectures, whose performance will be investigated.

Table 3.3: Preliminary GBNS architecture candidates

1 Beacon	**Measurements**	**2 Beacons**
1-A	Range	2-A
1-B	Range-Rate	2-B
1-C	Bearing	2-C
1-D	Range + Range-Rate	2-D
1-E	Range + Bearing	2-E
1-F	Range-rate + Bearing	2-F
1-G	Range + Range-Rate + Bearing	2-G
3 Beacons	**Measurements**	**4 Beacons**
3-D	Range + Range-Rate	4-D

With the aim of having a pool of maximum six options, it has been decided to:

- discard the single measurements, since it is very unlikely that such an effort to enable this system would be made only for measuring relative velocities to beacons, for example;
- always put together range and range-rate measurements, for all considerations already stated in this chapter.

With these two constraints, the list in table 3.3 reduces to six options, which are reported in table 3.4.

Referring to table 3.4, it can be noticed that:

- A places the lander on a circular pattern;
- B enables unambiguous positioning in plane;
- C places the lander at the intersections of two circumferences;
- D, E and F give enough data to unambiguously locate the lander in space.

The cases in table 3.4 will be studied in the following order:

Table 3.4: Selected GBNS architectures to be analyzed

	ID	Measurements
1 Beacon	A	Range + Range-Rate
	B	Range + Range-Rate + Bearing
2 Beacons	C	Range + Range-Rate
	D	Range + Range-Rate + Bearing
3 Beacons	E	Range + Range-Rate
4 Beacons	F	Range + Range-Rate

- with the interest in minimizing the number of beacons (GBNS-3, table 3.1), after having implemented observations models for range, range-rate and bearing, first it will be studied case B (table 3.4), since it maximizes the information passed to the filter; it is expected better results than case A;
- as consequence case D will be analyzed prior to case C; moreover it is of great interest because it is the option with the least number of beacons that enables 3D positioning;
- case E will then be treated before case F.

Therefore, no "ranking" is provided for the cases, but, according to aforementioned reasons, at this stage, cases B and D are expected to be the more interesting ones.
For the preliminary analyses which are carried out in this thesis it will be assumed that all clocks are synchronized.
The trade-offs will be presented assuming exact knowledge of the positions of the beacons and fixed update frequency of the new measurements. Eventually, sensitivity analyses will be shown to have an idea of the influence of the position uncertainty and working frequency on the obtained results.

CHAPTER 4

Models and Algorithms Description

4.1 Reference Frames

First of all it is useful to give some information about the reference systems used throughout the work and cited in this thesis.

4.1.1 Inertial Reference Frame

The inertial reference frame used in this study is defined with the x-axis pointing towards the mean vernal equinox, the z-axis to the geodetic north pole of the Moon and the y-axis completing the orthogonal tern.
This is the reference frame in which the dynamics (landing trajectory and attitude) is integrated inside the Simulink model.

4.1.2 Moon Centered Fixed (MCF) Reference Frame

This coordinate system is fixed with respect to the Moon and has its origin in the center of mass of the Moon. It is defined with the x-axis pointing towards the point on the surface with null latitude and longitude, the z-axis towards the geodetic north pole and the y-axis completing the orthogonal reference frame [1].

[1] For the sake of simplicity, throughout the text, unless specified with the appropriate superscript, the nominal reference frame is the MCF.

4.1.3 Down-Range Cross-Range and Altitude (DCA) Reference Frame

This relative frame is defined with same origin of MCF frame, the z-axis, altitude (A), directed as the Zenith, the y-axis, cross-range (CR) obtained from:

$$\mathbf{CR} = \frac{\mathbf{v}^{MCF}}{\|\mathbf{v}^{MCF}\|} \times \mathbf{A} = \frac{\mathbf{v}^{MCF}}{\|\mathbf{v}^{MCF}\|} \times \frac{\mathbf{r}^{MCF}}{\|\mathbf{r}^{MCF}\|} \tag{4.1}$$

and eventually the x-axis, down-range (DR), computed as:

$$\mathbf{DR} = \mathbf{CR} \times \mathbf{A} \tag{4.2}$$

There is a singularity in equation (4.1) when velocity and position vectors are aligned: in this situation it is kept the DCA frame defined the time instant before. Moreover, if the lander is overstepping the landing site while descending, in the moment it comes back, the down and cross-range change sign. The corresponding rotation from MCF frame to DCA frame is expressed as:

$$\mathbf{R}_{MCF}^{DCA} = \begin{bmatrix} \mathbf{DR} & \mathbf{CR} & \mathbf{A} \end{bmatrix}^T \tag{4.3}$$

4.1.4 Local Horizon (LH) Reference Frame

This reference frame is defined with origin as for the MCF frame, the x-axis directed towards the Zenith of the local observer on the surface (the beacon) and the other two axes parallel to the local horizon, such that y-axis heads to the East and z-axis to the North

Being the MCF x-axis passing through the point at zero longitude and latitude, the relation among MCF and LH is expressed as:

$$\mathbf{R}_{MCF}^{LH} = \mathbf{R}_2(\phi)\,\mathbf{R}_3(\lambda_E) = \begin{bmatrix} \cos\phi\cos\lambda_E & \cos\phi\sin\lambda_E & \sin\phi \\ -\sin\lambda_E & \cos\lambda_E & 0 \\ -\sin\phi\cos\lambda_E & -\sin\phi\sin\lambda_E & \cos\phi \end{bmatrix} \tag{4.4}$$

where λ_E and ϕ are respectively the East longitude and the latitude. The matrices describing these rotations are constant, since in this study it will be considered that beacons are fixed on the surface.

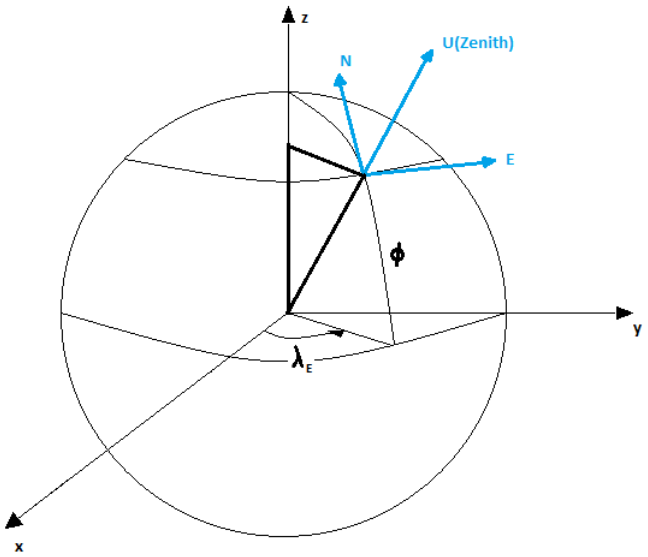

Figure 4.1: Local Horizon Reference Frame

Beacon Position Evaluation

In this study every beacon position on the surface is given in terms of East longitude ($\lambda_{E,BC}$), latitude (ϕ_{BC}) and altitude (h_{BC}) with respect to the landing site, therefore the surface curvature, which affects visibility from the beacon, is accounted. The routine used to compute the position of a beacon is here presented.
Relative displacements of the beacon along the North (ΔN) and East (ΔE) direction with respect to the landing site are introduced. These are converted in radians ($\Delta\phi$ and $\Delta\lambda_E$), under the assumption that the Moon radius is the radius at the landing site (R_{LS}), which, for small displacements around the landing site is a valid assumption. In particular:

$$\Delta\phi = \frac{\Delta N}{R_{LS}} \longrightarrow \phi_{BC} = \phi_{LS} + \Delta\phi \tag{4.5}$$

Being the latitude defined in the interval $[-\pi,\pi]$, if the landing site is close to one of the poles, it should be checked whether the beacon has "crossed the pole" after applying (4.5), and the value of ϕ_{BC} has to be corrected accordingly, in order to fit in the aforementioned interval. In this work, this event does not happen being the landing site near to the equator.
The longitude of the beacon is then computed by:

$$\Delta\lambda_E = \frac{\Delta E}{R_{LS}\ \cos\phi} \longrightarrow \lambda_{E,BC} = \lambda_{E,LS} + \Delta\lambda_E \tag{4.6}$$

The rotation matrix associated to the beacon is then computed through equation (4.4) and used to compute the position of the beacon in MCF frame.

$$\mathbf{r}_{BC} = \mathbf{R}_{MCF}^{LH\ T}\, \mathbf{r}_{BC}^{LH} \tag{4.7}$$

where $\mathbf{r}_{BC}^{LH} = [R_{LS} + h_{BC}, 0, 0]^T$

4.1.5 Body (B) and Sensors Reference Frame

The SINPLEX body frame is the body frame of the housing. This is composed of three orthogonal axes that are fixed to the housing and centered at a defined point. All sensors reference frames, i.e. accelerometer, star tracker, gyro and navigation camera have their own reference frames which are linked to the body frame through proper rotation matrices [18].
Under the assumption of a non-directional antenna on-board of the lander, there is no need to define a reference frame for the radiometric measurements from the beacons.

4.2 Scenario

The scenario, as already stated, is a lunar soft landing. The landing trajectory, adapted from the ones used in the Autonomous Terrain based Optical Navigation (ATON) project of DLR, starts with a maneuver to be inserted in a 100x10 km descent orbit, from a 100x100 km polar orbit. At perigee the powered descent is initiated and at 2 km altitude, i.e. at high gate when the landing site is in view, the landing phase starts. Finally a vertical descent is performed from around 1 km altitude (figure 4.2).
More in detail, the DO is chosen such to provide optimal lighting condition for optical navigation. A variable thrust is used to slow down the lander as it descends towards the landing site, which is located near the equator. A small constant acceleration is also given during PD in cross-range direction in order to cope with the lunar surface rotation. Figure 4.4a shows the specific force profile.
The S/C attitude is initiated such that the main thruster is oriented for the DO burn, after which the S/C is oriented to be in the best attitude for optical navigation. Before PD a small rotation is performed to reorient the main thruster for PDI, while throughout the PD the attitude is constrained by the thrust profile. It is assumed to have the antenna used for the beacon navigation near the NC on the bottom surface of the lander, so that it is directly visible from the beacons during PD, when lander is visible. Figure 4.4b presents the angular velocity profile.

The simulation starts with the DO burn and ends at an altitude of 1 m above the LS, so it includes all parts of the landing. The final velocity is less than 0.5 m/s.

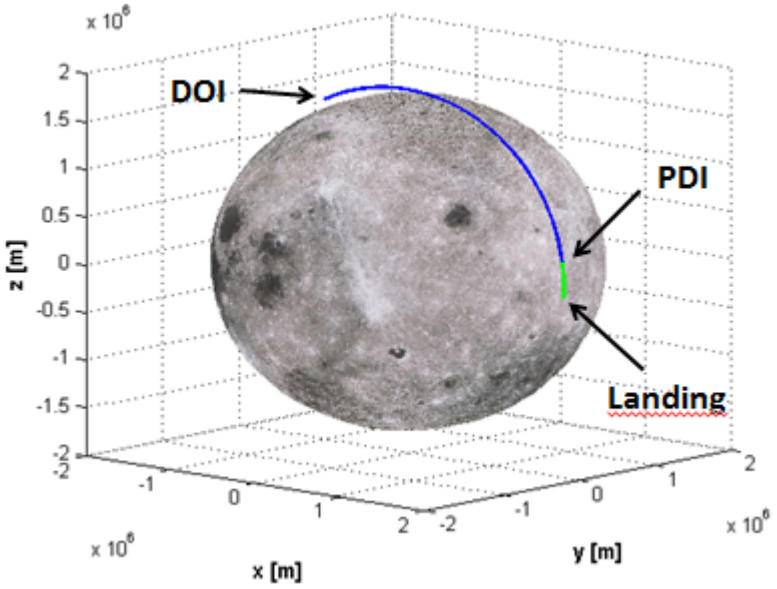

Figure 4.2: Landing trajectory

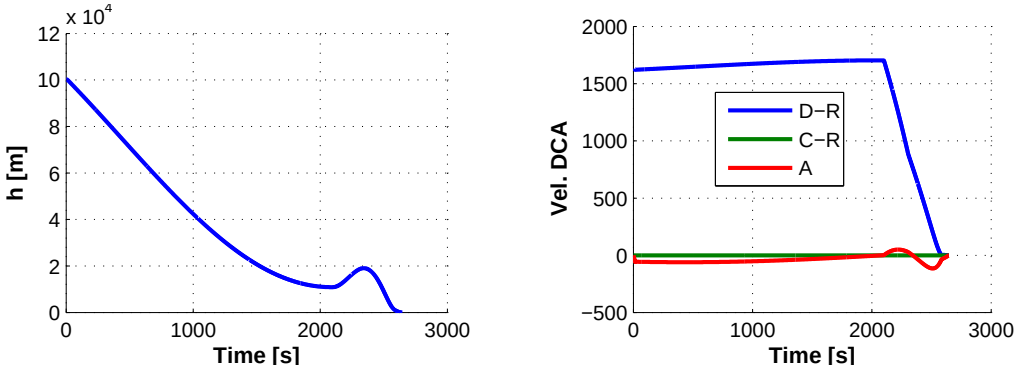

(a) Altitude (b) Vel. profile DCA

Figure 4.3: Landing

Eventually, it is useful to report the powered descent footprint on the LH plane of an observer in the LS, in order to better understand some considerations during the analyses (figure 4.5).

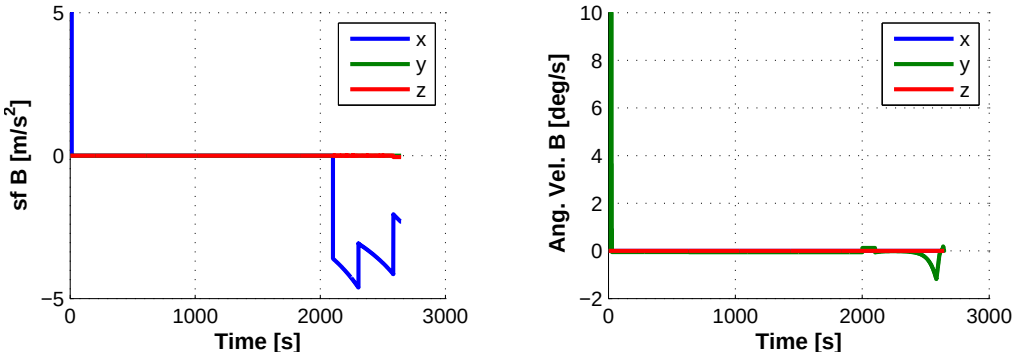

(a) sf^B (b) ω^B

Figure 4.4: Control profile

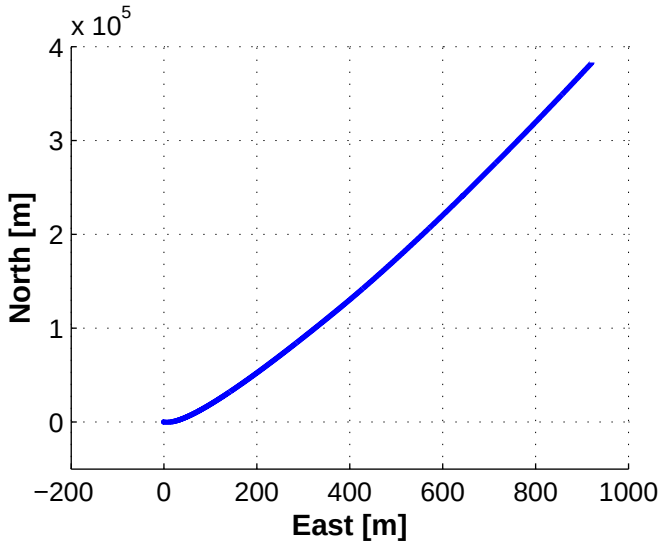

Figure 4.5: Powered Descent footprint in LH plane

4.3 Truth Model

The lander dynamics truth model implemented in the SINPLEX Simulink model is run in continuous time.
Given the initial conditions and trajectory dynamics as inputs, the model integrates the following equations of motion in inertial frame:

$$\begin{cases} \dot{\mathbf{r}}^I = \mathbf{v}^I \\ \dot{\mathbf{v}}^I = \mathbf{R}(\mathbf{q}_B^I)\ \mathbf{a}^B + \mathbf{R}(\mathbf{q}_{MCF}^I)\ \mathbf{g}(\mathbf{r}^{MCF}) \\ \dot{\mathbf{q}}_B^I = -\dfrac{1}{2}\ \mathbf{q}_B^I \otimes [\ \boldsymbol{\omega}_{I,B}^B \quad 0\ ]^T \end{cases} \tag{4.8}$$

where $\mathbf{a}$ is the specific force, $\mathbf{g}$ is the gravity model, $\mathbf{q}$ is an attitude quaternion and $\mathbf{R}(\mathbf{q})$ is the direction cosine matrix associated to the quaternion.
S/C states are then transformed in MCF frame which is needed by several sensors models, including the beacon one. The transformation equations are:

$$\begin{cases} \mathbf{r}^{MCF} = \mathbf{R}(\mathbf{q}_I^{MCF})\ \mathbf{r}^I \\ \mathbf{v}^{MCF} = \mathbf{R}(\mathbf{q}_I^{MCF})\ \mathbf{v}^I - \boldsymbol{\omega}_{I,MCF}^{MCF} \times \mathbf{r}^{MCF} \\ \mathbf{a}^{MCF} = \mathbf{R}(\mathbf{q}_I^{MCF})\ \mathbf{a}^I - 2\ \boldsymbol{\omega}_{I,MCF}^{MCF} \times \mathbf{v}^{MCF} - \boldsymbol{\omega}_{I,MCF}^{MCF} \times \boldsymbol{\omega}_{I,MCF}^{MCF} \times \mathbf{r}^{MCF} \\ \boldsymbol{\omega}_{MCF,B}^B = \boldsymbol{\omega}_{I,B}^B - \mathbf{R}(\mathbf{q}_{MCF}^B)\ \boldsymbol{\omega}_{I,MCF}^{MCF} \end{cases} \tag{4.9}$$

4.4 Navigation Filter

This section is intended to briefly present to the reader the navigation filter used in this work, which is an implementation of the SINPLEX navigation algorithms. The navigation filter exploited in this work is coded in Matlab.

4.4.1 Navigation Scheme

SINPLEX uses a multi-rate scheme for the navigation algorithm to be executed:

- an high-rate (HR) task runs at 100 Hz on the IMU and integrates the IMU data and also compensates the IMU data with its stored calibration coefficients and the bias and scale factor values sent from HR;
- a medium-rate (MR) task runs at 10 Hz for the propagation of the whole states with the integrated IMU data using strapdown navigation and calculates the state transition matrix;
- a low-rate (LR) task at the end of each 1 Hz filter time step receives the state transition matrix. Principally, the LR task runs at 1Hz and

propagates the filter and then updates the filter when measurement data are available using data passed from the MR task.

The navigation scheme is represented in figure 4.6, where τ_j and t_k represent the time respectively for the MR and LR processes.

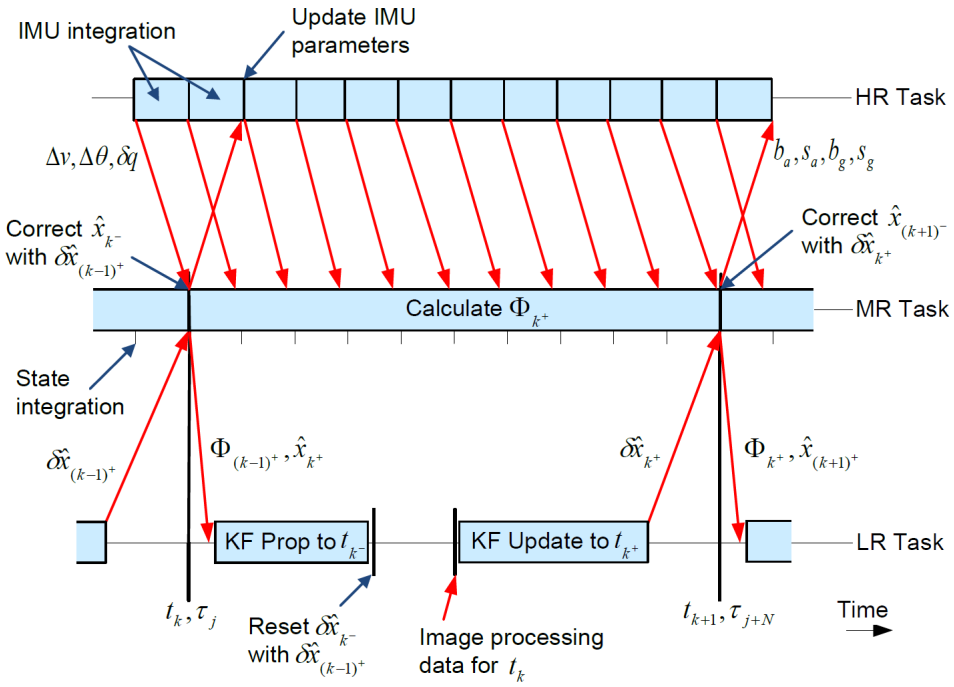

Figure 4.6: Time line of navigation algorithm and the data passed between the HR, MR and LR tasks. Red arrows indicate data exchanges. Blue arrows are for descriptions (taken from [19]).

4.4.2 Discrete Error-State Extended Kalman Filter

The real-time implementation of SINPLEX software is a discrete delayed error-state EKF (eEKF), which copes with the fact that measurements are not in the real system available at the same time but with delays. It is reported that error-state EKF avoids some problems arising with the delays for standard EKF and is more computationally efficient [8].
Although SINPLEX exploits a discrete *delayed* eEKF, i.e. with whole state corrections which are delayed by 1 time step (as it can also be seen from figure 4.6), in this analysis work a preparatory version of the navigation software without the 1 time step delay for the updates has been used. The equations for the discrete eEKF are reported in table 4.1, while figure 4.7 shows the timing diagram for the discrete eEKF.

Table 4.1: Summary of discrete eEKF equations, taken from [8]

Whole State System Model	$\mathbf{x}_{k+1} = \phi_k(\mathbf{x}_k) + \mathbf{w}_k;\ \mathbf{w}_k \sim \mathcal{N}(0, Q_k)$
Error State System Model	$\delta\mathbf{x}_{k+1} = \phi_k(\hat{\mathbf{x}}_k + \delta\mathbf{x}_k) - \phi_k(\hat{\mathbf{x}}_k) + \mathbf{w}_k$
Measurement Model	$\mathbf{z}_k = \mathbf{h}_k(\hat{\mathbf{x}}_k + \delta\mathbf{x}_k) - \mathbf{h}_k(\hat{\mathbf{x}}_k) + \nu_k;\ \nu_k \sim \mathcal{N}(0, R_k)$
Initial Conditions	$\mathbf{x}_0 \sim \mathcal{N}(\hat{\mathbf{x}}_0, P_0);\ \delta\hat{\mathbf{x}}_0 = 0$
Other Assumptions	$E\left\langle \mathbf{w}_k \nu_l^T \right\rangle = 0;\ \forall k;\ \forall l$
Whole State Propagation	$\hat{\mathbf{x}}_{(k+1)^-} = \phi_k(\hat{\mathbf{x}}_{k^+})$
Error State Propagation	$\delta\hat{\mathbf{x}}_{(k+1)^-} = \phi_k(\hat{\mathbf{x}}_{k^+} + \delta\hat{\mathbf{x}}_{k^+}) - \phi_k(\hat{\mathbf{x}}_{k^+})$
Covariance Propagation	$P_{(k+1)^-} = \Phi_{k^+} P_{k^+} \Phi_{k^+}^T + Q_k$
Kalman Gain Matrix	$K_k = P_{k^-} H_{k^-}^T \left[H_{k^-} P_{k^-} H_{k^-}^T + R_k\right]^{-1}$
Error State Update	$\delta\hat{\mathbf{x}}_{k^+} = \delta\hat{\mathbf{x}}_{k^-} + K_k\left(\mathbf{z}_k - \mathbf{h}_k(\hat{\mathbf{x}}_{k^-} + \delta\hat{\mathbf{x}}_{k^-}) + \mathbf{h}_k(\hat{\mathbf{x}}_{k^-})\right)$
Filter Reset	$\hat{\mathbf{x}}_{k^+} = \hat{\mathbf{x}}_{k^-} + \delta\hat{\mathbf{x}}_{k^+};\ \delta\hat{\mathbf{x}}_{k^+} \leftarrow 0$
Covariance Update	$P_{k^+} = \left[I - K_k H_{k^-}\right] P_{k^-}$
Definitions	$\Phi_{k^+} \equiv \left.\frac{\partial\phi_k(\mathbf{x}_k)}{\partial\mathbf{x}_k}\right\|_{\mathbf{x}_k=\hat{\mathbf{x}}_{k^+}}$ $H_{k^-} \equiv \left.\frac{\partial\mathbf{h}_k(\mathbf{x}_k)}{\partial\mathbf{x}_k}\right\|_{\mathbf{x}_k=\hat{\mathbf{x}}_{k^-}}$

This filter differs from the EKF in that it estimates the error states rather than the whole states of the system and the whole state vector is reset with corrections; it can be defined by substituting $\delta\mathbf{x}$ for $\mathbf{x}$ in the standard EKF equations. It is basically the same of an EKF but it allows the whole states to be integrated as quickly as possible while error state integration is separated. The estimated whole state vector can then be regularly corrected after each propagate (contrary to the EKF, which corrects right after the update step) with the error state estimates [8].
For states with additive errors the error state vector is defined as:

$$\delta\mathbf{x} = \mathbf{x} - \hat{\mathbf{x}} \tag{4.10}$$

It can be shown that, due to the fact $\dfrac{\partial\mathbf{x}_k}{\partial(\delta\mathbf{x}_k)} = \mathbf{I}$, both the linearized state transition matrix $\mathbf{\Phi}_k$ used to propagate the state covariance, and the linearized observation matrix $\mathbf{H}_k$ are respectively Jacobians of the whole state system and measurement models, same to the standard EKF [8].

4.4.3 Filter States

The states necessary for the strapdown navigation are position and velocity in MCF frame, attitude error angles and accelerometers and gyros bias and scale

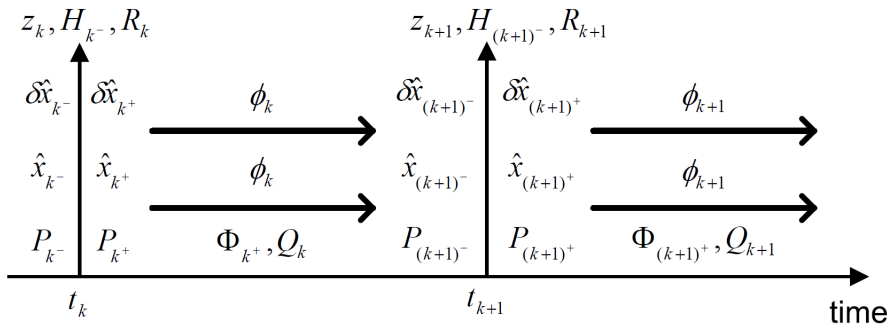

Figure 4.7: Timing diagram for the discrete eEKF, taken from [8]

factors. There are then additional states necessary for the terrain relative navigation, which are feature positions needed to build the terrain model and estimate changes in the S/C navigation states. There are so 4 added "map states", corresponding to feature positions. The terrain model is estimated through the solution of the SLAM problem [20].
The state vector is:

$$\mathbf{x} = \left\{ \begin{array}{c} \mathbf{r}^{MCF} \\ \mathbf{v}^{MCF} \\ \boldsymbol{\theta}^{B} \\ \mathbf{b}_{a}^{B} \\ \mathbf{s}_{a}^{B} \\ \mathbf{b}_{g}^{B} \\ \mathbf{s}_{g}^{B} \\ \boldsymbol{\xi}_{i}^{MCF} \end{array} \right\} \tag{4.11}$$

where $\boldsymbol{\xi}_i^{MCF}$, with i=1:4 are the tracked feature positions. The length of the state vector is 33.

4.5 Baseline Sensor Suite Models

In this section a brief description of the modeling of the sensors composing the SINPLEX sensor suite for the lunar landing scenario will be presented [18, 19]. It has to be remarked that the modeling of these sensors has not been part of this thesis work, with the exception of part of the laser altimeter update model, which will be therefore more extensively presented later in this section.
In this work, every sensor updates at a frequency of 1 Hz (LR task), with the exception of the IMU, whose working frequency is 100 Hz (HR task).
The sensors models are implemented in a Simulink model, as done for the truth model.

4.5.1 Inertial Measurement Unit

The Generic IMU model from the High Performance Satellyte Dynamics Simulator (HPS) is used for this simulation. This model uses a generic error model for the accelerometers and gyros and uses an analog to digital converter (ADC) model to sample the outputs [18].
The true specific force $\mathbf{f}^B$ and angular rate of the body with respect to the inertial in B frame ($\boldsymbol{\omega}^B_{I,B}$) are given as inputs to the model. The outputs of this model are the measured angular rates and specific forces for all gyros and accelerometers and the sampled IMU clock value.
The scalar angular rate measured by each gyro is modeled as:

$$\omega = \mathbf{e}^T \mathbf{R}^G_B \, \boldsymbol{\omega}^B_{I,B} \tag{4.12}$$

where $\mathbf{e}$ is the unit vector of the gyro measurement direction and $\mathbf{R}^G_B$ is the rotation from body to gyro frame.
The scalar input for the given accelerometer is instead:

$$f = \mathbf{e}^T \mathbf{R}^A_B (\mathbf{f}^B + \mathbf{f}^B_{cent} + \mathbf{f}^{Euler}_B) \tag{4.13}$$

where the centripetal and Euler term of the acceleration due to the angular velocity have to be taken into account.
These inputs are then fed in the HPS generic sensor model which models the bias and scale factor errors. The analogue output is then converted to digital with the ADC model.

4.5.2 Star Tracker

The ST model from the HPS is used. This simulates the attitude quaternion measurement of the ST frame with respect to the inertial frame. This is calculated by using the input quaternion from truth.
The model simulates the location and appearance of each star in the current field of view (FOV) based on camera attitude with respect to the inertial frame. This model is based on the pin-hole camera principle. The centroiding errors are added as typical star tracker errors (an input parameter to the model). A simulated set of unit vectors of the measured stars is generated; these vectors are then used to solve the Wahba problem through the Paul Davenport's q-method in order to obtain the measured attitude quaternion.

4.5.3 Crater Navigation

The crater navigation model estimates the measurement returned by the crater navigation image processing algorithm. This sensor uses the navigation camera images to detect craters on the surface and match them to a database of known craters. The result is used to calculate the absolute position of the camera in the MCF frame.
The simulation of the crater navigation is given through a first order error model. In particular, the measured S/C position is modeled as a white noise added to the true position in MCF frame.
The model also checks if the altitude is above 10 km and if at least half of the image contains the surface, which are necessary conditions in order to consider the measurements valid.

4.5.4 Feature Tracking

The feature tracker model simulates measured feature positions and IDâĂŹs. The features are randomly chosen over the surface of a sphere, which simulates the surface of the Moon. Once chosen, the features are fixed to the sphere and are projected into the camera image at each time point.
The inputs of the FT model are the position vector in the MCF frame and the quaternion in the MCF frame with respect to the B frame, while the outputs is a table which includes the pixel coordinates and unique ID number of every feature in the image. An overview over the algorithm is shown in figure 4.8.
The measurement of the FT algorithm are not directly used in the EKF, but they are first converted into an optical flow measurement. This update model is discussed in more detail in [9].

In this work, the FT is updating the navigation solution from 20 km height.

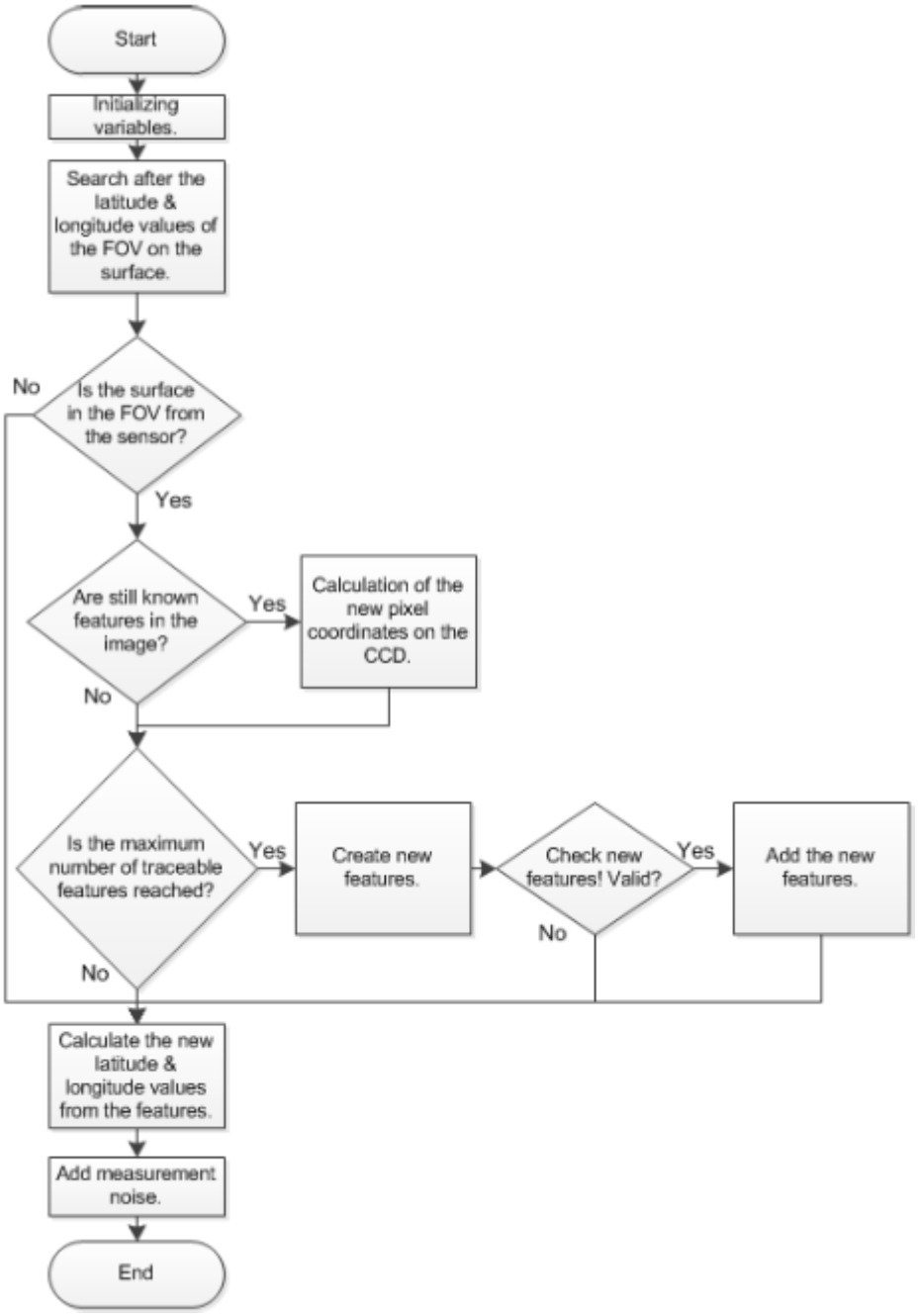

Figure 4.8: Feature tracking algorithm overview

4.5.5 Laser Altimeter

The LA measures the slant-range (SR), i.e. the distance along the LA measurement direction between the sensor and the intersection with the surface. In SINPLEX, the distance to the intersection points is calculated by finding the roots of the equation:

$$SR^2 + 2\,\mathbf{r}^{MCF^T}\,\boldsymbol{\zeta}^{MCF}\,SR + \|\mathbf{r}^{MCF}\|^2 - R_{LS}^2 = 0 \tag{4.14}$$

where $\boldsymbol{\zeta}^{MCF}$ is the LA measurement direction unit vector in MCF frame and it has been assumed that the radius of the Moon is equal to the one of the landing site. The output measurement, if valid (the LA measurement direction intersects the sphere), is equal to this distance to which random noise is added.
This measurement is not directly used in the navigation filter, but it is used within the terrain relative navigation together with the estimated $\boldsymbol{\xi}_i^{MCF}$ which are describing the terrain model. In this way, it is modeled the uncertainty in the terrain slope and altitude when updating, which is not considered in computing the slant-range.
In this work, the LA, as the FT, is updating the navigation solution from an altitude of 20 km.

Vertical Descent Update Equations

In order to cope with the fact that the lander, in the scenario analyzed, is landing in a well determined landing site, whose altitude is known a priori, the update equations from the laser altimeter measurement have to be different from the previous ones during the vertical descent phase.

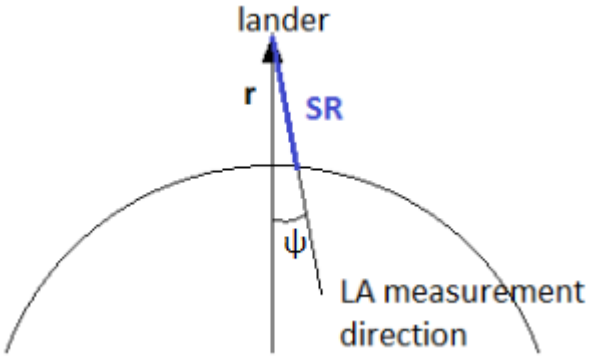

Figure 4.9: Slant-range measurement

With reference to figure 4.9, if the altitude of the S/C and the angle ψ between the LA measurement direction and the position vector of the LA are small enough, then the following approximate expression for the slant-range can be used:

$$SR \cong (\|\mathbf{r}_{LA}\| - R_{LS}) \frac{1}{\cos\psi} \tag{4.15}$$

where

$$\mathbf{r}_{LA} = \mathbf{r} + \mathbf{R}_B^{MCF} \boldsymbol{\ell}_{LA}^B \tag{4.16}$$

being $\boldsymbol{\ell}_{LA}^B$ the lever arm of the LA with respect to the IMU.
Then, the cosine of ψ is given by:

$$\cos\psi = -\boldsymbol{\zeta}^{B^T} (\mathbf{R}_{MCF}^B \frac{\mathbf{r}_{LA}}{\|\mathbf{r}_{LA}\|}) \tag{4.17}$$

where $\boldsymbol{\zeta}^B$ is the LA measurement direction unit vector in body frame. At this stage, in order to have an easier expression to compute the Jacobian, the following approximation is used:

$$\frac{1}{\cos\psi} = \pm\sqrt{1+\tan^2\psi} \approx \pm\sqrt{1+\sin^2\psi} \approx \pm\sqrt{2-\cos^2\psi} \tag{4.18}$$

The equation (4.15) can be now rewritten as:

$$SR \cong \sqrt{2 - (\frac{\mathbf{r}_{LA}^T}{\|\mathbf{r}_{LA}\|} \mathbf{R}_B^{MCF} \boldsymbol{\zeta}^B)^2} (\|\mathbf{r}_{LA}\| - R_{LS}) \tag{4.19}$$

The dependency on the attitude error angles is in the rotation matrix, expressed as:

$$\mathbf{R}_B^{MCF} = \hat{\mathbf{R}}_B^{MCF} (\mathbf{I} - [\boldsymbol{\theta}^B\times]) \tag{4.20}$$

being $\hat{\mathbf{R}}_B^{MCF}$ the rotation matrix estimated by the filter, and $\mathbf{I} - [\boldsymbol{\theta}^B\times]$ the linearized small rotation matrix.
Introducing the following terms for the sake of having more compact expressions:

$$
\begin{aligned}
A &= \sqrt{2 - (\frac{\mathbf{r}_{LA}^T}{\|\mathbf{r}_{LA}\|}\, \mathbf{R}_B^{MCF}\, \boldsymbol{\zeta}^B)^2} \\
B &= \|\mathbf{r}_{LA}\| - R_{LS} \\
C &= \mathbf{R}_B^{MCF}\, \boldsymbol{\zeta}^B \\
D &= \frac{\mathbf{r}_{LA}{}^T}{\|\mathbf{r}_{LA}\|}\, \mathbf{R}_B^{MCF}\, \boldsymbol{\zeta}^B
\end{aligned}
\tag{4.21}
$$

the partial derivatives of equation (4.19) with respect to the state variables are:

$$
\frac{\partial SR}{\partial \mathbf{r}} = A\, \frac{\mathbf{r}_{LA}{}^T}{\|\mathbf{r}_{LA}\|} - \frac{B\, C^T\, D}{A}\, (\frac{1}{\|\mathbf{r}_{LA}\|}\, \mathbf{I} - \frac{1}{\|\mathbf{r}_{LA}\|^3}\, \mathbf{r}_{LA}\, \mathbf{r}_{LA}{}^T) \tag{4.22}
$$

$$
\frac{\partial SR}{\partial \boldsymbol{\theta}^B} = -\frac{B\, D}{A}\, \frac{\mathbf{r}_{LA}{}^T}{\|\mathbf{r}_{LA}\|}\, \hat{\mathbf{R}}_B^{MCF} [\boldsymbol{\zeta}^B \times] \tag{4.23}
$$

where it has been exploited the relation $\mathbf{a} \times \mathbf{b} = -\mathbf{b} \times \mathbf{a}$.
It has to be noticed that in the derivation of equation (4.23) it has been neglected the dependency of the attitude on $\mathbf{r}_{LA}$, being it much smaller with respect to the depencency on the cosine of ψ.
The Jacobian $\mathbf{H}_{SR}$ is:

$$
\mathbf{H}_{SR} = [\ \frac{\partial SR}{\partial \mathbf{r}} \quad \boldsymbol{\emptyset}_{1\times 3} \quad \frac{\partial SR}{\partial \boldsymbol{\theta}^B} \quad \cdots\ ] \tag{4.24}
$$

The innovation processed by the eEKF is eventually the difference between the measured and the estimated slant-range:

$$
z_{SR} = \delta SR = \tilde{SR} - \hat{SR} \tag{4.25}
$$

In this work, these update equations are applied when the altitude is 1 km with respect to the LS one. At this height, the lander is starting to descent vertically and the angle ψ is small enough to consider applicable equation (4.19).

4.6 Beacon

4.6.1 Observation Models

In the following, the observation models used for the radiometric measurements considered are reported.
The equations presented in this section have been appropriately implemented in:

- the beacon Simulink model which has been then added to the SINPLEX sensor and truth Simulink model for the simulation of the measurements;
- the Matlab code running the eEKF, for the fusion of those measurements with the others.

Range

The range is the measurement of the distance between the beacon and the antenna on-board of the S/C (figure 4.10).

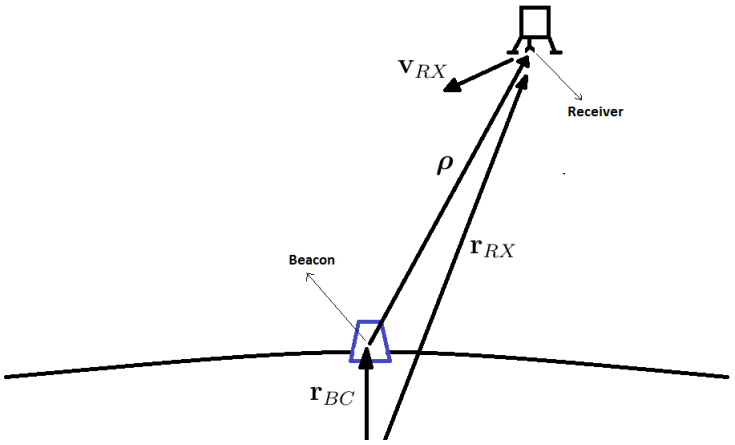

Figure 4.10: Representation of S/C and beacon on lunar surface

The lever arm of the receiver is first added to the position of the IMU in the MCF frame (a state of the filter):

$$\mathbf{r}_{RX} = \mathbf{r} + \mathbf{R}_B^{MCF}\, \boldsymbol{\ell}_{RX}^B \tag{4.26}$$

The vector between the beacon and the receiver is:

$$\boldsymbol{\rho} = \mathbf{r}_{RX} - \mathbf{r}_{BC} = \mathbf{r} + \mathbf{R}_B^{MCF}\, \boldsymbol{\ell}_{RX}^B - \mathbf{r}_{BC} \tag{4.27}$$

Under the assumption of neglecting the clock biases, which brings to the equality between range and pseudo-range, the range is expressed as:

$$\rho = \rho(\mathbf{r}, \boldsymbol{\theta}^B) = \|\boldsymbol{\rho}\| + w_\rho \tag{4.28}$$

where w_ρ is the range measurement noise which is assumed to be normally distributed [2].

The partial derivatives of equation (4.28) with respect to the state variables are:

$$\frac{\partial \rho}{\partial \mathbf{r}} = \frac{\partial \rho}{\partial \boldsymbol{\rho}} \frac{\partial \boldsymbol{\rho}}{\partial \mathbf{r}} = \frac{\boldsymbol{\rho}^T}{\rho} \tag{4.29}$$

$$\frac{\partial \rho}{\partial \boldsymbol{\theta}^B} = \frac{\partial \rho}{\partial \boldsymbol{\rho}} \frac{\partial \boldsymbol{\rho}}{\partial \boldsymbol{\theta}^B} = \frac{\boldsymbol{\rho}^T}{\rho} \mathbf{R}_B^{MCF} [\boldsymbol{\ell}_{RX}^B \times] \tag{4.30}$$

being,

$$\frac{\partial \boldsymbol{\rho}}{\partial \boldsymbol{\theta}^B} = \mathbf{R}_B^{MCF} [\boldsymbol{\ell}_{RX}^B \times] \tag{4.31}$$

These derivatives are properly fed into the Jacobian $\mathbf{H}_\rho$:

$$\mathbf{H}_\rho = [\ \frac{\partial \rho}{\partial \mathbf{r}} \quad \emptyset_{1\times 3} \quad \frac{\partial \rho}{\partial \boldsymbol{\theta}^B} \quad \cdots \ ] \tag{4.32}$$

The innovation processed by the eEKF is eventually the difference between the measured and the estimated ranges:

$$z_\rho = \delta\rho = \tilde{\rho} - \hat{\rho} \tag{4.33}$$

Range-Rate

The range-rate is the relative velocity between the on-board receiver and the beacon. The observation equation used is the following:

$$\dot{\rho} = \dot{\rho}(\mathbf{r}, \mathbf{v}, \boldsymbol{\theta}^B, \mathbf{b}_g^B, \mathbf{s}_g^B) = -\mathbf{v}_{RX}^T \frac{\boldsymbol{\rho}}{\rho} + w_{\dot{\rho}} \tag{4.34}$$

where it can be shown that the velocity of the receiver in MCF frame is:

$$\mathbf{v}_{RX} = \mathbf{v} + (\mathbf{R}_B^{MCF} [\boldsymbol{\omega}_{I,B}^B \times] - [\boldsymbol{\omega}_{I,M}^M \times] \mathbf{R}_B^{MCF}) \, \boldsymbol{\ell}_{RX}^B \tag{4.35}$$

[2] In lack of references to consider different distribution for the noises, all noises in this work are considered to be normally distributed.

For evaluating the angular velocity of the S/C the following approximation is used:

$$\boldsymbol{\omega}_{I,B}^{B} \cong \frac{\Delta\boldsymbol{\Theta}^{B}}{\Delta\tau} \tag{4.36}$$

where the observation equation for the angular variation used is:

$$\Delta\boldsymbol{\Theta}^{B} \cong diag(\mathbf{s}_{g}^{B})\ \Delta\tilde{\boldsymbol{\Theta}}^{B} + \Delta\tau\ \mathbf{b}_{g}^{B} + w_{\Delta\boldsymbol{\Theta}} \tag{4.37}$$

In (4.37) $\Delta\tilde{\boldsymbol{\Theta}}^{B}$ and $\Delta\tau$ are respectively the angular variation measured by the IMU and its sampling interval.
In the following equations, the partial derivatives of the observation equation (4.34) with respect to the states variables are reported.

$$\frac{\partial\dot{\rho}}{\partial\mathbf{r}} = \frac{\partial\dot{\rho}}{\partial\boldsymbol{\rho}}\ \frac{\partial\boldsymbol{\rho}}{\partial\mathbf{r}} = -\frac{\mathbf{v}_{RX}^{T}}{\rho}\ (\mathbf{I} - \frac{1}{\rho^{2}}\ \boldsymbol{\rho}\ \boldsymbol{\rho}^{T}) \tag{4.38}$$

$$\frac{\partial\dot{\rho}}{\partial\mathbf{v}} = \frac{\partial\dot{\rho}}{\partial\mathbf{v}_{RX}}\ \frac{\partial\mathbf{v}_{RX}}{\partial\mathbf{v}} = -\frac{\partial\rho}{\partial\mathbf{r}} \tag{4.39}$$

$$\begin{gathered}\frac{\partial\dot{\rho}}{\partial\boldsymbol{\theta}^{B}} = \frac{\partial\dot{\rho}}{\partial\mathbf{v}_{RX}}\ \frac{\partial\mathbf{v}_{RX}}{\partial\boldsymbol{\theta}^{B}} + \frac{\partial\dot{\rho}}{\partial\boldsymbol{\rho}}\ \frac{\partial\boldsymbol{\rho}}{\partial\boldsymbol{\theta}^{B}} = \\ -\frac{\partial\rho}{\partial\mathbf{r}}\ (\mathbf{R}_{B}^{MCF}[(\boldsymbol{\omega}_{I,B}^{B} \times \boldsymbol{\ell}_{RX}^{B})\times] - [\boldsymbol{\omega}_{I,M}^{M}\times]\ \mathbf{R}_{B}^{MCF}[\boldsymbol{\ell}_{RX}^{B}\times]) + \frac{\partial\dot{\rho}}{\partial\boldsymbol{\rho}}\ \frac{\partial\boldsymbol{\rho}}{\partial\boldsymbol{\theta}^{B}}\end{gathered} \tag{4.40}$$

$$\frac{\partial\dot{\rho}}{\partial\mathbf{b}_{g}^{B}} = \frac{\partial\dot{\rho}}{\partial\mathbf{v}_{RX}}\ \frac{\partial\mathbf{v}_{RX}}{\partial\mathbf{b}_{g}^{B}} = \frac{\partial\rho}{\partial\mathbf{r}}\ \mathbf{R}_{B}^{MCF}[\boldsymbol{\ell}_{RX}^{B}\times] \tag{4.41}$$

$$\frac{\partial\dot{\rho}}{\partial\mathbf{s}_{g}^{B}} = \frac{\partial\dot{\rho}}{\partial\mathbf{v}_{RX}}\ \frac{\partial\mathbf{v}_{RX}}{\partial\mathbf{s}_{g}^{B}} = \frac{\partial\dot{\rho}}{\partial\mathbf{b}_{g}^{B}}\ diag(\Delta\tilde{\boldsymbol{\Theta}}^{B})\ \frac{1}{\Delta\tau} \tag{4.42}$$

Eventually the consequent Jacobian $\mathbf{H}_{\dot{\rho}}$ and the innovation used to update the state are respectively:

$$\mathbf{H}_{\dot{\rho}} = [\ \frac{\partial\dot{\rho}}{\partial\mathbf{r}}\quad \frac{\partial\dot{\rho}}{\partial\mathbf{v}}\quad \frac{\partial\dot{\rho}}{\partial\boldsymbol{\theta}^{B}}\quad \boldsymbol{\emptyset}_{1\times6}\quad \frac{\partial\dot{\rho}}{\partial\mathbf{b}_{g}^{B}}\quad \frac{\partial\dot{\rho}}{\partial\mathbf{s}_{g}^{B}}\quad \cdots\ ] \tag{4.43}$$

$$z_{\dot{\rho}} = \delta\dot{\rho} = \tilde{\dot{\rho}} - \hat{\dot{\rho}} \tag{4.44}$$

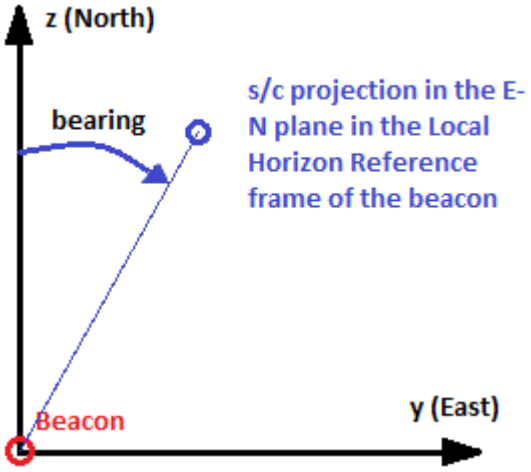

Figure 4.11: Bearing measurement definition

Bearing

The bearing is here defined as the Azimuth, i.e. the angle, positive clockwise, between the projection of the S/C position vector on the LH plane of the beacon and the North (figure 4.11). It is meant as a similar measurement to what VOR system performs on Earth. In order to compute the bearing, the position of the receiver has to be rotated in the LH frame of the beacon with respect to whom the bearing is measured.

$$\mathbf{r}_{RX}^{LH} = \mathbf{R}_{MCF}^{LH}\, \mathbf{r}_{RX} \tag{4.45}$$

It has to be noticed that, since what it is necessary for the bearing evaluation are the East and North components, i.e. the y and z components in LH frame, the use of $\mathbf{r}_{RX}^{LH}$ or $\boldsymbol{\rho}_{RX}^{LH}$ is equivalent. In the following the equations will be presented using $\mathbf{r}_{RX}^{LH}$.
In order to project the position vector in the E-N plane, the following matrix is introduced:

$$\mathbf{L} = \begin{bmatrix} 0 & 0 & 0 \\ 0 & 1 & 0 \\ 0 & 0 & 1 \end{bmatrix} \tag{4.46}$$

Having introduced this matrix, the bearing can be computed as the arccosine of:

$$X = \mathbf{n}^T \frac{\mathbf{L}\, \mathbf{r}_{RX}^{LH}}{\|\mathbf{L}\, \mathbf{r}_{RX}^{LH}\|} \tag{4.47}$$

where $\mathbf{n}$ is the unit vector parallel to E-N plane and heading to the north. Being the arccosine function defined in the interval [0,π], the following relations are introduced in order to have the bearing observation equation defined in the interval [0,2π]:

$$y_{RX}^{LH} \geq 0 \implies b = b(\mathbf{r}, \boldsymbol{\theta}^B) = \arccos(X) + w_b \tag{4.48}$$

$$y_{RX}^{LH} < 0 \implies b = b(\mathbf{r}, \boldsymbol{\theta}^B) = 2\pi - \arccos(X) + w_b \tag{4.49}$$

At this stage, as for the range and range-rate, the partial derivatives needed by the eEKF are evaluated.

$$\begin{gathered} \frac{\partial b}{\partial \mathbf{r}} = \frac{\partial b}{\partial X} \frac{\partial X}{\partial \mathbf{r}_{RX}^{LH}} \frac{\partial \mathbf{r}_{RX}^{LH}}{\partial \mathbf{r}} = \\ \mp \frac{1}{\sqrt{1-X^2}} \mathbf{n}^T \left(\frac{1}{\|\mathbf{L}\ \mathbf{r}_{RX}^{LH}\|} \mathbf{I} - \frac{(\mathbf{L}\ \mathbf{r}_{RX}^{LH})(\mathbf{L}\ \mathbf{r}_{RX}^{LH})^T}{\|\mathbf{L}\ \mathbf{r}_{RX}^{LH}\|^3} \right) \mathbf{R}_{MCF}^{LH} \end{gathered} \tag{4.50}$$

$$\frac{\partial b}{\partial \boldsymbol{\theta}^B} = \frac{\partial b}{\partial X} \frac{\partial X}{\partial \mathbf{r}_{RX}^{LH}} \frac{\partial \mathbf{r}_{RX}^{LH}}{\partial \boldsymbol{\theta}^B} = \frac{\partial b}{\partial \mathbf{r}} \mathbf{R}_B^{MCF} \left[\boldsymbol{\ell}_{RX}^B \times \right] \tag{4.51}$$

In equation (4.50) the negative or positive sign is respectively related to the application of equations (4.48) or (4.49).
Eventually, the $\mathbf{H}$ matrix and the innovation are:

$$\mathbf{H}_b = \left[\begin{array}{cccc} \dfrac{\partial b}{\partial \mathbf{r}} & \boldsymbol{\emptyset}_{1\times 3} & \dfrac{\partial b}{\partial \boldsymbol{\theta}^B} & \cdots \end{array} \right] \tag{4.52}$$

$$z_b = \delta b = \tilde{b} - \hat{b} \tag{4.53}$$

Simplified Models

Under the assumption of neglecting the lever arm between IMU and receiver ($\boldsymbol{\ell}_{RX}^B = \mathbf{0}$), the measurement equations and especially the Jacobians become simpler.
In particular, as far as the range is concerned, the equations reduce to:

$$\rho = \|\mathbf{r} - \mathbf{r}_{BC}\| \tag{4.54}$$

$$\frac{\partial \rho}{\partial \mathbf{r}} = \frac{\mathbf{r} - \mathbf{r}_{BC}}{\rho} \tag{4.55}$$

For the range-rate equations become:

$$\dot{\rho} = -\frac{\mathbf{v} \cdot (\mathbf{r} - \mathbf{r}_{BC})}{\|\mathbf{r} - \mathbf{r}_{BC}\|} \tag{4.56}$$

$$\frac{\partial \dot{\rho}}{\partial \mathbf{r}} = -\frac{\mathbf{v}}{\rho} + \frac{\mathbf{v} \cdot (\mathbf{r} - \mathbf{r}_{BC})}{\rho^2} \frac{\partial \rho}{\partial \mathbf{r}} \tag{4.57}$$

$$\frac{\partial \dot{\rho}}{\partial \mathbf{v}} = -\frac{\partial \rho}{\partial \mathbf{r}} \tag{4.58}$$

Eventually for the bearing it is also possible to use the arctangent, for which it is available in the simplified case an easy expression of the partial derivatives. It has then the advantage of being defined in the interval $[-\pi,\pi]$ ("atan2" function). The bearing observation model therefore can be reduced to:

$$b = \arctan(\frac{y^{LH}}{z^{LH}}) \tag{4.59}$$

$$\mathbf{r}^{LH} = \mathbf{R}_{MCF}^{LH}\, \mathbf{r} = \left\{ \begin{array}{c} \cdots \\ -\sin\lambda_E\, x + \cos\lambda_E\, y \\ -\sin\phi\cos\lambda_E\, x - \sin\phi\sin\lambda_E\, y + cos\phi\, z \end{array} \right\} \tag{4.60}$$

$$\frac{\partial b}{\partial \mathbf{r}} = \frac{1}{1+X^2}\, \frac{1}{(z^{LH})^2} \left\{ \begin{array}{c} -\sin\lambda_E\, z^{LH} + \sin phi \cos\lambda_E\, y^{LH} \\ \cos\lambda_E\, z^{LH} + \sin phi \sin\lambda_E\, y^{LH} \\ -\cos\phi\, y^{LH} \end{array} \right\} \tag{4.61}$$

where $X = \dfrac{y^{LH}}{z^{LH}}$.

With the aforementioned assumption the dependency on the attitude is everywhere dropped, leading to a much simpler expression of the derivatives needed by the EKF.
Throughout the analyses performed in this study, it has been noticed, as it is expected, that there is not much influence in the navigation performance if the real position of the receiver is considered or not. However, in order not to lose generality, in this study it has been considered $\boldsymbol{\ell}_{RX}^{B} \neq \mathbf{0}$.

4.6.2 Visibility Model

The measurements from a beacon are available when the lander is inside the visibility window.

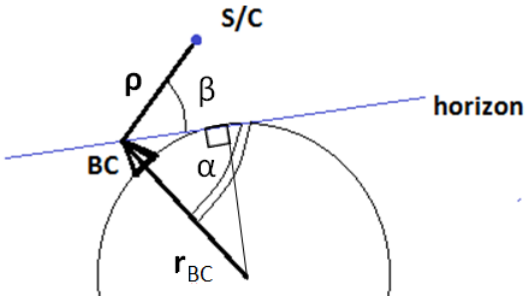

Figure 4.12: Visibility model

With reference to figure 4.12, the condition for the visibility is:

$$\arccos\left(-\frac{\boldsymbol{\rho}^T\ \mathbf{r}_{BC}}{\|\boldsymbol{\rho}\|\ \|\mathbf{r}_{BC}\|}\right) - \alpha \geq \beta_{LIM} \tag{4.62}$$

where,

$$\alpha = \arcsin\left(\frac{R_{LS}}{\|\mathbf{r}_{BC}\|}\right) \tag{4.63}$$

Being the real morphology of the surface unknown, it has been assumed a minimum elevation angle (β_{LIM}) of 10 degrees with respect to the horizon in order to consider the lander visible from the beacon and the update valid.

4.7 Error Models

In this section the errors models for the measurements in the navigation system will be defined.

4.7.1 Baseline Sensor's Suite

First, the error parameters for the baseline sensor's suite are presented.
In table 4.2, the parameters for the IMU used in the simulations are reported.
In table 4.3 the noise figures associated to the rest of the baseline sensor suite are listed.
Studies are on-going to characterize the noise associated to crater navigation: for this work, as preliminary approach, the noise related to the position determination of the CN has been set to be normally distributed with standard

deviation proportional to the slant-range, i.e. decreasing with the altitude. Both the error in the CN and FT algorithm were tuned from comparison of the obtained navigation solution with the results from ATON, in which a more realistic model for the CN is used.

Table 4.2: IMU parameters (1-σ)

Parameter	Value	Units
Accelerometer		
- Bias level	25.5	mg
- Bias stability	1.5	mg
- Random walk	0.0106	$\mathrm{m/s}/\sqrt{hr}$
- Scale factor error	$3.33 \cdot 10^{-4}$	-
- Scale factor error stability	$1.67 \cdot 10^{-6}$	-
Gyroscope		
- Bias level	825	deg/hr
- Bias stability	4	deg/hr
- Random walk	0.9	$\mathrm{deg}/\sqrt{hr}$
- Scale factor error	$3.33 \cdot 10^{-5}$	-
- Scale factor error stability	10^{-6}	-

Table 4.3: STR, CN, FT, LA error parameters (1-σ)

Parameter	Value	Units
STR accuracy	9.1	arcsec
CN accuracy	3 % of slant-range	m
FT accuracy	1	pixel
LA accuracy	0.04	m

4.7.2 Beacon

In table 4.4 the noise figures associated to the measurements from the beacons, used in this work, are reported. First of all, the main driver has been to be conservative in their selection.
The chosen level of the range noise is comparable with the user equivalent range error (UERE) for the GPS C/A code with no selective availability.

Table 4.4: Beacon measurements error parameters (1-σ)

Parameter	Value	Units
Range	10	m
Range-rate	0.1	m/s
Bearing	1.4	deg

Dominant error in UERE is related to the atmosphere as it can be seen from table 4.5. Since the lunar atmosphere is negligible it could be expected then that the level of noise experienced in the scenario of this work is less.

Table 4.5: Standard error model - L1 C/A (no SA), taken from [22]

	One-sigma error, m			
Error source	Bias	Random	Total	DGPS
Ephemeris data	2.1	0.0	2.1	0.0
Satellite clock	2.0	0.7	2.1	0.0
Ionosphere	4.0	0.5	4.0	0.4
Troposphere	0.5	0.5	0.7	0.2
Multipath	1.0	1.0	1.4	1.4
Receiver measurement	0.5	0.2	0.5	0.5
User equivalent range error (UERE), rms*	5.1	1.4	5.3	1.6
Filtered UERE, rms	5.1	0.4	5.1	1.5
Vertical one-sigma errors--VDOP= 2.5			**12.8**	**3.9**
Horizontal one-sigma errors--HDOP= 2.0			**10.2**	**3.1**

Moreover, studies about relative navigation system for space applications using GPS receivers have shown r.m.s. errors in the relative state vector components of typically 0.5 m and 1 cm/s in hardware-in-the-loop simulations [23]. Eventually, with the aim of not underestimating the errors and considering all the uncertainties in the observation models used, the noise figures selected for range and range-rate can be considered a good compromise.
Taking the bearing into account, the literature concerning VOR navigation system claims it is not a precision aid. It is reported a 2-σ predictable accuracy of 1.4 deg although it seems that seldom worst case errors of around $\pm$4-5 deg are possible [24]. In this study, for similar considerations regarding the choice of range and range-rate noise, it has been decided to use the value reported in table 4.4 for the bearing measurement noise.

CHAPTER 5

Analyses and Results

5.1 Simulation Overview

The results that will be later presented in this chapter are the outcomes of Monte Carlo analyses, where the noise histories on the measurements from the various sensors in the SINPLEX sensor's suite, together with the ones coming from the beacons, are changing in each simulation (i.e. different seeds in the random normal numbers generators are used). The number of data sets per each Monte Carlo has been chosen to be 100, which is a compromise between high enough number of sets and affordable computational time.
First of all a pool of 100 simulations without the beacon's updates has been generated, in order to have reference navigation solutions for further analyses concerning the use of the beacons. For each simulation, first, the results of the integration of the true dynamics (which is the same for each simulation, being the landing trajectory fixed) is used to generate the sensor's measurements. This part of the simulation is performed in a dedicated Simulink model which contains the truth model and the sensor's models. Then, these results are processed by the navigation algorithm, which is implemented in a Matlab script, in order to evaluate the navigation solution (figure 5.1).
At the end of the Monte Carlo analysis, 100 navigation solutions are available. From this set a worst case navigation solution is extracted. In fact, it has been considered appropriate to perform trade-offs analyses on worst case navigation solutions, comparing them to 3-σ requirements. In detail, this worst case is evaluated extracting the maximum absolute navigation er-

ror per each time instant of the navigation solution, along the whole set of simulations available ($N_{MC} = 100$).

$$\Delta E_i = max(|\Delta e_i|)_{j=1}^{N_{MC}} \tag{5.1}$$

where Δe_i is the error between the result of the navigation solution at a given time instant and the truth. This error is, for example, the position error in the DR. Being the navigation solution available at MR, with a different time step with respect to the integrated truth (more refined), an interpolation is performed in order to compute the errors at consistent times. It has been also evaluated the variance and compared it with the covariance analysis, in order to check if the covariances set in the EKF, for the SINPLEX sensor's suite, were appropriately tuned.

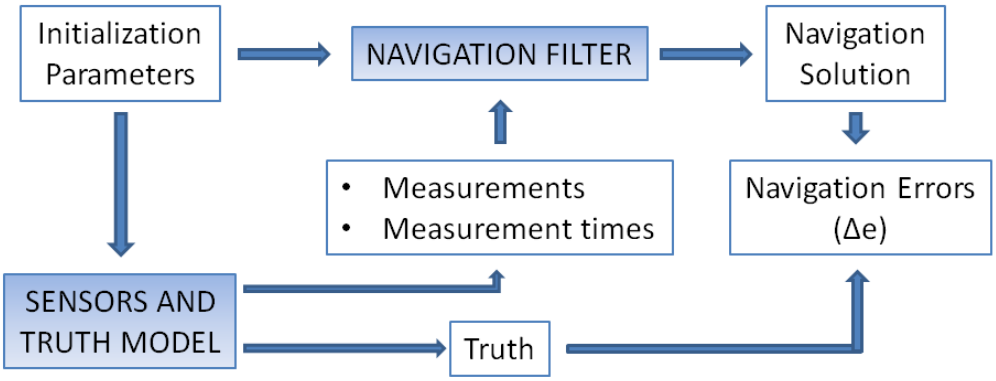

Figure 5.1: Simulation scheme

For the analyses involving the beacons, the same process just described has been applied, but, in order to speed up the analyses, a reduced Simulink model has been used exclusively for the evaluation of the beacon measurements, while the navigation algorithm is performed starting from the first valid beacon update. In practice, the already available Monte Carlo data sets from the reference simulation (without beacon) is used as baseline.
The navigation solutions for the last intervals, the ones influenced by the beacons, can then be merged with the ones before the beacons start updating (figure 5.2).
These operations make the computational time of each simulation with beacon to be of about 30-35 s, i.e. about 10% of the time that it is required by a complete simulation within the Monte Carlo, as illustrated before (figure 5.1).

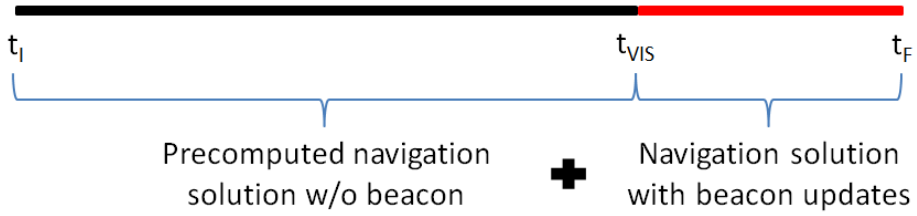

Figure 5.2: Navigation solution evaluation scheme for beacon

This resulted in a computational time of about 1 hour for a complete Monte Carlo simulation for a given beacon configuration, practically not sensitive to the number of beacon in the analysis, since the largest computational effort is taken by the strap-down integration and filter propagation, which respectively take place at 100 and 10 times the frequency the beacons and the other sensor's in SINPLEX are updating.
The output of each Monte Carlo analysis for a given beacon configuration under study, was then processed through equation (5.1), in the same way the baseline worst case solution without beacon has been obtained.

5.2 Cost Functions Definition

5.2.1 Reference Error Profile

The trade-offs presented in this chapter require the definition of some parameters useful to compare a configuration to another and to the baseline, in order to be able to understand which are the best options.
First, reference navigation errors, both for the position and the velocity have been generated. This correspond to a 3-σ desirable navigation error that could guarantee the success of the landing.

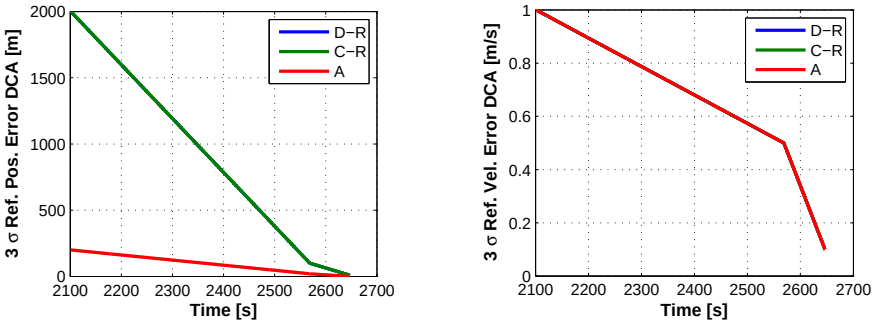

(a) Position Error (b) Velocity Error

Figure 5.3: Reference error profile

The error profile in figure 5.3 have been extrapolated by comparison of some relevant references lunar landing navigation requirements (e.g. SINPLEX, ATON, ALHAT). The profiles start from the PDI, although the navigation solution is available from the beginning of the DO: this both because the PD is the most relevant part of the landing, where higher accuracy is searched, and because the first valid beacon updates are more or less available from the middle of the PD, when beacons are near to the LS.
To generate the profiles in figure 5.3 errors at given time instants, corresponding to relevant landing phases have been imposed. The values in detail can be read in table 5.1.

Table 5.1: 3-σ reference error values

	PDI		**HG**		**Landing**	
	$\Delta\bar{E}_r[m]$	$\Delta\bar{E}_v[m/s]$	$\Delta\bar{E}_r[m]$	$\Delta\bar{E}_v[m/s]$	$\Delta\bar{E}_r[m]$	$\Delta\bar{E}_v[m/s]$
DR	2000	1	100	0.5	10	0.1
CR	2000	1	100	0.5	10	0.1
A	200	1	20	0.5	0.5	0.1

It can be noticed that higher accuracy is requested as the landing site is approached. The velocity profiles are the same for the down-range, cross-range and altitude, while the position error in the altitude has to be generally one order of magnitude smaller than in the other components. The 3-σ position errors imposed at landing are challenging for current technology, but in this study it was considered as mandatory if a precise landing relatively to a well defined landing site is wanted.

5.2.2 Cost Functions

The general form for the cost functions used in the upcoming analyses is:

$$J = \frac{1}{N}\sum_{i=I_0}^{I_F}\left(\frac{\Delta E_i}{\Delta\bar{E}_i}\right)^2 \tag{5.2}$$

where i is the index for the time of the navigation solutions; I_0 and I_F are respectively the initial and final time indexes corresponding to the time interval in which the cost function has to be evaluated; N is eventually the number of samples in the interval.
Equation (5.2) is basically similar to an integral of the worst case navigation solution errors (equation (5.1)), weighted with the reference errors defined in

the previous subsection. The term inside the summation is squared so that everything that exceeds the reference errors is weighted more.
A number of 4 intervals have been defined, in which to evaluate the cost functions. The main interval goes from the first valid beacon update (called t_{VIS}) to the landing (cost function class J). This interval is meant to study the performance for the whole period in which the beacon measurements are impacting on the navigation solution.
The other 3 are sub-intervals of the main one, and they are needed in order to enter deeper in the evaluation of the performance of a given configuration: this way it is possible to see how the studied option is impacting on the different relevant phases of the landing. In particular (see also figure 5.4):

- first sub-interval, corresponding to cost function class J_1, starts at t_{VIS} and ends at t_{MID}, which is defined as the mid point between t_{VIS} and t_{HG}, i.e. the time in which s/c reaches high gate;
- second sub-interval (cost function class J_2), starts at t_{MID} and ends at t_{HG};
- third sub-interval (cost function class J_3), goes from t_{HG} to the landing.

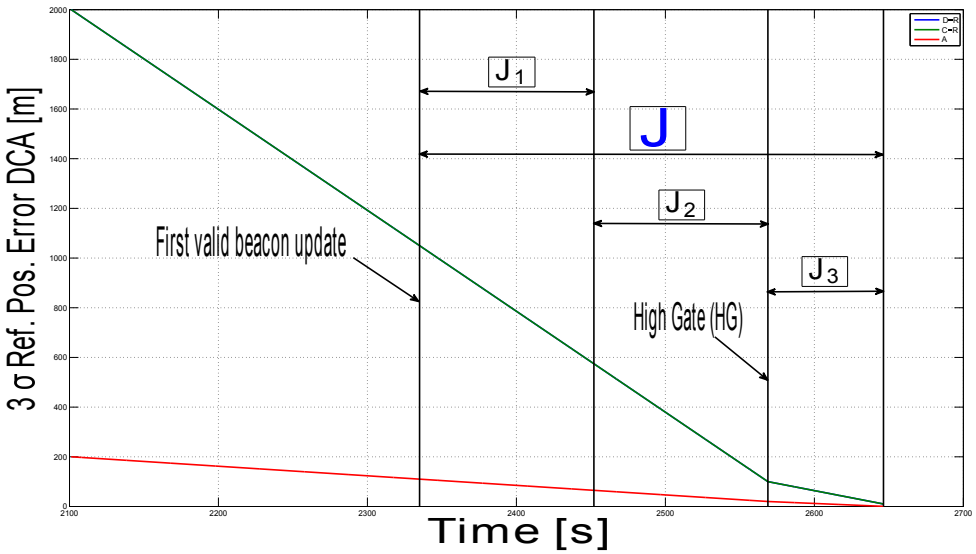

Figure 5.4: Cost function intervals

Eventually a total of 24 independent cost functions is available, i.e. 4 (classes of J) times 3 (components of DCA frame) times 2 (position and velocity errors). In table 5.2, a notation overview is reported, for the cost

function class 1, in order to make the reader to understand the notation with which analyses results will be presented.

Table 5.2: Cost function notation (example for J_1)

	DR	CR	A	Total
Position	$J_{1,r}^{DR}$	$J_{1,r}^{CR}$	$J_{1,r}^{A}$	$J_{1,r}^{tot} = J_{1,r}^{DR} + J_{1,r}^{CR} + J_{1,r}^{A}$
Velocity	$J_{1,v}^{DR}$	$J_{1,v}^{CR}$	$J_{1,v}^{A}$	$J_{1,v}^{tot} = J_{1,v}^{DR} + J_{1,v}^{CR} + J_{1,v}^{A}$

5.3 Baseline Navigation Solution

In this section the baseline worst case navigation solution is presented (figures 5.5, 5.6 and 5.7); it is the output of the Monte Carlo analysis on SINPLEX without the use of beacon updates, as already explained in section 5.1.

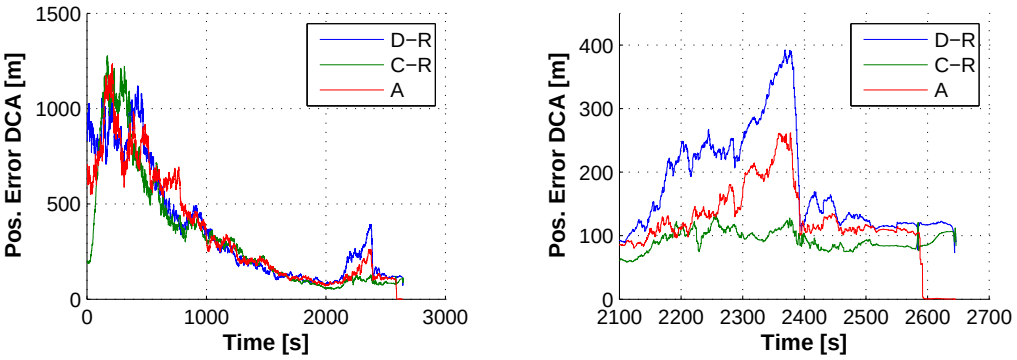

(a) Position errors

(b) PD detail

Figure 5.5: Baseline position worst case absolute errors (DCA)

It can be noticed that the navigation solution resents the high noise in the CN at the beginning of the simulation (figures 5.5a and 5.6a), when the S/C is entering in the DO. In fact, in that phase the navigation is relying only on the IMU and the CN, as far as the position and velocity determination are concerned, therefore the error is driven by this last one. As it is expected, as time goes by, the navigation solution improves, being the noise in the CN decreasing. Before PD initiate, also LA and FT are updating, since they start working from 20 km altitude. As PD starts it is possible to notice a sudden increase on the errors, especially in the velocity ones (figures 5.5b and 5.6b), due to the quick rotation of the S/C to orient the thrust [9].

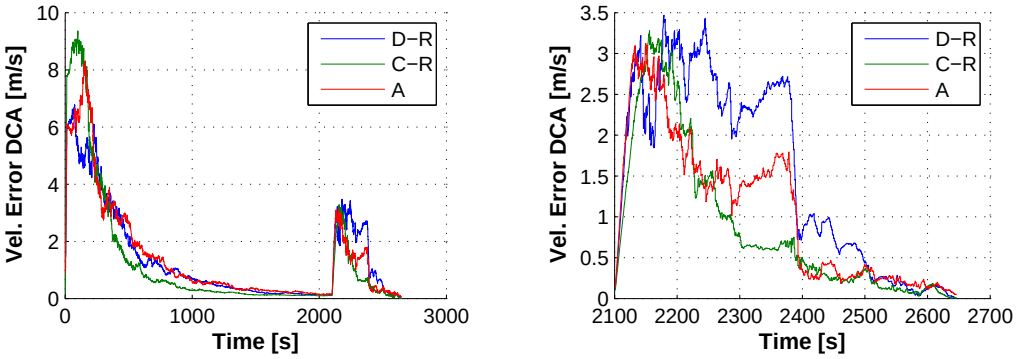

(a) Velocity errors (b) PD detail

Figure 5.6: Baseline velocity worst case absolute errors (DCA)

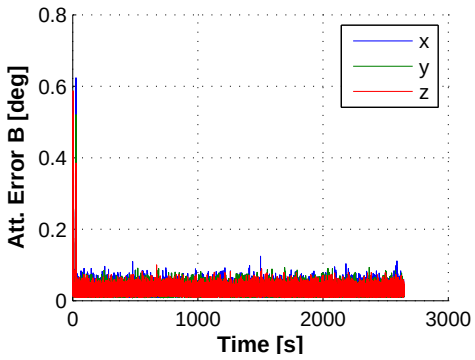

Figure 5.7: Baseline attitude worst case absolute errors (B)

In particular, the error in the CR maintains more or less constant throughout the whole PD, and also the velocity in the CR seems to be the one better determined; this is a contribute of the FT, that is sensitive to the cross-range. The errors in down-range and altitude are instead larger; in particular, for what concerns the position they reach a maximum around the middle of the PD, which corresponds more or less to the point of maximum altitude reached during PD: this larger error is probably driven by the larger noise on the CN that is experienced at that point. At the end of the power descent, when the CN is no more updating, being altitude falling below the limit of 10 km, the position error sets to values of around 100 m for all the components except the altitude, whose determination is drastically improved by the LA once the landing site is in view and the update model is switched (figure 5.5b). The velocity error, thanks to the FT, is instead approaching low values of around 0.1 m/s as the LS is reached (figure 5.6b).
Comparing figures 5.5b and 5.6b with figures 5.3, it is noticeable that the po-

sition error output of the baseline navigation is generally below the imposed values of the reference profile, except in the last phase for the DR and CR and from the middle of the PD, i.e. until the LA improves its determination, as far as the altitude is concerned. In any case the final error is much larger than what is required for a precise landing relative to a given landing site. The velocity errors instead experience a different behavior, being them larger than needed at the beginning and nice at the landing.
Eventually, the attitude is well determined throughout the whole simulation, thanks to the ST, which, as expected, keeps the attitude error rather small (figure 5.7).

5.3.1 Baseline Cost Function Evaluation

The values of the cost functions presented in 5.2.2, computed for the baseline solution, are reported in tables 5.3.

Table 5.3: Reference cost function values

(a) J

J_r^{DR}	**3.16**	J_v^{DR}	**2.73**
J_r^{CR}	**2.63**	J_v^{CR}	0.27
J_r^{A}	**7.28**	J_v^{A}	1.06
J_r^{tot}	13.07	J_v^{tot}	4.05

(b) J_1

$J_{1,r}^{DR}$	0.09	$J_{1,v}^{DR}$	**6.61**
$J_{1,r}^{CR}$	0.01	$J_{1,v}^{CR}$	0.51
$J_{1,r}^{A}$	**3.77**	$J_{1,v}^{A}$	**2.43**
$J_{1,r}^{tot}$	3.88	$J_{1,v}^{tot}$	9.55

(c) J_2

$J_{2,r}^{DR}$	0.25	$J_{2,v}^{DR}$	0.56
$J_{2,r}^{CR}$	0.12	$J_{2,v}^{CR}$	0.13
$J_{2,r}^{A}$	**9.30**	$J_{2,v}^{A}$	0.08
$J_{2,r}^{tot}$	9.68	$J_{2,v}^{tot}$	0.92

(d) J_3

$J_{3,r}^{DR}$	**12.14**	$J_{3,v}^{DR}$	0.13
$J_{3,r}^{CR}$	**10.34**	$J_{3,v}^{CR}$	0.09
$J_{3,r}^{A}$	**9.54**	$J_{3,v}^{A}$	0.26
$J_{3,r}^{tot}$	32.02	$J_{3,v}^{tot}$	0.48

Although there are no beacons updates here, being it necessary to define a t_{VIS} in order to use the equation 5.2 for J, J_1 and J_2, it has been decided to set it to the value it would have for a beacon placed exactly in the LS: this choice is related to the fact that the LS is in the center of the grid that will be later defined to study the single beacon configuration, therefore, the value of t_{VIS} available there is kind of an average[1].

[1]It has been in any case noticed, that the values of cost functions for the baseline were

From the values in table 5.3, the baseline navigation during PD is worsening its performance in positioning with respect to the required one as landing site is approached, while the opposite happens for the velocity. Values around unity or lower mean that the related error profile is good with respect to the requirement. Values exceeding unity have been highlighted in bold. As figure 5.5b and the values of $J_{3,r}$ highlight, the worst performance is achieved in the last phase of the landing, for what concerns the position.

5.4 Single Beacon with Bearing (Case B)

In this section, the trade-off analysis results on the impact of the 3 new measurements defined in section 4.6.1 from a single beacon and of its positioning are presented.

5.4.1 Test Scenario

First of all the disposition of the beacon to be tested around the LS has been taken into account.
In principle, it could be of interest to make the analysis for whichever beacon positioned on the surface, as far as it is able to provide some valid updates to the S/C, i.e., as far it is visible.
In figure 5.8 it is possible to see that the longest visibility is for a beacon placed in the LS, which is somehow expected, being the lander slower in the final phase of the PD. It is also expected that the smaller the visibility window, the smaller the impact on the navigation. It is hard then to believe that an effort to place a beacon on the lunar surface is made, if that beacon is far from the landing site, or at least from the landing trajectory; on the other hand, since when using the model presented in 4.1.4 to dispose the beacons, a regular surface is assumed (i.e. same height of LS), this hypothesis would be probably unrealistic for beacons placed too far, where the real morphology of the surface could play an important role, and the consequent results could be inaccurate. Moreover, it is clear from the previous analyses of the baseline solution (see table 5.3d) that the portion requiring more improvements is the final phase of the PD, where especially DR and CR positioning need to be better fixed.
For all these reasons and also to limit the points to analyze and the computational time, beacons too distant from the landing site have not been taken into account.
It was therefore decided to build a square grid with the LS in the middle,

not much influenced by the choice of this time, in the range of t_{VIS} applicable.

20 km wide along the North and East directions[2]. This results in having the farthest beacon at a distance of about 14.1 km from the LS.

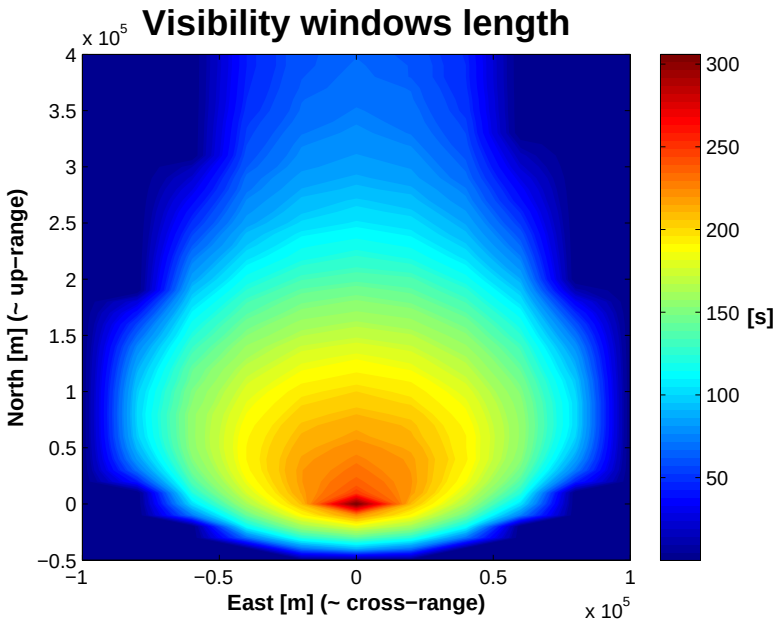

Figure 5.8: Duration of visibility windows

In figure 5.9 are shown the points in the aforementioned grid for which the Monte Carlo analysis has been performed. It can be seen that the points are uniformly distributed and the beacons in the grid are quite dense (121 points). As it can be seen, there are also 4 curves shown in the image, which represent the $\pm\ 3\ \sigma$ (in green) and the $\pm\ (2\ km + 3\ \sigma)$ (in red) boundaries. These boundaries come from NASA's recommendations about avoiding to land nearer than 2 km from objects on the surface to be protected and to make sure not to intersect the landing footprint with 3 σ uncertainty[3] (either up-range and down-range) with this 2 km avoidance circle around the object [25]. These objects in this scenario are the beacons, which could be harmed either by the plume of the lander, or by dust and particles on the soil projected at high velocity by this plume impinging on the surface, or by a potential loss of the lander during landing, which could fall near it, even destroying it [25].
However, it can be noticed from figure 5.9, that also points inside the avoid-

[2]It has to be remarked that the grid is spread over the sphere of the Moon, with the radius equal to the height of the LS; therefore 10 km North are not meant on the LH plane, but North-ward along the sphere.

[3]This value has been set to 100 m, as assumption.

ance area have been inserted in the trade-off analysis: this, both to have a more uniform data distribution for the data processing and interpolations, and for the interest in checking what happens for beacons located very near to the lander footprint.

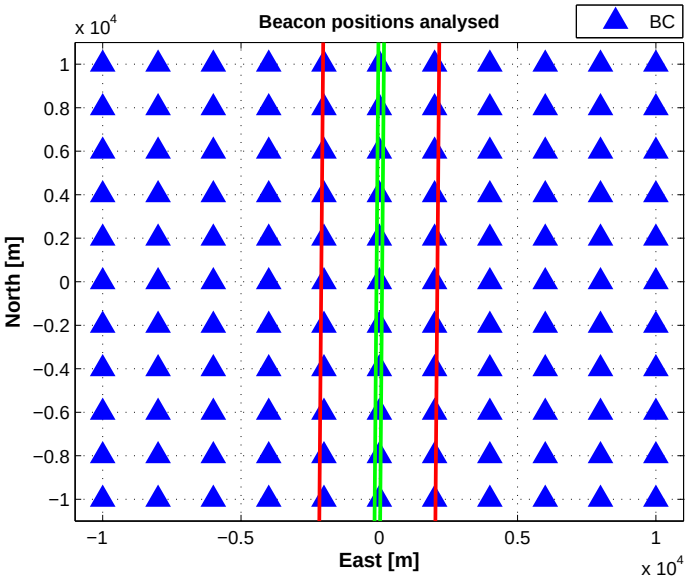

Figure 5.9: Test grid for the single beacon configuration

It is also considered of interest, as complement to the presentation of the results, to show the detail of the visibility window length for the beacons inside the grid (figure 5.10).

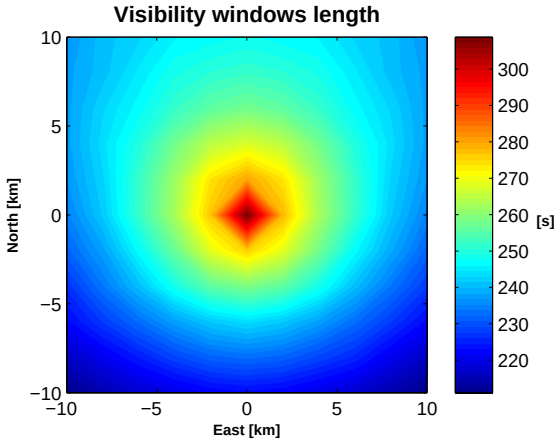

Figure 5.10: Visibility windows for the tested beacons in the grid

5.4.2 Results

In figures 5.11 to 5.20 the results of the analyses are shown. Starting with the grid of uniform distributed data, the available values have been exploited to create filled contour plots, which allow to see trends, if there are, and more in general to immediately look at what is happening inside the test grid and make comparisons. It has been decided to plot the actual value that the cost functions (figures 5.11 to 5.18) and the final errors (figures 5.19 and 5.19) assume in the grid points: these values can be read beside the color bars. On top of the color bars, instead, the corresponding reference values are reported (taken from tables 5.3 for the cost functions). This has been done in order to make confrontations with the reference case easier and more immediate; the possibility of generating contour plots scaled with the reference values has been discarded, since some results are not fully interpretable from relative plots.
The first and most important conclusion, looking at these plots, is that wherever the beacon is positioned inside the test grid, the overall impact on the navigation solution is positive, in particular for what concerns the position determination. In fact, from figures 5.11d to 5.18d, it is possible to see that, with the exception of figure 5.18d, the values of the various J^{tot} cost functions are always below the ones evaluated for the baseline. The best improvement is in the position determination during the last phase, starting from HG ($J_{3,r}$): it is possible to see from figure 5.17d that the values drop from 32 to around 0, for beacons near to the LS, but in any case never above 4.
The velocity does not resent of the same level of improvement, which is also due to the fact that the original sensor suite is already performing well with respect to the defined error profile in figure 5.3b. This is true especially for the CR component in the phases before the S/C approaches HG; looking at figures 5.14b and 5.16b the beacons are even worsening the performance when located in some areas. The fact that in $J_{1,v}$ and $J_{2,v}$ the performance is somewhere decreased in CR component could be due to the larger impact of the bearing noise on the state estimation when S/C is further from the BC. To confirm this, looking at 5.18b, i.e. when S/C is near to the beacon, the deterioration is no more detectable. However, for the last three cost functions examined, the values on the corresponding color bars show both that the range of variation is very limited and that the maximum value is relatively low, compared to the one reached for the DR and altitude components (see e.g. figures 5.14a, 5.14c, 5.16a and 5.16c).
Figure 5.18c shows that in the final part of the PD the beacon is worsening that performance, unless it is placed in proximity of the LS for example; the fact is that the laser altimeter there is already doing a very nice job in keep-

ing the error small, and the beacon measurements are noisier than LA ones. This is also noticeable in figures 5.19c and 5.20c: the final error in altitude is everywhere larger than the baseline, although being acceptable since always smaller than the corresponding one in the error profile from table 5.1.
Looking at figures 5.11, 5.13, 5.15 and 5.17 for the DR but especially for the A components, it is possible to see a common trend: the related cost functions assume larger values going down-range, i.e. South, which is somehow correlated with the visibility interval which naturally decreases going DR, as figure 5.10 highlights. The minimums are instead generally located along the landing ground track, a bit up-range. The trend assumed by these position cost functions related to the altitude is then reflected in the J^{tot}'s ones, being the absolute values larger than in the DR and CR components, which is a direct consequence of the fact that the requirements in altitude errors are one order of magnitude more accurate (see table 5.1). What said is especially valid for figure 5.15, where the baseline altitude errors are exceeding the required, and the beacon is reducing them. An exception is instead noticeable in figure 5.17, where instead the larger contribution is from the CR component (figure 5.17b); but also in this case the aforementioned trend can be detected.
As far as the velocity is concerned, having an overall look at figures 5.12, 5.14, 5.16 and 5.18, it is difficult to detect trends, with the exception of figure 5.18c. The range of variation inside the grid is limited, as already noticed, therefore the noisy aspect of some contour plots could be correlated with the Monte Carlo analyses performed, i.e. it can happen to have some outlier at some spots processing through equation (5.1). It is possible that an increase in the number of simulation inside each Monte Carlo would smooth these contours.
It was somehow then expected to find a symmetry with respect to the North axis in the contour plots, since the landing trajectory is substantially coming from North, from the perspective of an observer in the LS. This was also considered during the definition of the test grid, i.e. whether it would have been the case to assume symmetry in the impact of beacons located East or West. Apparently, looking throughout the figures, there is not symmetry in the performance underlined by some cost functions, in particular the ones related to the CR, especially when the S/C is still outside the grid (J_1 and J_2), since in J_3 it can be noticed that there is substantially symmetry. It seems that especially for CR, e.g. figure 5.13b, 5.14b, 5.16b (but see also figure 5.14c for the altitude), the fact that the lander is slightly coming from East plays a role, although this has to be considered together with the limited range of variation above mentioned. However, overall (look J^{tot}'s) the performance show symmetry with respect to North axis, as expected.

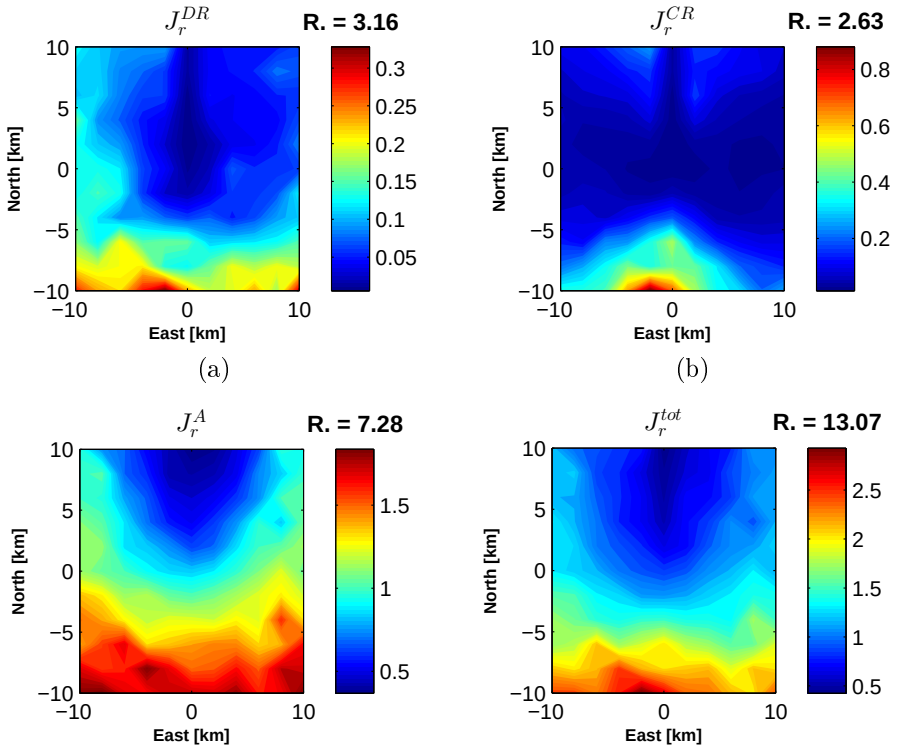

Figure 5.11: J_r cost functions

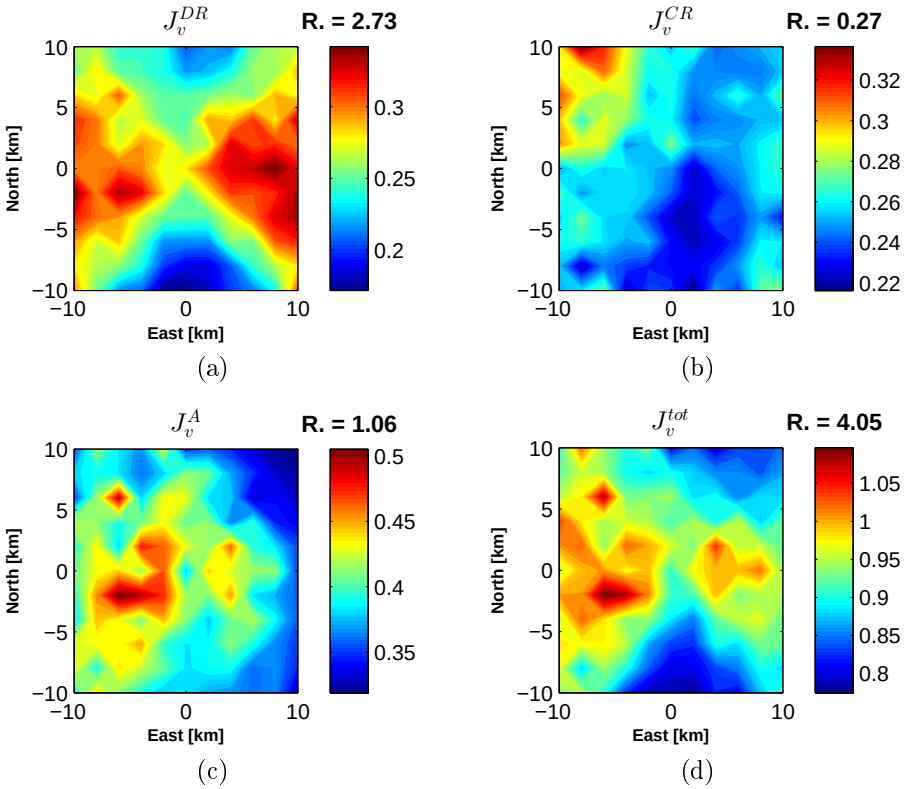

Figure 5.12: J_v cost functions

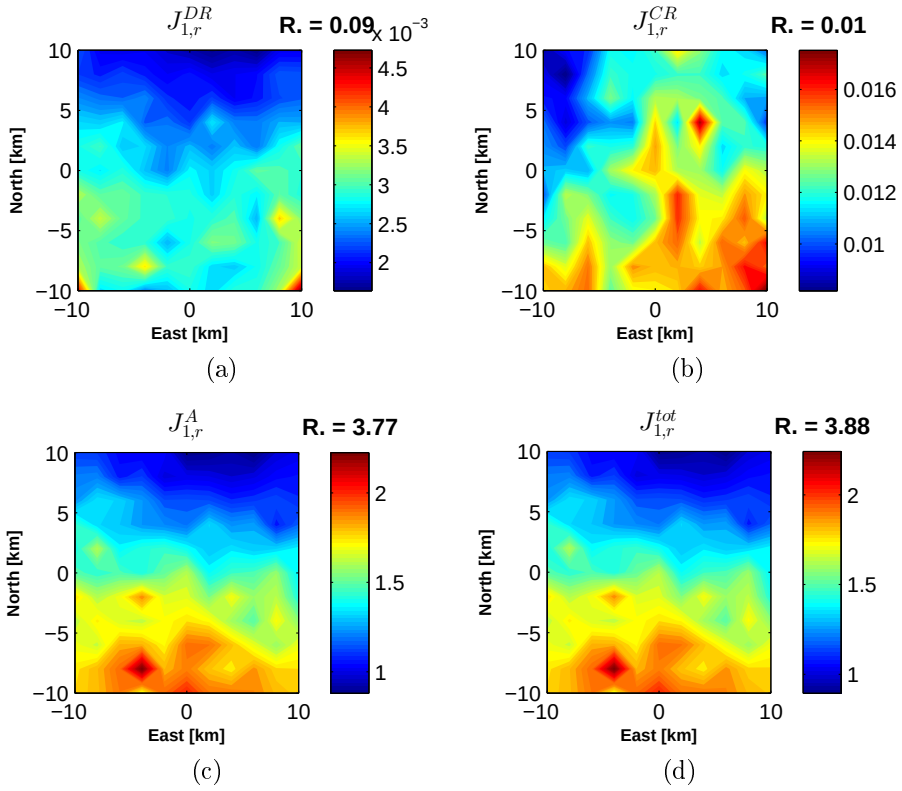

Figure 5.13: $J_{1,r}$ cost functions

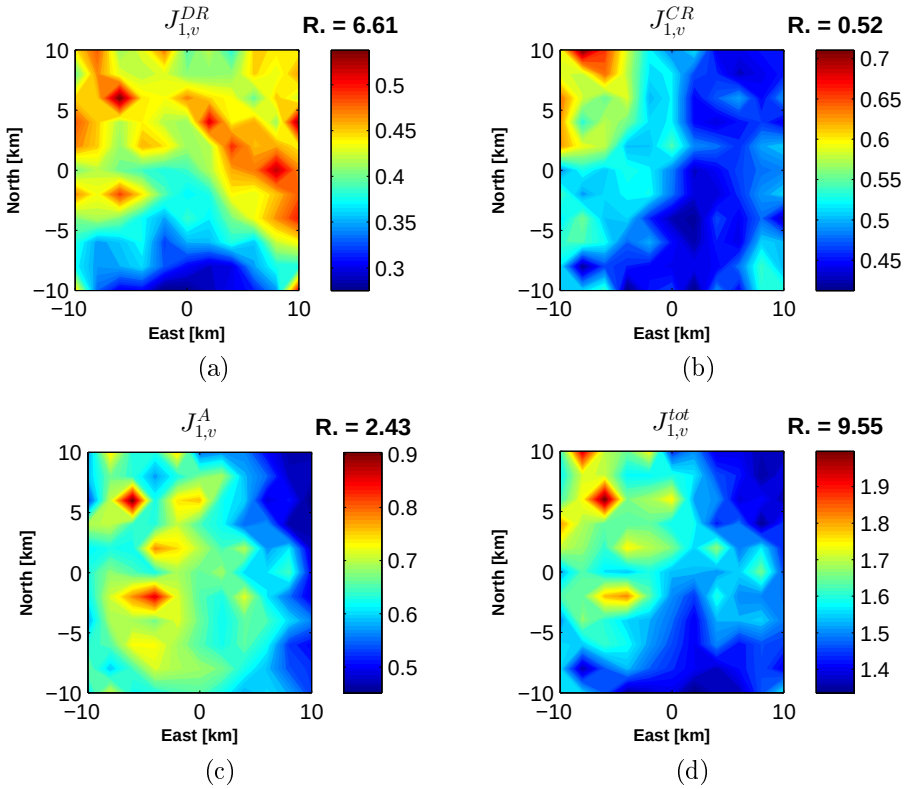

Figure 5.14: $J_{1,v}$ cost functions

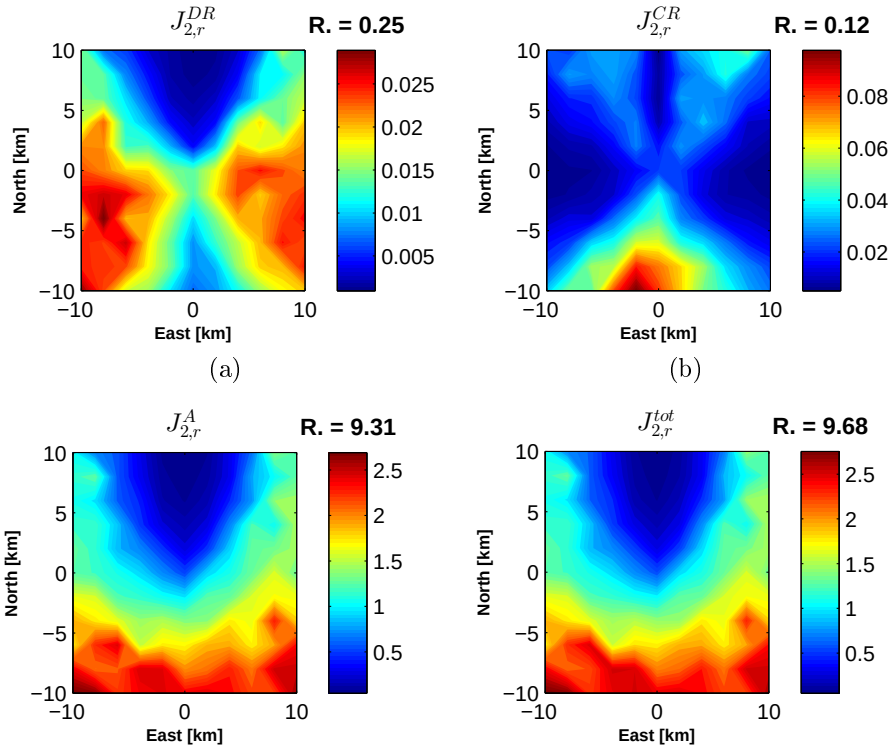

Figure 5.15: $J_{2,r}$ cost functions

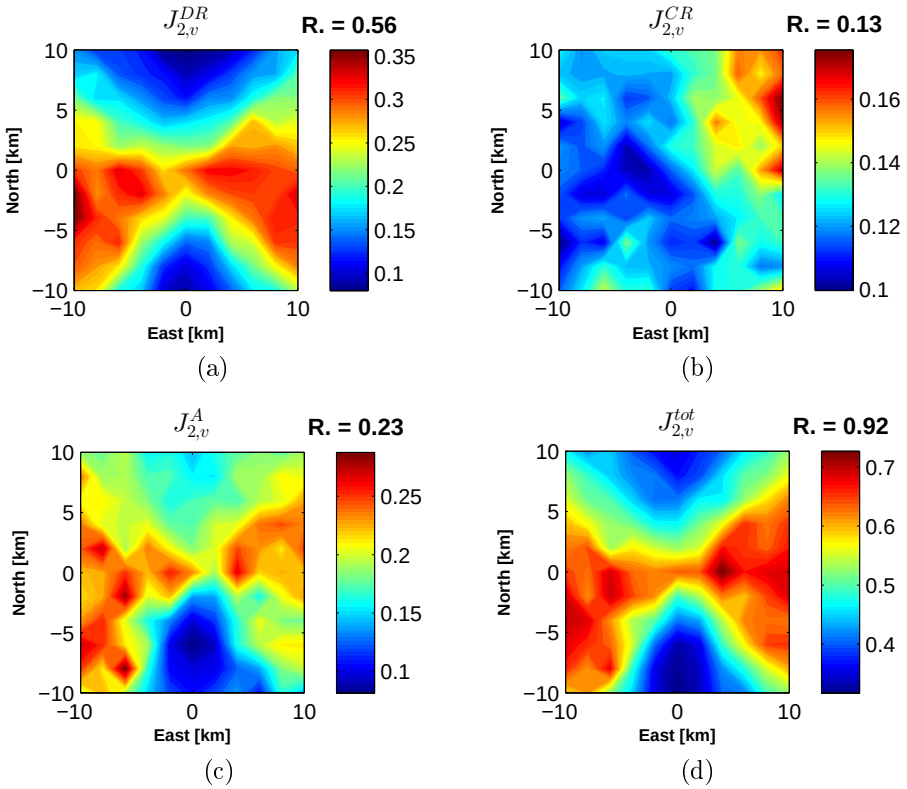

Figure 5.16: $J_{2,v}$ cost functions

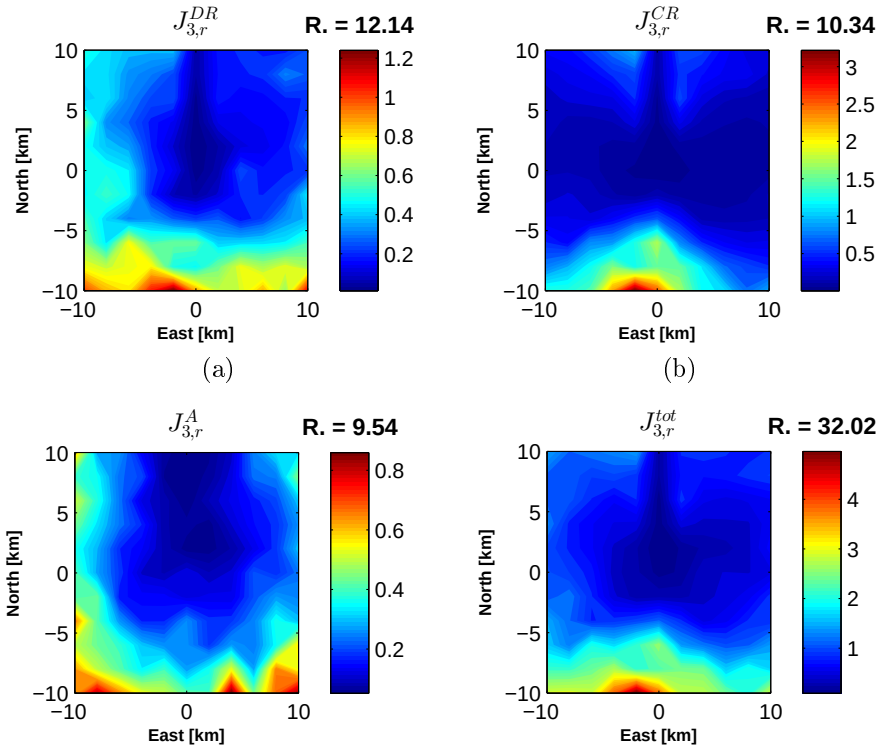

(a) (b) (c) (d)

Figure 5.17: $J_{3,r}$ cost functions

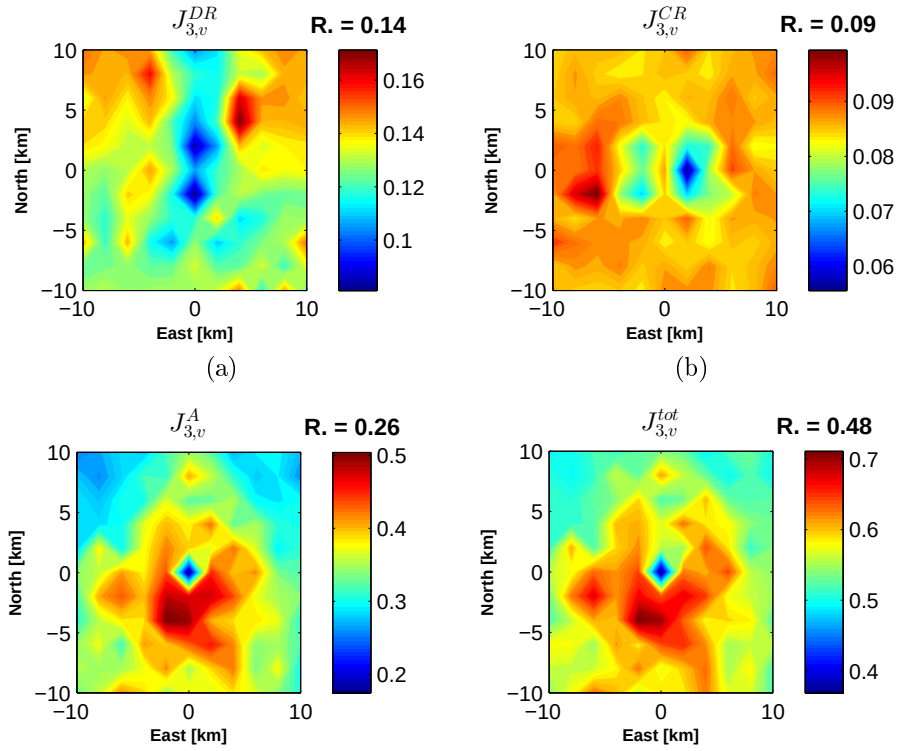

(a) (b) (c) (d)

Figure 5.18: $J_{3,v}$ cost functions

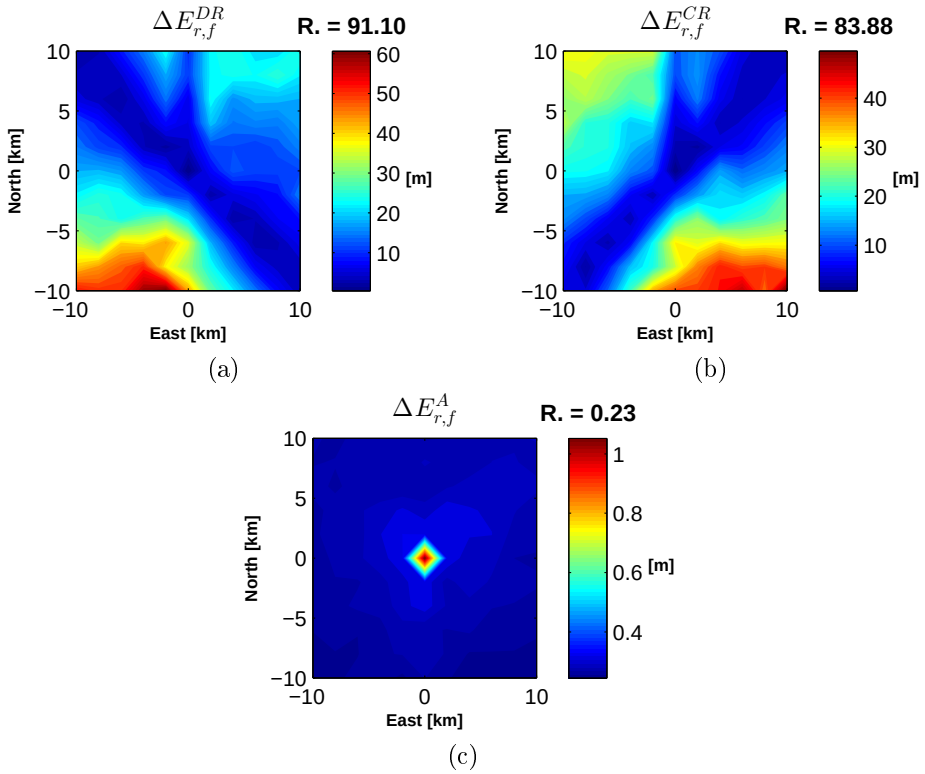

Figure 5.19: Final position errors ($\Delta E_{r,f}$)

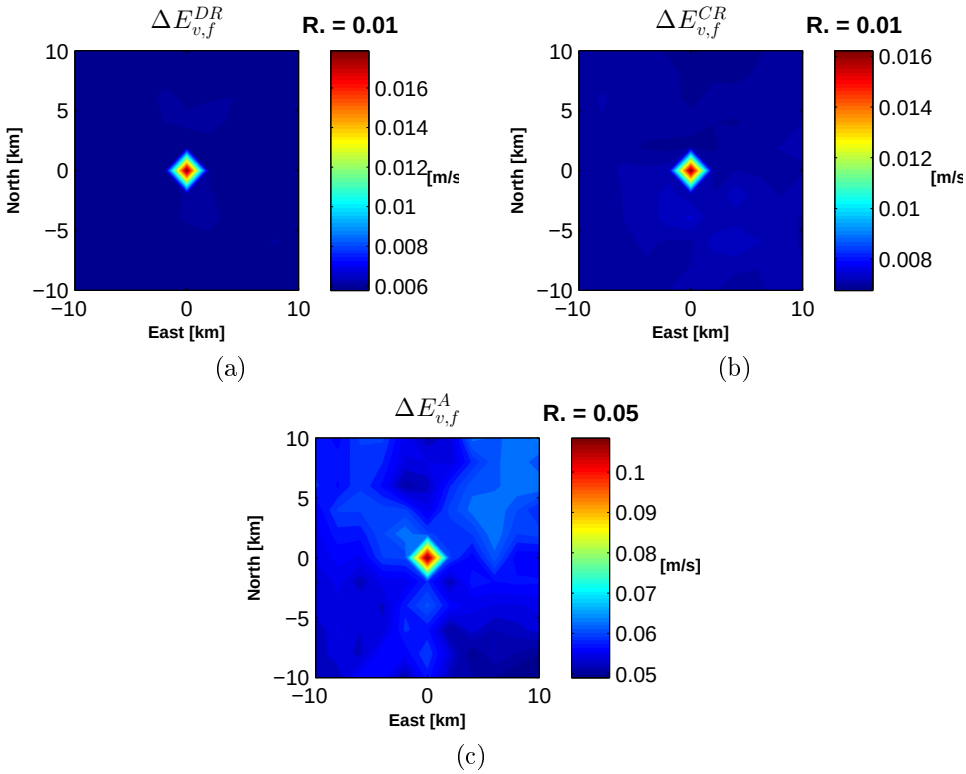

Figure 5.20: Final velocity errors ($\Delta E_{v,f}$)

There is a general improvement, as already discussed, in adding the beacon updates (case B ,table 3.4) to the baseline on-board navigation system.
An overall look into figures 5.11 to 5.20 suggests that the best area in which to locate the beacon is along the landing footprint, slightly up-range with respect to the LS. This area guarantees both general low values of cost functions and values of the final errors for position below the limit from requirements. This result is somehow expected since:

- the best configuration for the down-range improvement is to lie along the ground-track while the S/C is approaching (in this case the range and range-rate measured are more or less aligned with the DR position and velocity);

- the best configuration for the altitude is having the beacon under the S/C, since in that case the range more or less coincides with the altitude;

- the presence of the bearing measurement gives information from which cross-range can be retrieved, also while beacon is displaced in that zone, which would not be the case if only the range is measured, as it will be shown in the analysis of case A (table 3.4); in fact, looking at equation (4.59), bearing depends both on East and North component y^{LH} and z^{LH}, therefore making it possible to retrieve information both in DR and CR more or less independently on where it is placed, as it seems from figures 5.11b, 5.13b, 5.15b and 5.17b.

Unfortunately, this area falls inside the one that should be avoided for reasons presented before [25].
Taking into account the final position error in DR and CR, figures 5.19a and 5.19b prove that these worst case errors are below the required 10 m at 3-σ not everywhere in the grid, and in some areas located down and cross-range they reach values around 60 m, i.e. much higher.
In particular, it seems that these errors increase the farther the beacon is with respect to the LS, which is expected at least for a couple of reasons:

- for those beacons the visibility window does not cover the very last part of the navigation, when the S/C falls below the horizon;

- the bearing is a more precise update for the position and velocity estimation when the S/C is nearer to the beacon, as already claimed.

These errors are also small almost everywhere along the bisectors NW-SE for the DR and NE-SW for the CR: this behavior, symmetric due to the

orthogonality of the two components, is probably connected to the direction from which the LS is approached. The LS is in fact approached from more or less S/SE, at the very end of the PD since it goes a bit down-range, therefore beacons along NW-SE direction are more sensitive to the DR, while the ones perpendicular, i.e. along NE-SW are more sensitive to the CR[4], from geometric considerations.
In figures 5.22, 5.23 and 5.24 it is eventually presented a comparison between the baseline worst case navigation solution, and the one obtained with adding a beacon 3000 m East and 1000 m North of the LS (5.21). It has been chosen to present results for this configuration, since, looking at the previous contours, this position is a good trade-off between minimization of cost functions and final errors, which are 11.4 m in DR 5.5 m in CR and 0.3 m in A; moreover, this beacon falls outside of the avoidance zone, still being not so far from the landing site.

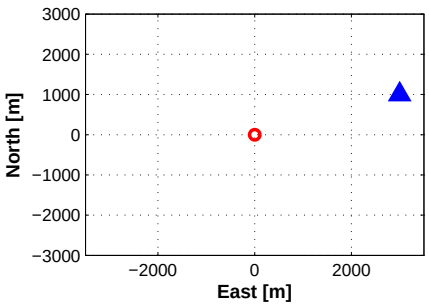

Figure 5.21: Selected positions of the single beacon

From the figures it is possible to see the impact that the addition of the updates from the beacon has on the second part of the PD:

- the most noticeable is the effect on the DR errors, which suddenly diminish as the lander gets visible from the beacon (figure 5.22b and 5.23b);

- the CR error component at the beginning seems not to be influenced by the presence of the beacon, while then it starts decreasing following more or less the same profile of the altitude error; this behavior is expected, since, as already remarked, the CR improvement is mostly given to the presence of the bearing, for a beacon placed near to the

[4]It must be remembered that the DCA frame considered is defined locally for every point on the landing trajectory, as presented in section 4.1.3.

landing footprint, and the bearing is more effective as the S/C gets nearer to the beacon;

- the errors in velocity seem to decrease with similar trend, and they look similar to the ones obtained without the use of the beacon, at least during the last 100-150 s;
- there is also a small improvement on the attitude determination, which shall be the consequence of the overall improvement in the navigation (figure 5.24b);
- it is finally worth noticing also the small increase in the position DR and CR errors that starts 30-40 seconds before the landing, which is correlated to the exit from the visibility window.

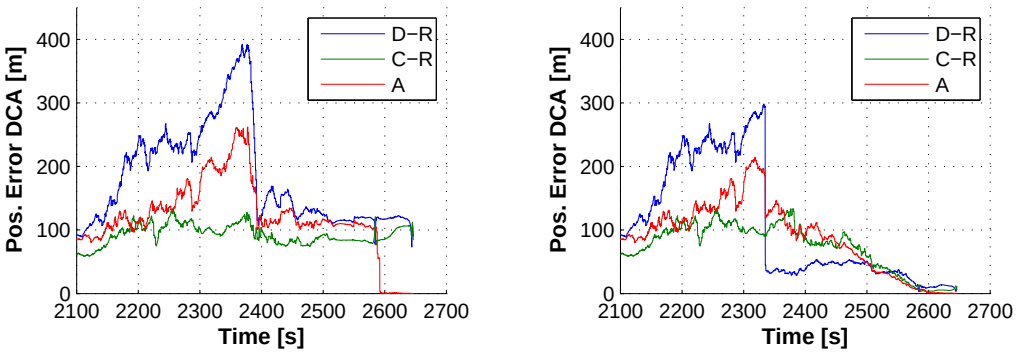

(a) Baseline

(b) Beacon, case B

Figure 5.22: Comparison of worst case position errors during PD

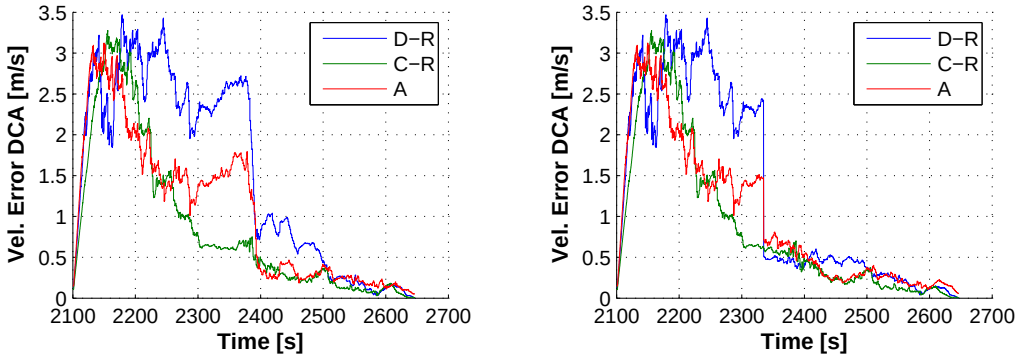

(a) Baseline (b) Beacon, case B

Figure 5.23: Comparison of worst case velocity errors during PD

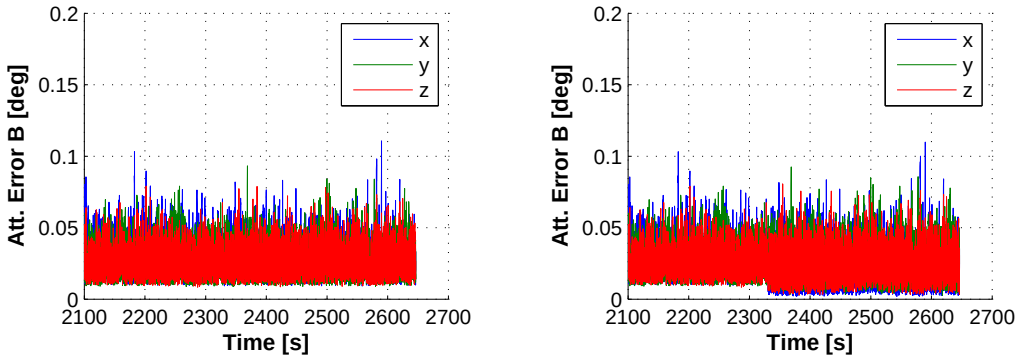

(a) Baseline (b) Beacon, case B

Figure 5.24: Comparison of worst case attitude errors during PD

5.5 Single Beacon without Bearing (Case A)

The results for the single beacon configuration without the bearing measurement are now presented. The same points in the grid in figure 5.9 have been used also in this analysis and the resulting filled contours can be seen in figure 5.25 to 5.34.
The first result is, as in the above case, that the performance is generally improved: from the figures it can be said that the impact of the beacon updates, even without the bearing measurement, is positive. From a geometrical point of view, it was expected to see that, without the bearing update, the CR determination is worse for beacons along the landing footprint. The clear trends detectable in figures 5.25b, 5.29b and 5.31b are therefore consistent with what expected: the more distant, i.e. perpendicular with respect to the ground-track, the more the CR is improved, as it can be clearly seen. In particular, when the beacon is along the footprint, the values of the cost functions under discussion are similar to the baseline, and just in figure 5.31b, when the final phase of the landing is taking place, the peak value is smaller then the baseline. These performances are quite different from what happens in presence of the bearing, which helps the CR fixing also when beacon is placed along the footprint as seen in the previous section. There seems to be an exception looking at figure 5.27b, which seems very similar to figure 5.13b; but, this must be considered together with the very limited range of variation inside the grid of the related cost function.
On the other hand, being the DR perpendicular to the CR, always from a geometrical point of view, it was foreseen to see the opposite behavior, i.e. a stronger impact on the DR position fixing for beacons along the DR. This is only detectable in figure 5.29a, i.e. for the phase of the landing when the lander is approaching HG. Figure 5.27a is then also similar to its corresponding one in case B analysis, as seen for the cross-range. During the last phase of the landing (figure 5.31a), the trend is instead analogous to the one in CR, which is probably due the fact the lander is in this case passing over beacons along footprint, which is not the best configuration to observe DR. However the peak value is here definitely smaller than the baseline, differently from the CR one which is comparable. The fact that also figure 5.25a shows this trend does not then mean that what said regarding the DR observation is not verified, but this result is given to the large weight $J_{3,r}^{DR}$ peak values have on J_r^{tot}, since $J_{1,r}^{DR}$ and $J_{2,r}^{DR}$ ones are at least 2 orders of magnitude less. Therefore, it seems that everything also for what concerns the position in DR is as expected, with the performance improved with respect to the baseline, but less than what happens in presence of the bearing measurement.
It is worth then noticing that, comparing the cost functions for the altitude

component of case A and B, these are similar, although a bit worse. It seems therefore clear that the bearing update does not influence much the determination of the altitude, which was an expected behavior, being the bearing depending on components in the LH plane of the beacon, which are just slightly influenced by the altitude.
It is clearly now confirmed, looking at figure 5.31c, that best geometric configuration for altitude determination through range measurement is when beacon is displaced under the lander: a circular pattern is detectable in this figure (as it was also in figure 5.17c), with the minimums in the center which is located where the lander more or less finds itself during the last phase of landing, when it is descending almost vertically.
Comparing the contours of the cost functions related to the velocity with and without bearing, it is possible to see that they are similar, both in the range of values and trends. It seems that the values are slightly smaller for cost functions $J_{1,v}$ and $J_{2,v}$, while slightly larger for $J_{3,v}$, although this difference is very marginal. This weak change could be related to the larger effectiveness of the bearing when nearer to the beacon. It seems clear that the bearing is not bringing any sensitive improvement on the velocity determination. As before, some areas of the test grid still have values of velocity cost functions in CR larger than the baseline (figure 5.26b, 5.28b and 5.30b): the cause, which in the analysis of case B was assumed to be the larger impact of the bearing noise when far from the beacon, could then be related to the worse performance that the range-rate update brings in some configuration with respect to what the feature tracking is already bringing. In fact, now it is at least possible to say that the bearing is not the responsible, being it absent in this last analysis. Beside this consideration, being the velocity related contours similar, same conclusions of the discussion about case B can be inferred.
Eventually, it can be recognized from figures 5.33a and 5.33b a similar trend to the one experienced with the bearing included, except that the peak values are now along the footprint. It is then possible to confirm that that trend is due to a geometric consideration about the range, as assumed in previous section. It is worth noticing that should the beacon be in the LS, then the errors in DR and CR would be small while the one in altitude would exceed the requirement from table 5.1. The peak values are higher than what available in presence of bearing, which is another indicator of the positive effect that the bearing has on the position improvement. In particular it is possible to see that for beacon placed along the footprint, the CR error is the same of the baseline, indicating that the beacon is not helping for this.

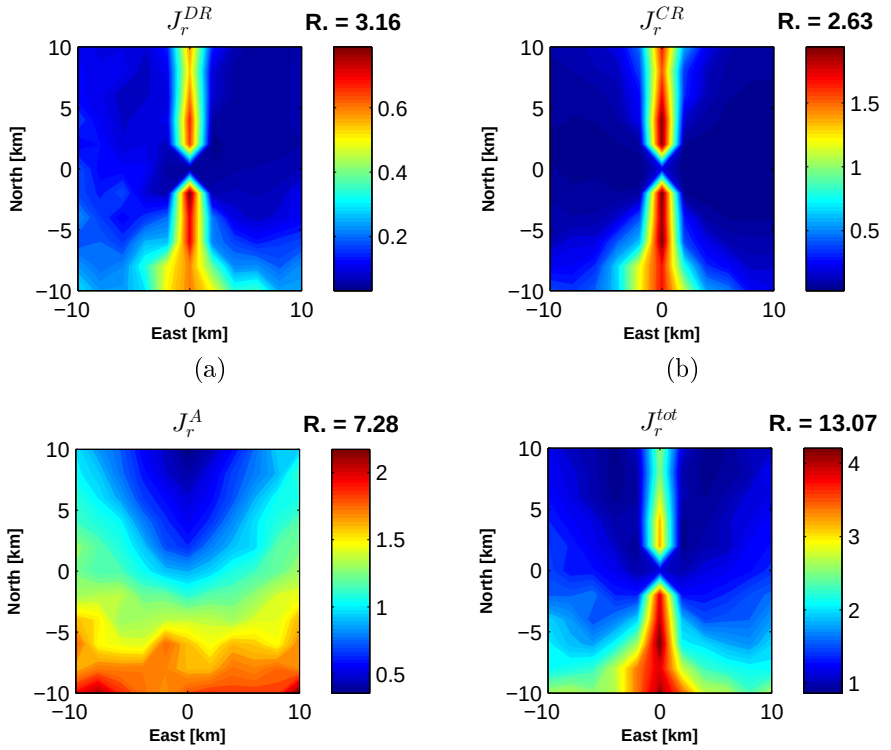

Figure 5.25: J_r cost functions

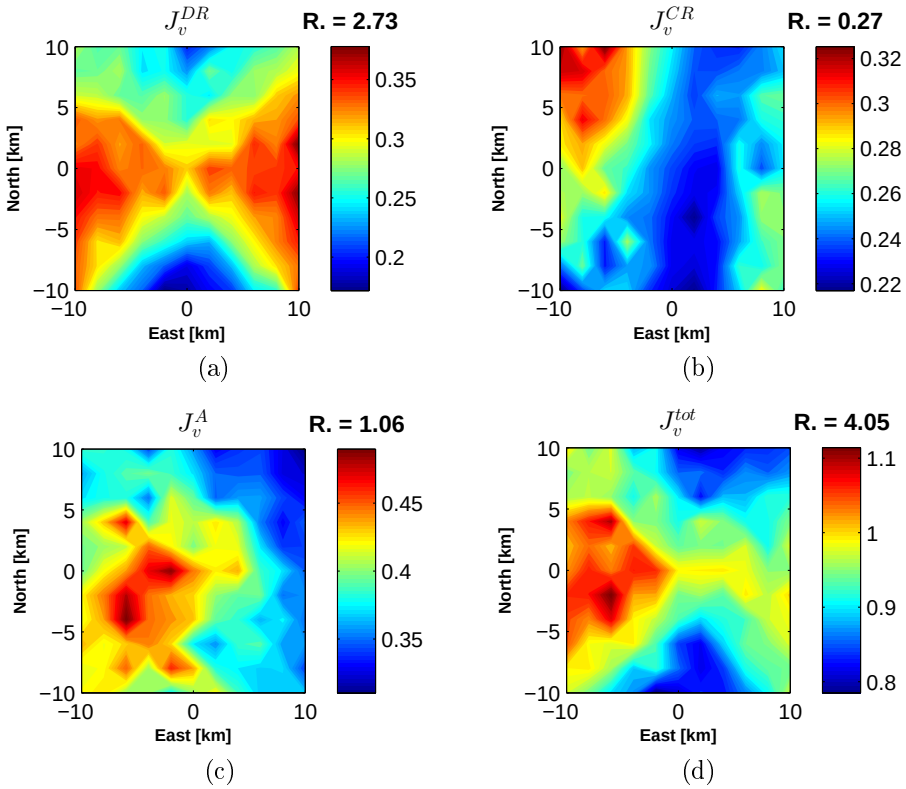

Figure 5.26: J_v cost functions

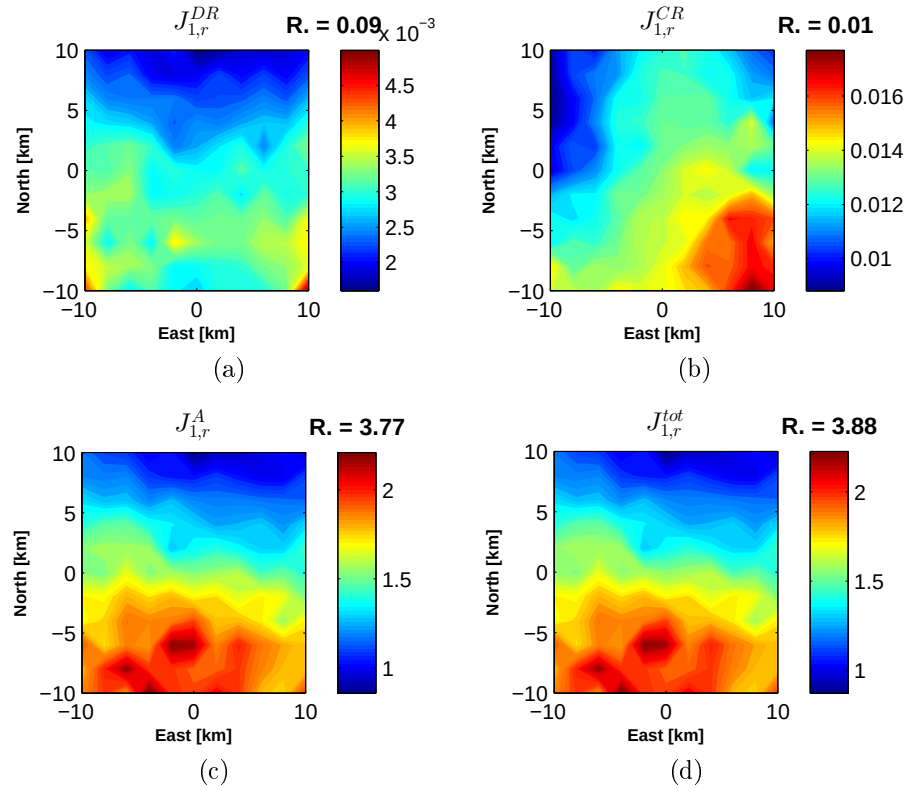

(a) (b) (c) (d)

Figure 5.27: $J_{1,r}$ cost functions

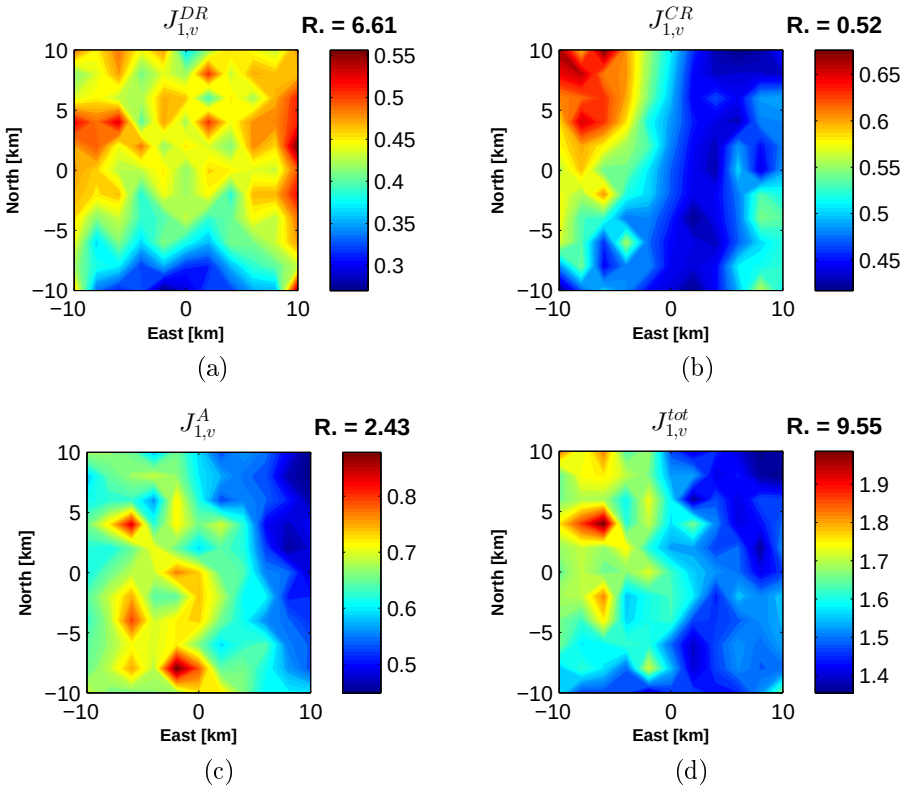

(a) (b) (c) (d)

Figure 5.28: $J_{1,v}$ cost functions

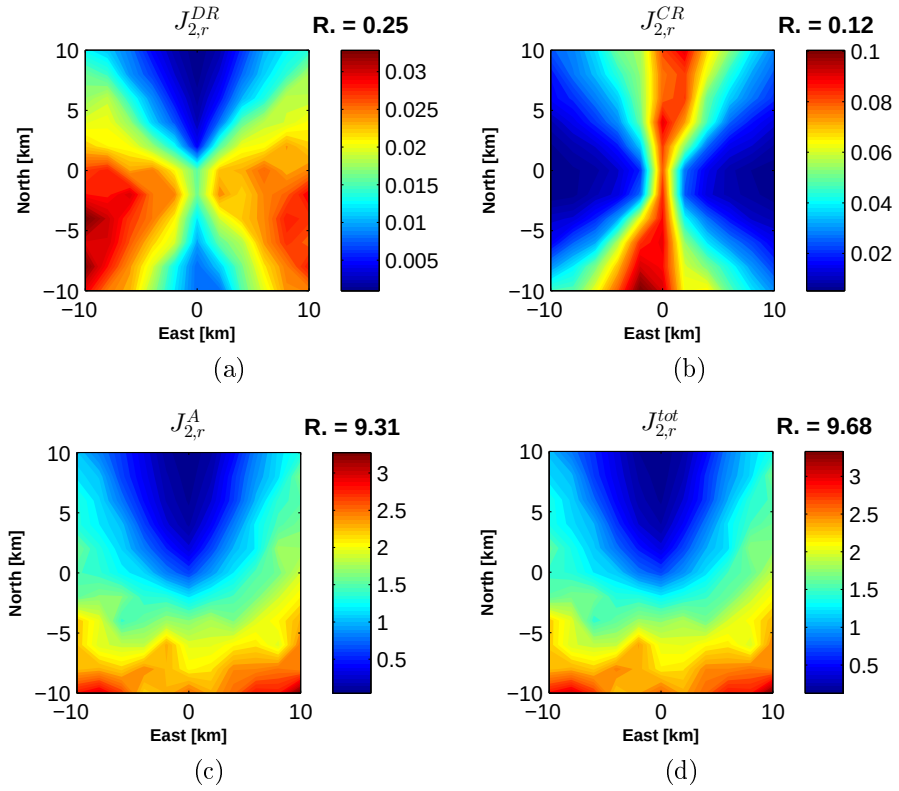

Figure 5.29: $J_{2,r}$ cost functions

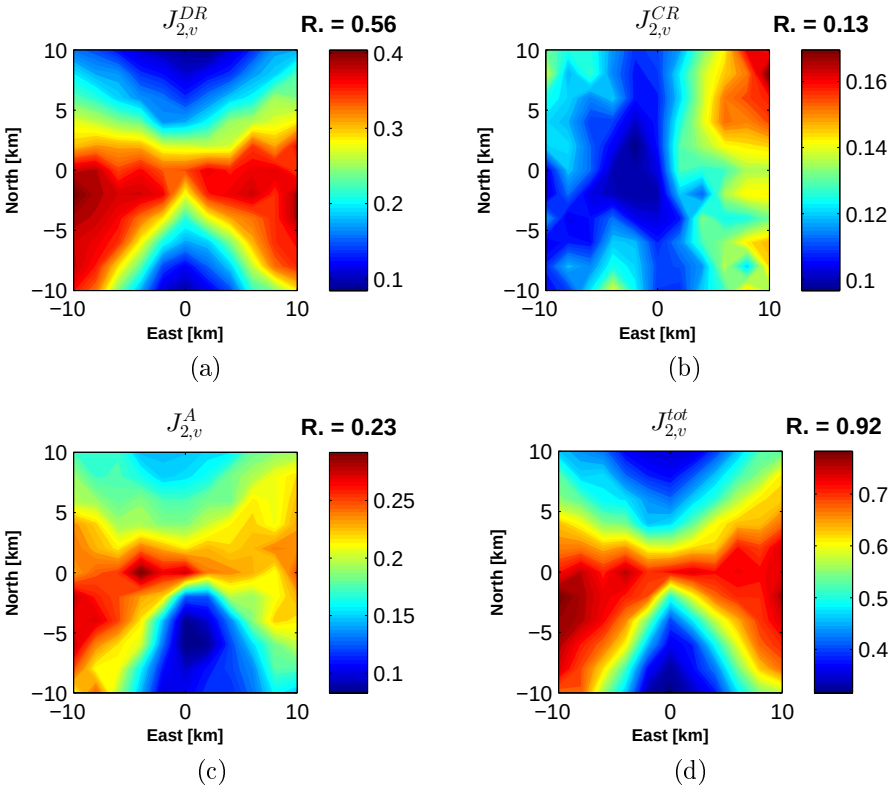

Figure 5.30: $J_{2,v}$ cost functions

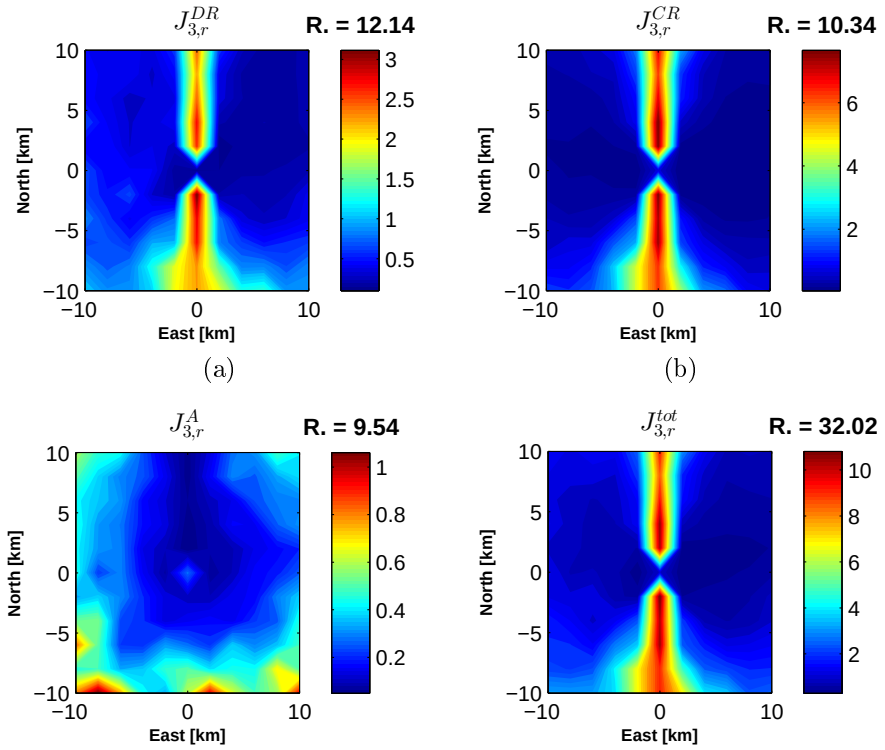

(a) (b) (c) (d)

Figure 5.31: $J_{3,r}$ cost functions

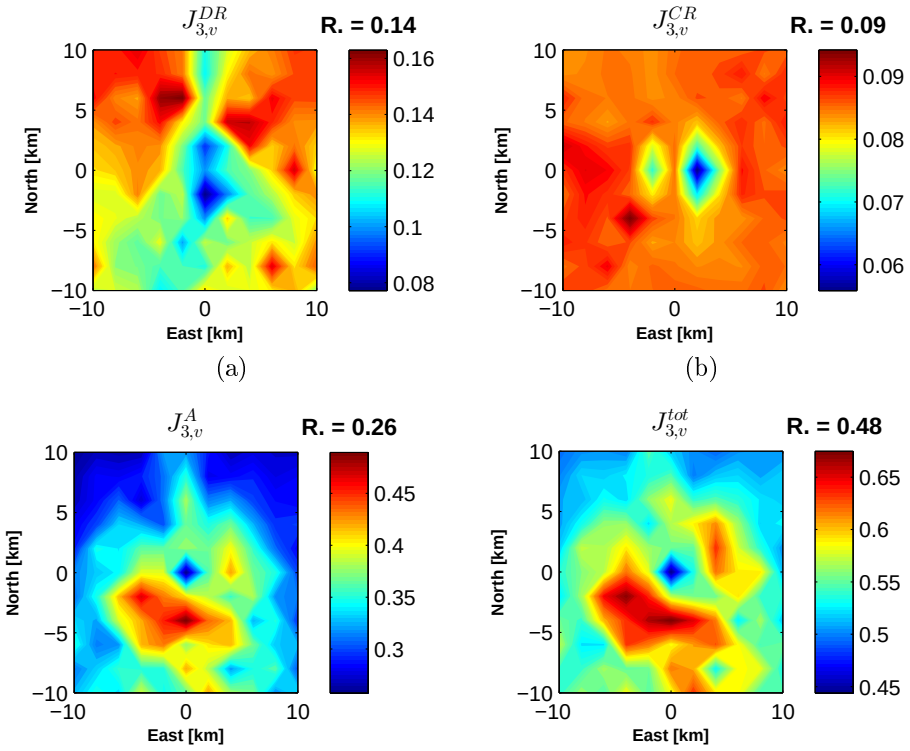

(a) (b) (c) (d)

Figure 5.32: $J_{3,v}$ cost functions

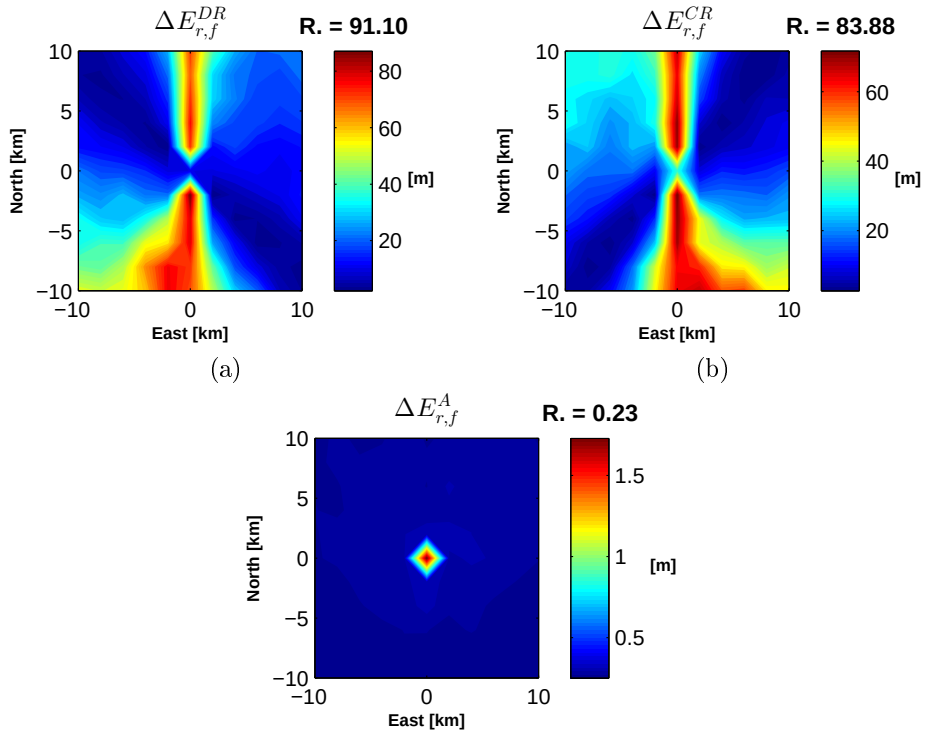

Figure 5.33: Final position errors ($\Delta E_{r,f}$)

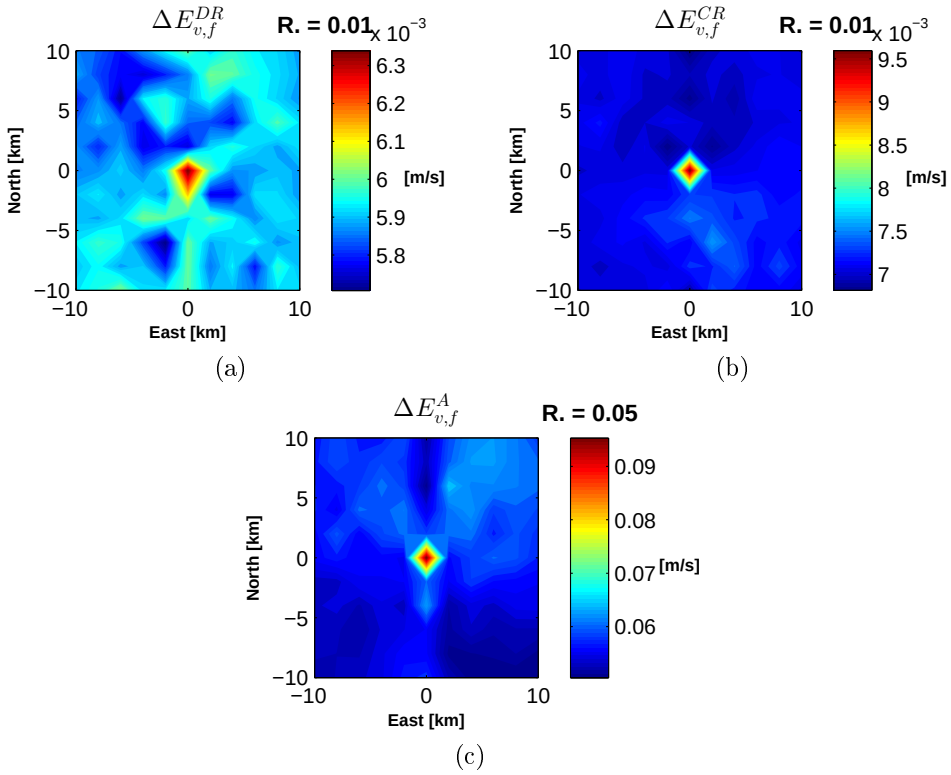

Figure 5.34: Final velocity errors ($\Delta E_{v,f}$)

It seems therefore, as foreseen, that the impact of a beacon on navigation performances, even without the measurement of the bearing, is positive. In particular, taking the position into account, an improvement is experienced wherever the beacon is located inside the grid, except for the final error in altitude as already remarked. In the analysis of case B it was made the hypothesis that the bearing was slightly worsening the velocity determination when far from the beacon; the analysis of the cost functions related to velocity for case A somehow confirms this, being them a little smaller in absence of bearing. Still the impact on the velocity is overall positive for whichever position of the beacon, discarding some local deterioration already discussed for case B especially for the CR. However this impact is not as strong as for the position, also because of the already good performance of the baseline during the landing phase, where the beacons inside the test grid are updating. Comparing cases A and B analyses, main noticeable effects in removing the bearing measurement are here summarized:

- looking throughout figures 5.25 to 5.34 it is possible to see that the best area in which to maximize the performance is no more up-range along the footprint, but it seems that up-range and a little cross-track, or even very near to the LS (except the error in altitude above the requirement) is the most favorable position;

- position related cost functions are overall larger, especially in the last phase of landing (see figure 5.17 and 5.31), in which the bearing is more effective;

- velocity related cost functions have substantially similar trends and values;

- the altitude position error, as expected, although decreasing a little with bearing enabled, is not much affected by it (its improvement is mainly given to the range measurement).

However, although it is clear that adding the bearing is better for the reduction of the errors, the single beacon configuration providing only range and range-rate measurements is already helping significantly the on-board baseline navigation system, as said.
Eventually it is interesting to show representative worst case errors profiles also for case A, as it has been done in previous section for case B. Also for this analysis it seems that the position chosen for case B (figure 5.21) is overall good, looking at the performance contours, both in term of cost functions and final errors. Therefore this point has been selected.

The worst case navigation errors, both for options A and B are presented in figures 5.35 and 5.36, where the two cases are compared in terms of position and velocity errors during the PD. It is hardly possible to see the slight improvement in position fixing in figure 5.35 of case B brought by the bearing. Apparently, for beacon located there the performance with and without bearing is very similar; this is consistent with the fact that minimums of cost functions and final position errors are searched, and the minimums are similar in the test grid both for case A and B, having a general look at all contours previously shown.
The velocity plots are substantially equal, which is expected comparing the contours of the related cost functions, while no noticeable difference has been instead highlighted for what concerns the attitude errors, which therefore are not here displayed.

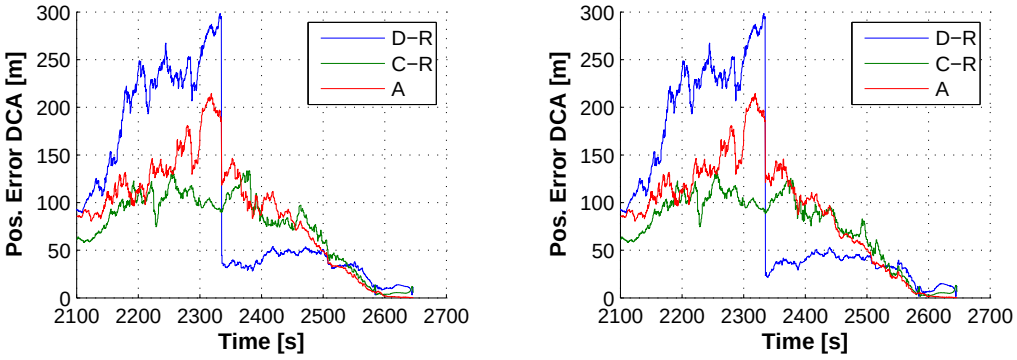

(a) Case B (with bearing) (b) Case A (without bearing)

Figure 5.35: Comparison of worst case position errors (cases A and B)

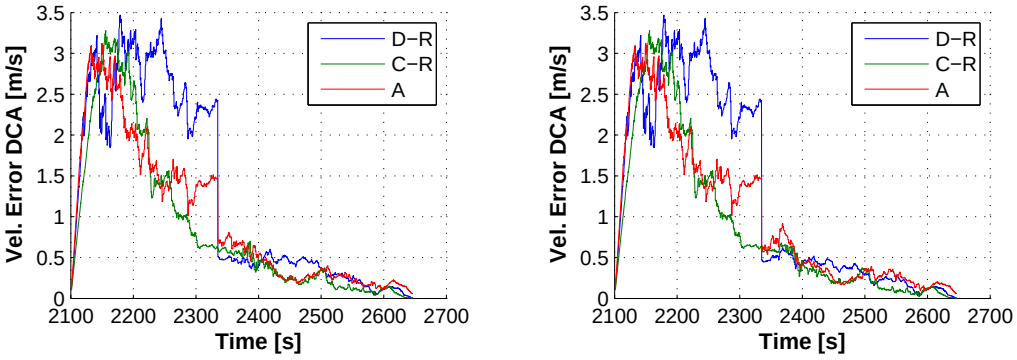

(a) Case B (with bearing) (b) Case A (without bearing)

Figure 5.36: Comparison of worst case velocity errors (cases A and B)

5.6 Double Beacons Analyses

In this section the results for the analyses involving the two beacons are presented (case C and D of table 3.4).

5.6.1 Test Scenario

The single beacon analyses results have been used as basis for the selection of the spatial configuration of the couple of beacons for which to perform these simulations. In particular, since one of those results is that generally the nearer to the landing site the better, either with or without bearing, it has been first decided to select 4 different points around the landing site (table 5.4). One of the two beacons was then fixed in each of these points, while the second beacon was located in different positions of the grid shown in figure 5.37b, similar to the grid for the single beacon analysis, but with less points. This resulted in having 100 different configuration tested both for options C and D. It can be noticed that all the 4 points in figure 5.37a are located on the East semi-plane: this choice is supported by the overall symmetric behavior shown by the single beacon analyses contours, which lead to the assumption that symmetric results are expected fixing first beacon symmetrically with respect to the North axis. Moreover, one of these points (P_4) is inside the avoidance area, but it was considered interesting to see performances also in that case. The number of points in the uniform grid, although less with respect to what used for the previous analyses, is still enough to have an outlook of the performances and highlight trends, if existing.

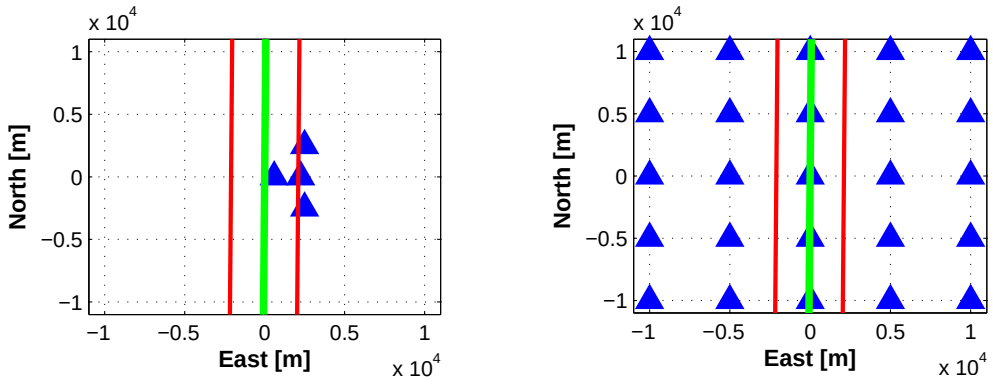

(a) 1^{st} beacon points (b) 2^{nd} beacon points

Figure 5.37: Double beacon analyzed positions

Therefore, in conclusion, this test scenario is a trade-off between reasonable number of simulations and choice of points in which to locate one of the two beacons. This approach is basically excluding from the analysis the possibility of having both beacons not in the immediate neighborhood of the landing site, but, as remarked, having to apply a criterion to reduce the number of simulation, the priority is for beacons nearer to the landing site. Moreover, from a geometric point of view, it is known that for case C, i.e. without bearing, the best situation is when the two lines in the plane departing from the S/C and intersecting the beacons are perpendicular each other: this eventuality happens nearer to the LS if both beacons are near to it.

Table 5.4: Coordinates of 1^{st} beacon position considered [m]

	P_1	P_2	P_3	P_4
East	2250	2500	2500	600
North	0	2500	-2500	0

5.6.2 Results

The results for options C and D are presented at this point. It has been decided not to discuss them separately, differently from what has been done for the analyses of the single beacon.
In figures 5.38 to 5.43 some significant contours generated in these analyses are reported as support. As it can be seen, they all refer to the first beacon located in P_2 and the contours have been reported both for case C and D, in order to compare them. The first important result is, as expected, that the performance improves with respect to the single beacon, either with the bearing measurement enabled or not. This is easily noticeable comparing the contours with the respective ones for the single beacon analyses. In particular the position is more improved, while the effect on the velocity is much more limited, as shown by the related cost functions values.
In particular, the study of all the contours generated in these simulations has shown that the range of variation of the cost functions is more limited, meaning that there is less influence on where the two beacons are located inside the test grid. In other words, it has been noticed more uniform results inside the test grid and especially this is more evident if compared to case A. It has been also noticed that having the two beacons too near each other is not the best configuration, which is somehow expected since this is not the

best from a geometric point of view.
Considering that values around or below the unity for the independent cost functions mean good performance with respect to the reference profile, the double beacon configuration has values below 1 for most cost functions in whichever configuration analyzed. In table 5.5 the values exceeding unity are reported with the indication of the related cost function and 1^{st} beacon for which this occurs. Basically, determination of velocity in all components and position in DR and CR are improved with respect to baseline and single beacon configuration (figures 5.38 to 5.41) bringing to navigation errors within the limits of the reference profiles (figure 5.3) almost independently from where the two beacons are located inside the test grid. The only exception is the position determination in altitude, although it is in any case improved with respect to the baseline.

Table 5.5: Cost functions maximums exceeding unity inside the test grid

Cost Function	1^{st} BC position	Maximum Value in Test Grid
J_r^A	P_3	1.1 (case C) / 1.2 (case D)
$J_{1,r}^A$	P_1, P_2, P_3, P_4	1.4-1.7 (case C) / 1.5-1.8 (case D)
$J_{2,r}^A$	P_3	1.3

The maximums for the position final errors inside the test grid are instead listed in table 5.6. It is worth noticing that in some cases the maximums are below the requirements set in table 5.1 and that in any case the values reported do not generally refer to the same configuration. In other words, it is possible to detect large portions of the test grid where to locate the second beacon for which the final error is acceptable (figure 5.43). This is a relevant and probably the most interesting improvement with respect to the single beacon analysis, where it was also possible to find locations satisfying all cost functions, but it was much harder to determine a position for which simultaneously also the final errors were within the requirements of table 5.1, excluding points too near to the LS that would fall inside the avoidance area. It has been noticed that generally the addition of the bearing (case D) seems to bring slightly worse results in DR and CR with respect to case C in the first phase the beacon is updating, i.e. when S/C is further from the LS, while better results are seen in the final part of the landing. Anyhow, this difference is hardly noticeable and could be explained with the increased effectiveness of the bearing when nearer to the beacons, as already previously remarked. For what concerns the altitude, the bearing measurement brings

Table 5.6: Maximum final position errors inside test grid [m]

(a) With bearing

	P_1	P_2	P_3	P_4
DR	9.1	18.5	3.2	3.4
CR	10.1	3.6	16.4	3.8
A	0.8	1.1	1.2	1.2

(b) Without bearing

	P_1	P_2	P_3	P_4
DR	14.4	26.5	3.4	4.8
CR	16	3.8	25.7	5.5
A	1.3	0.8	0.7	1

slightly better results in the whole time interval in which the beacons are updating, as it can be noticed from figure 5.42.
It is worth noticing that the respective contours for case C and D are quite similar to each other, both in trends and values. It could be therefore inferred that the impact of the bearing gets more marginal as the number of beacons in the configuration increases. This somehow legitimates the starting choice of not including the bearing measurement in configurations with more than 2 beacons.

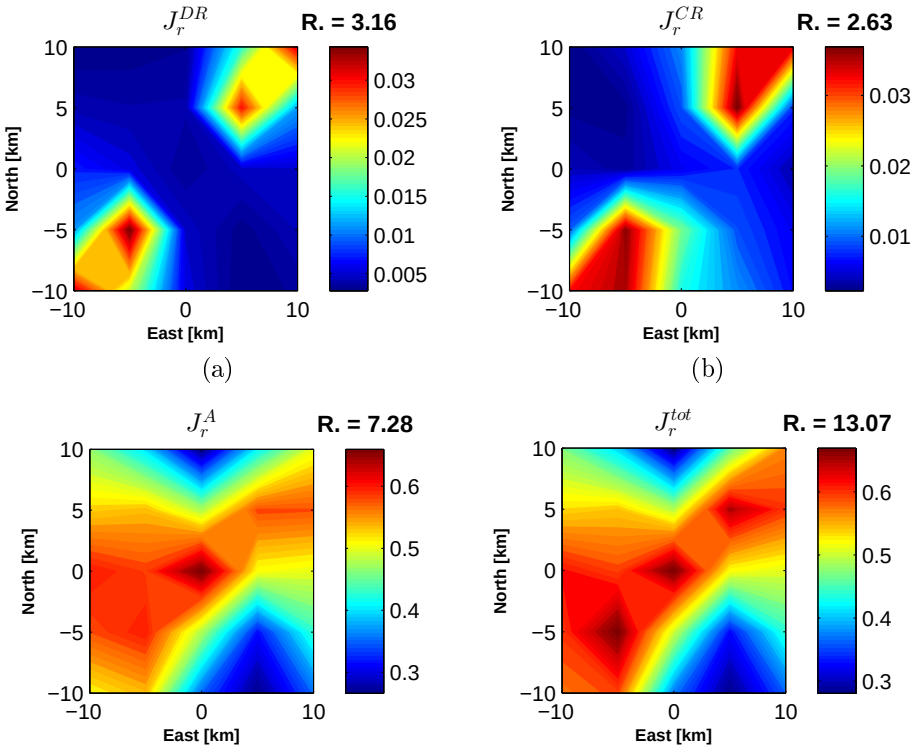

Figure 5.38: J_r cost functions, case D, 1^{st} beacon in P_2

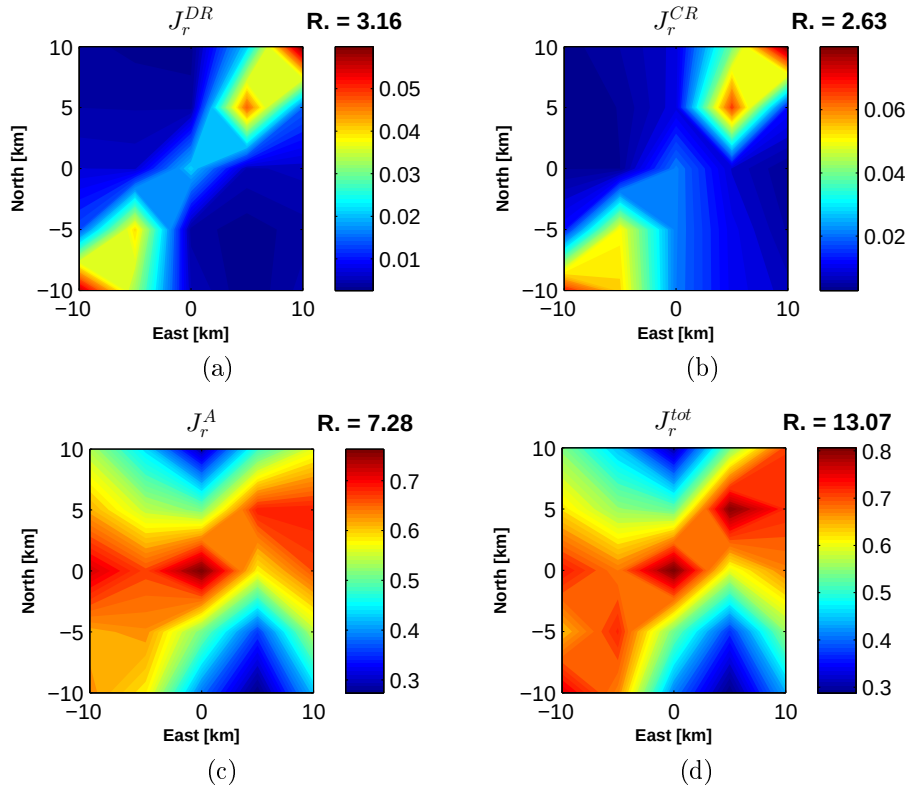

Figure 5.39: J_r cost functions, case C, 1^{st} beacon in P_2

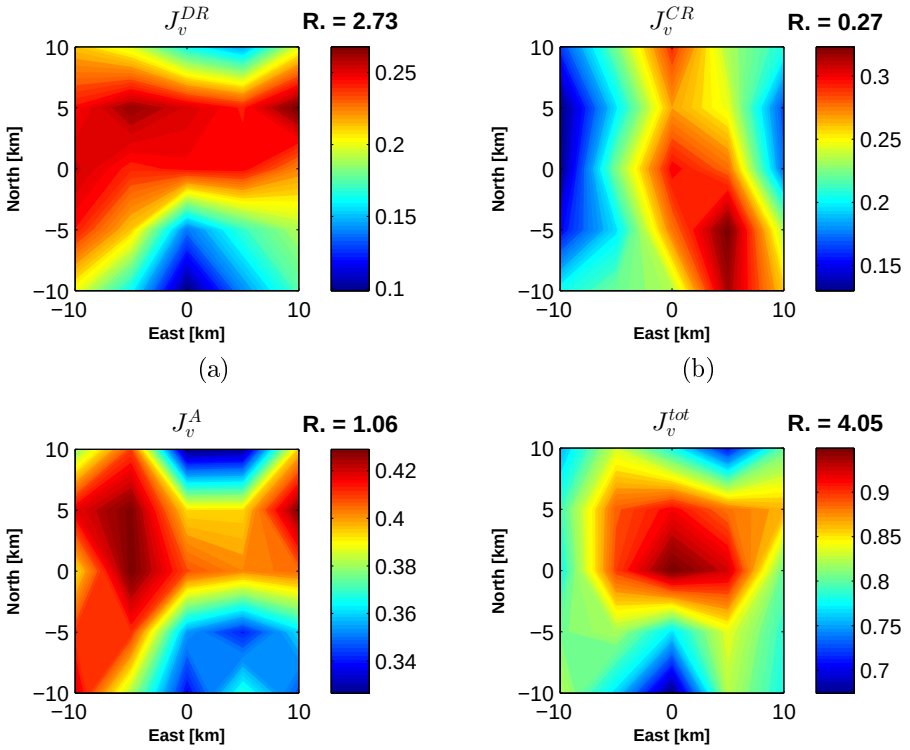

Figure 5.40: J_v cost functions, case D, 1^{st} beacon in P_2

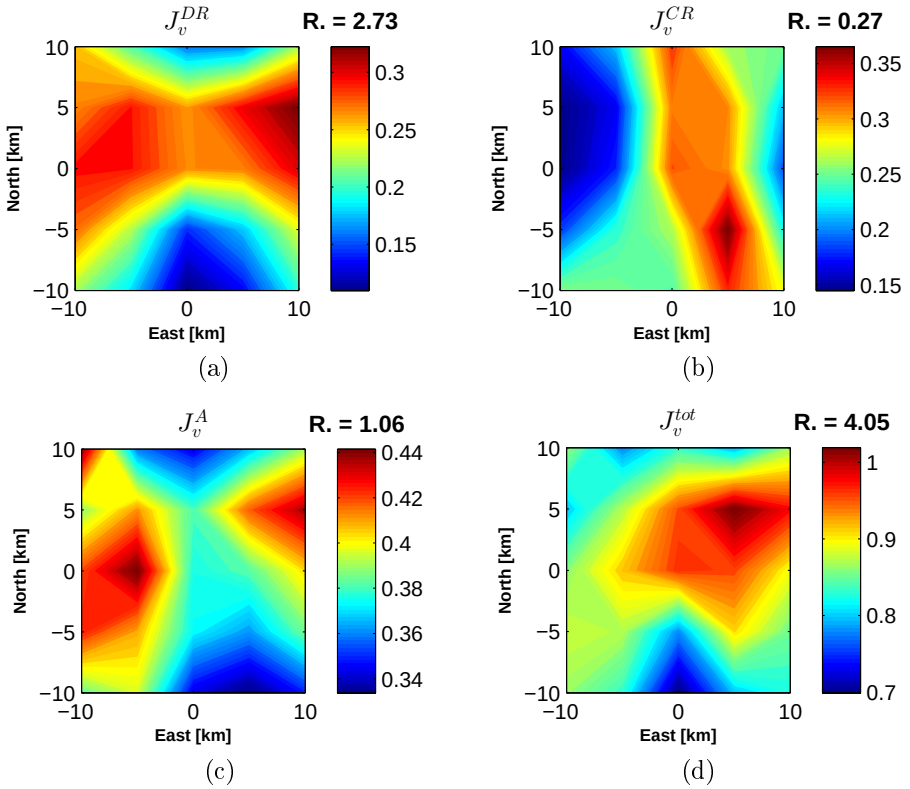

Figure 5.41: J_v cost functions, case C, 1^{st} beacon in P_2

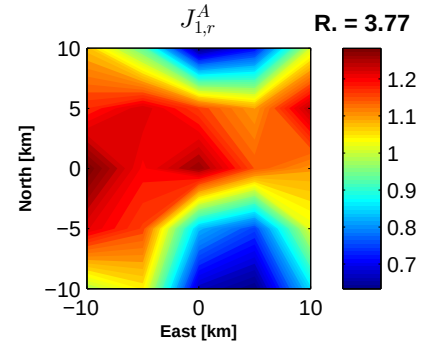

(a) case D

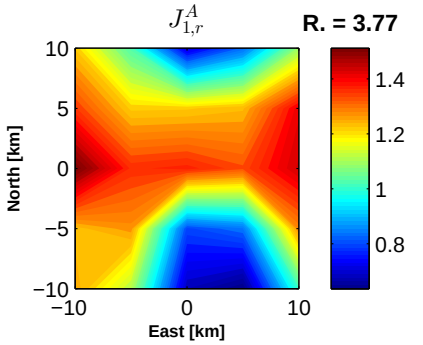

(b) case C

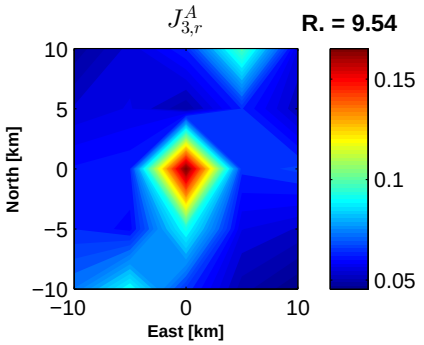

(c) case D

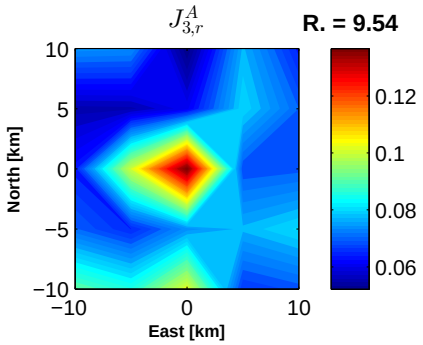

(d) case C

Figure 5.42: $J^A_{1,r}$ and $J^A_{3,r}$ cost functions, 1^{st} beacon in P_2

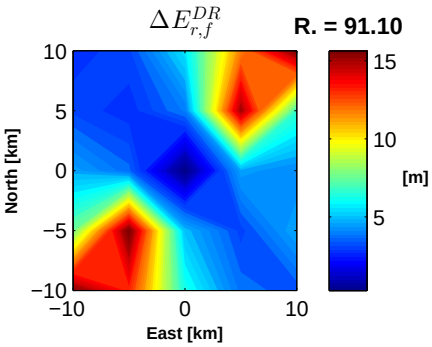

(a) case D

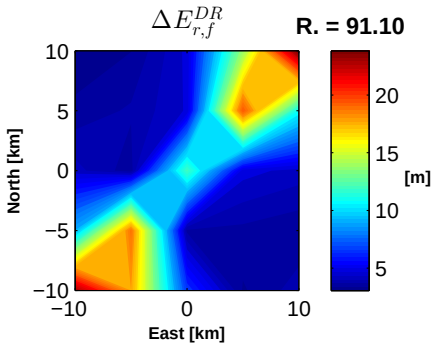

(b) case C

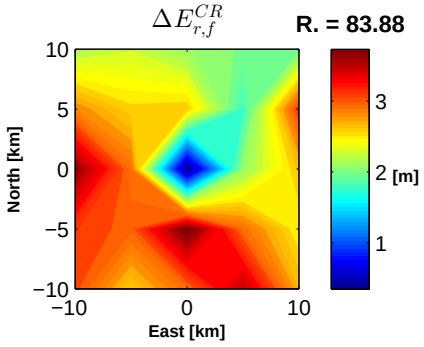

(c) case D

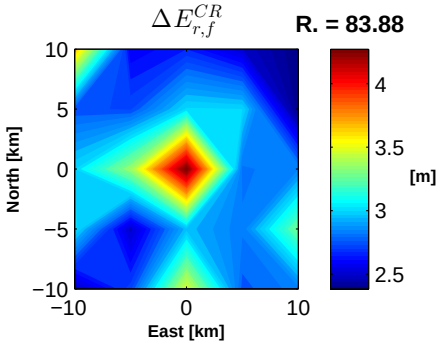

(d) case C

Figure 5.43: Final position errors in DR and CR ($\Delta E_{r,f}$), 1^{st} beacon in P_2

It has been decided to show worst case solution results for case C and D for the couple of beacons as in figure 5.44, which lie both on the same semi-plane: this is one possible configuration that guarantee all cost function to be less than 1 and also very small final errors. Moreover, both beacons are outside the avoidance area.

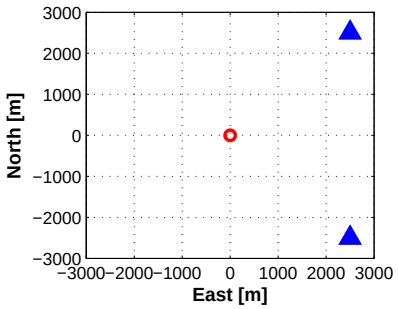

Figure 5.44: Selected positions of the beacon couple

Figures 5.45 and 5.46 respectively show the worst case position and velocity errors. It is possible to see in particular:

- the improvement with respect to the single beacon worst case solution shown in figures 5.35 and 5.36, expecially in the altitude component;
- the difference between cases C and D is more limited than the one between cases A and B;
- the error in the final part, say indicatively from HG, is visibly smaller than in the single beacon configuration.

It could be also noticed that the position error in CR is more or less unchanged with respect to the single beacon results especially at the beginning of the visibility window. This is expected since the configuration selected of figure 5.44 does not tell more to the filter to better estimate the CR. Although the CR error is already quite less than the related reference error profile, it is interesting to see that choosing a configuration geometrically favorable to sense the CR as the one in figure 5.47a makes error in CR decreasing significantly and fastly (figure 5.47b. In any case this configuration is worse being $J^A_{1,r}$ around 1.4 (the larger altitude error is also noticeable in figure 5.47b).

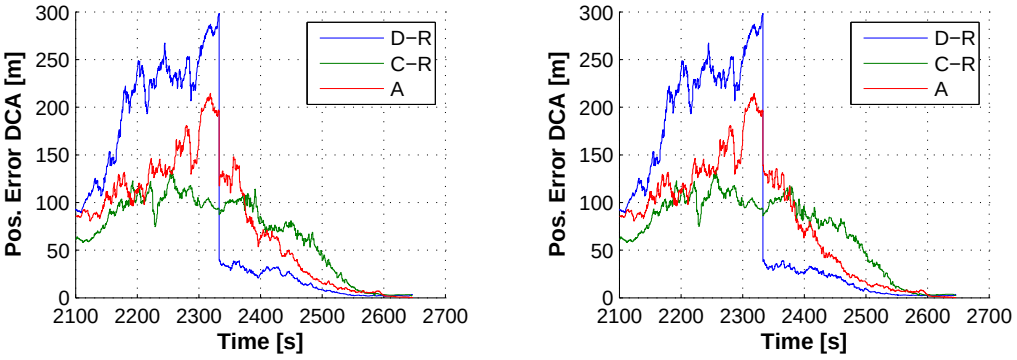

(a) Case D (with bearing) (b) Case C (without bearing)

Figure 5.45: Comparison of worst case position errors (cases C and D)

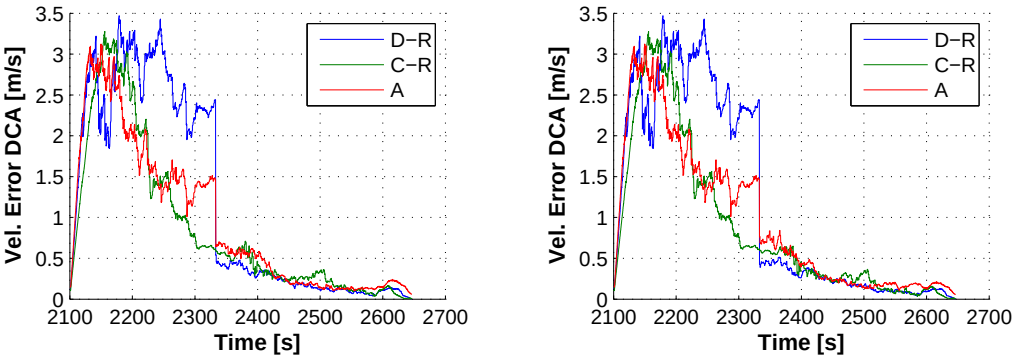

(a) Case D (with bearing) (b) Case C (without bearing)

Figure 5.46: Comparison of worst case velocity errors (cases C and D)

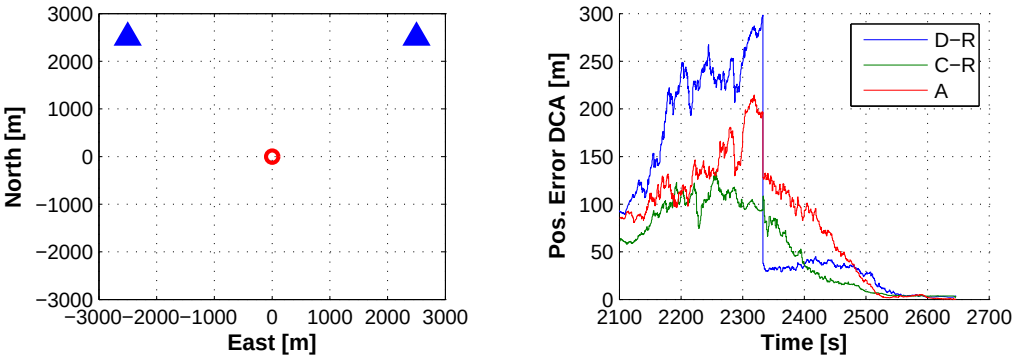

(a) Positions (b) Case C (without bearing)

Figure 5.47: Configuration of beacons minimizing position error in CR

5.7 Three Beacons Analysis

In this section the analysis and results for option E (table 3.4) are reported. The simulations have been performed fixing 2 of the beacons in the positions of figure 5.44, since in the previous section it has been shown this to be a possible promising configuration, i.e. it seems to be already enough to have navigation errors smaller than the ones imposed from requirements.
The interest is therefore to see what improvement could bring the addition of a third beacon to this couple.
It has been preferred this approach instead of a less constrained analysis with more DOF's, where also the first or second beacons are not fixed, since, beside requiring a huge number of simulations, in the light of what seen until this point it is assumed that optimal configuration for N number of beacons should be somehow connected to the optimal for $N-1$ through the superposition principle.
The third beacon is rotated in the points of the grid of figure 5.37b, following the same scheme used in the double beacons analyses.
It is remarked that this analysis excludes the presence of the bearing measurement.

5.7.1 Results

It is of particular interest to see if the third beacon brings to similar or better performance with respect to case D (with bearing) and for this reason it has been decided to compare the results with those for case D.
From the analysis of the contours it has emerged, as expected, that there are no substantial differences in terms both of cost functions and final errors, since it has already be shown that the two beacons deliver very good performance from the point of view of the requirements.
It has been thought that a possible interesting configuration is to combine the ones of figures 5.44 and 5.47a, bringing to the disposition presented in figure 5.48a. It can be noticed looking at the plot in figure 5.48b that the trend of the error is somehow the superposition of the profiles in figures 5.45a and 5.47b, as expected. After the first valid beacon update, the errors in all component decrease faster than what seen for the two beacons, especially the ones in DR and CR. Eventually these worst case errors are in the order of few meters (< 10 m) for the last 150 s of navigation, which is a really interesting and promising result in the light of enabling a very precise landing.
The plot of the velocity errors has been not reported since there is just a very slight and hardly noticeable improvement with respect to what can be seen in figure 5.46.

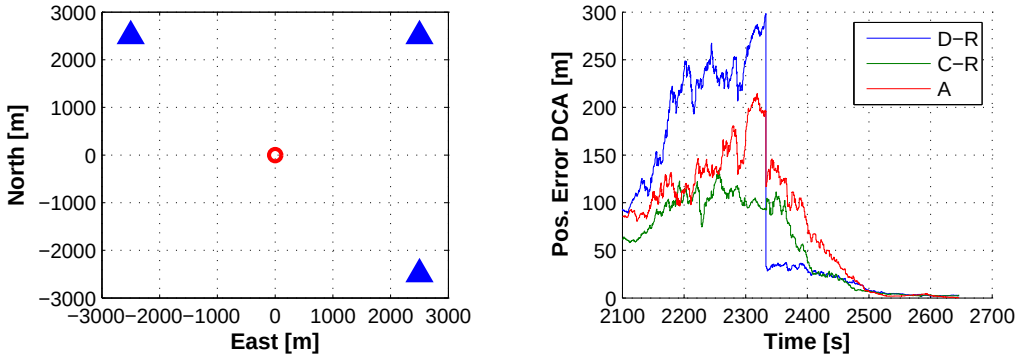

(a) Positions (b) Case E

Figure 5.48: Example of worst case position errors for case E

5.8 Four Beacons Analysis

This analysis has been performed with the same approach used for case E, fixing three beacons in the configuration of figure 5.48a.
In the light of the previous analyses it was not expected to find large improvements and/or dependency on the location of the fourth beacon; in fact, the study of the related contours confirms this expectation.
Figure 5.49b shows the worst case position errors for the example configuration in figure 5.49a, which from a GDOP point of view should be an overall good configuration for last part of the landing, in particular the vertical descent phase. These errors, although certainly smaller, are very similar to what obtained with three beacons (figure 5.48b): the observed variation in terms of performance is negligible.

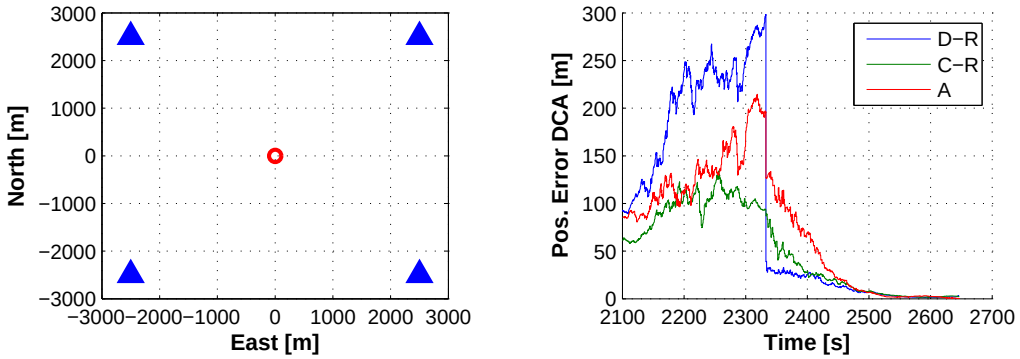

(a) Positions (b) Case F

Figure 5.49: Example of worst case position errors for case F

5.9 Sensitivity Analyses

In this section the sensitivity analyses on uncertainty in the beacon position and on the working frequency of the beacon measurement are presented.

5.9.1 Beacon Position Uncertainty

The trade-off analyses previously reported have been performed considering to know exactly where the beacons are. It is interesting now to check the influence of the existing uncertainty in the position of the beacons.
An error has been added to the East, North and altitude coordinates of the single beacon placed as in figure 5.21, and the results of the Monte Carlo analysis have been compared with the available ones without the uncertainty. All 3 measurements have been included, i.e. case B.
Recent studies about position determination of lander in the lunar surface reports that the accuracy of 10 minutes positioning combined USB and VLBI data can reach 10 m [26], therefore it has been decided to set an error of 10 m on the longitude, latitude and altitude.

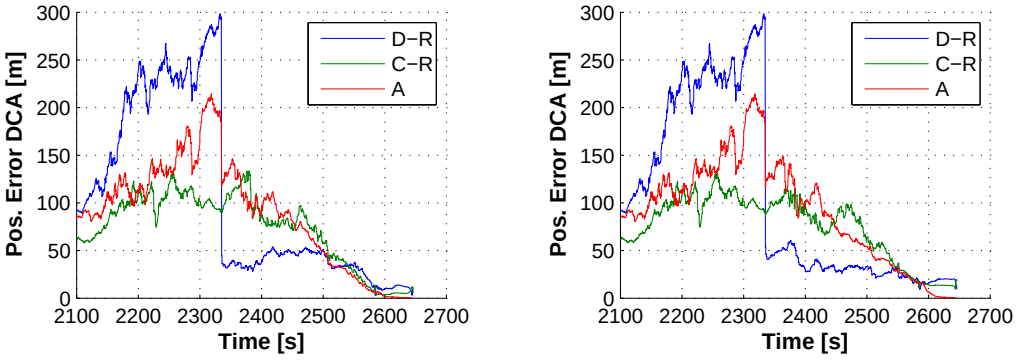

(a) Without uncertainty (b) With uncertainty

Figure 5.50: Comparison of worst case position errors with and without uncertainty in the beacon position (case B)

From the analysis of the figures in 5.50, it is possible to see that the imposed uncertainty is affecting in particular the last part of the navigation, with final errors in DR and CR larger with respect to the solution with no uncertainty. The influence in the velocity is instead negligible.
This position uncertainty analysis has not been performed for the other configurations, but it is reasonable to expect that for an increased number of beacons, on average the uncertainties on the different positions would compensate themselves, and possibly the effect noticeable in 5.50 would be smaller.

On the other hand, in the worst case where all uncertainties are "offsets" in the same direction, it could be expected a larger impact.
Eventually, this error is just the error in MCF frame: for the landing it might be more important to have an accurate relative position.

5.9.2 Frequency

It is here reported another analysis on the influence of different working frequency for the beacon measurements. It is remarked that until this moment it has been always assumed a frequency of 1 Hz for the measurements.
Taking always as reference the configuration of figure 5.21, case B, figure 5.51 and 5.52 show respectively the variation in the total position and velocity related cost functions, with varying update frequency of the beacon measurements.
Eventually figure 5.53 shows the variation in the final worst case position error.
From these figures it is possible to infer that there is not much difference in increasing the frequency above 1 Hz. The cost functions are not decreasing much after that point. Instead it clearly seems, especially from figure 5.51, that too small frequencies make the results much worse, as expected.
The benefits in having larger frequencies should be weighted with the complexity added to the system to allow faster measurements. In any case, from this last analysis it seems that 1 Hz is already performing well.

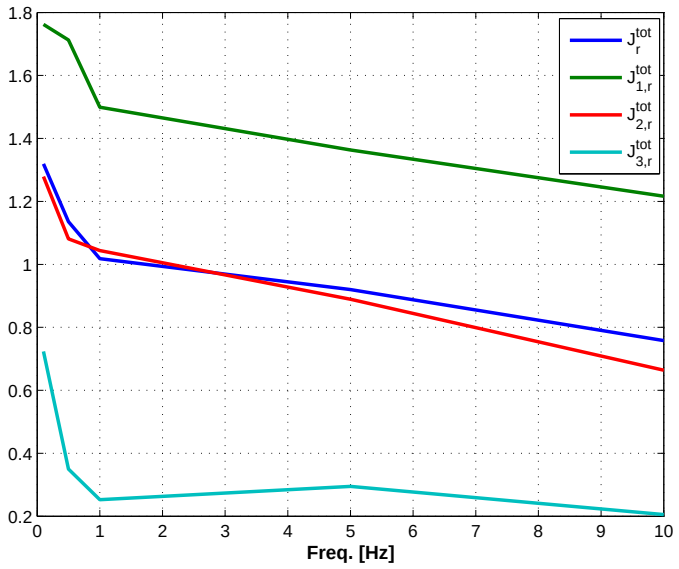

Figure 5.51: Position cost functions dependency on update frequency

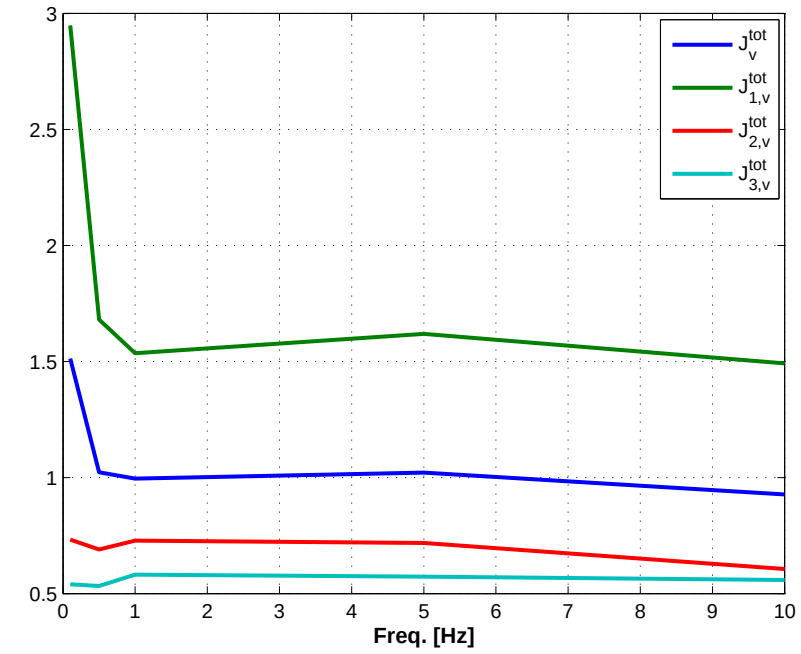

Figure 5.52: Velocity cost functions dependency on update frequency

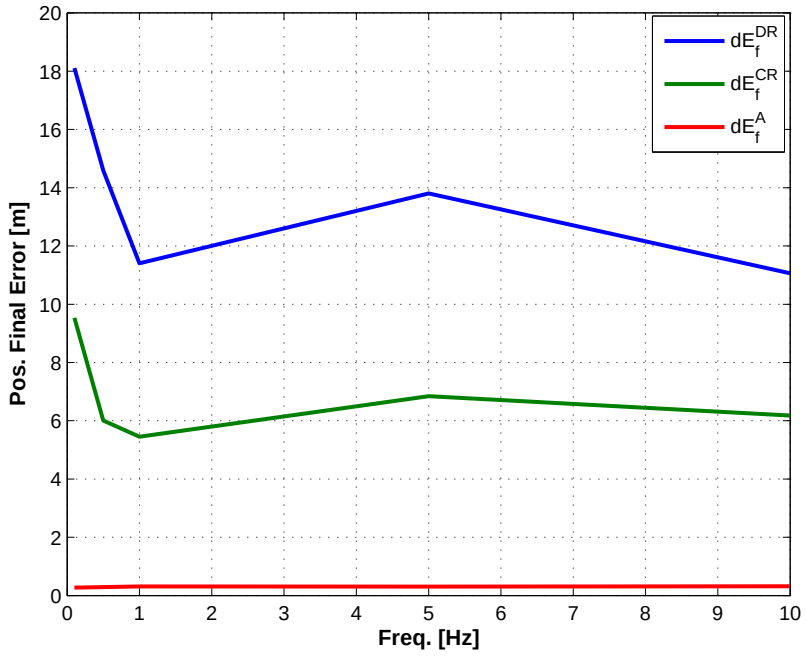

Figure 5.53: Worst case position error dependency on update frequency

5.10 Results Summary

It has been considered useful to summarize at this stage results for the configurations chosen throughout this chapter (table 5.7), i.e. the one in figures 5.21 for case A and B, 5.44 for case C and D, 5.48a for case E and 5.49a for case F. It has to be remarked that these example configurations have been chosen heuristically, with the constraint of being outside of the avoidance area [25]. From table 5.7 it could be said that a couple of beacons located near to the LS, even without the bearing measurement (case C), makes all the cost functions defined in section 5.2.2 to be less than one, in addition to having final worst case errors within the requirements imposed in table 5.1. Cases E and F substantially do not add much in terms of performance to this configuration: only the altitude fixing is slightly further improved. For what concerns the bearing, the expected added complexity to the on-ground system may not be worth the little benefit that it brings.
Therefore, in the light of enabling redundancy, a valid configuration for further studies could be the one of case E. In figure 5.54 it is presented a way this could be implemented, i.e. with a first mission carrying one beacon on a lander and the other beacons delivered by rovers, that would have to travel for 5 km along straight lines starting from the lander. In this scenario, the hypothetical lunar base could be located outside the avoidance area, for example either around the first beacon (blue triangle), or in any case not too far from the LS and from beacons (for their maintenance).

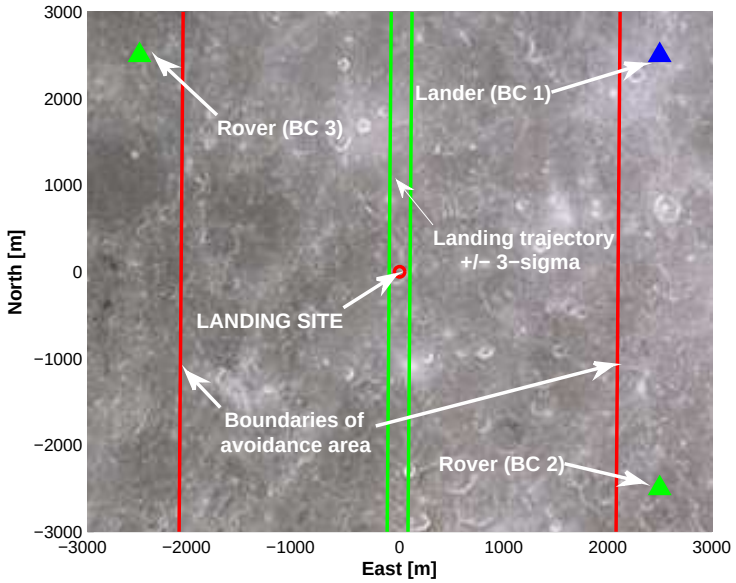

Figure 5.54: Possible case E configuration implementation

Another conclusion could be that two beacons with bearing (case D) are the nominal configuration (for example BC_1 and BC_2 from figure 5.54). If then one fails, case B is almost meeting all requirements as reported in table 5.7.

Table 5.7: Performance of analyzed cases with respect to the baseline

Parameter	Baseline	A	B	C	D	E	F
J_r^{DR}	3.16	0.05	0.04	<0.01	<0.01	<0.01	<0.01
J_r^{CR}	2.73	0.03	0.03	0.01	0.01	<0.01	<0.01
J_r^{A}	7.28	0.96	0.95	0.43	0.43	0.35	0.28
$J_{1,r}^{DR}$	0.09	<0.01	<0.01	<0.01	<0.01	<0.01	<0.01
$J_{1,r}^{CR}$	0.01	0.02	0.01	0.01	0.01	<0.01	<0.01
$J_{1,r}^{A}$	3.77	1.47	1.48	0.95	0.94	0.85	0.69
$J_{2,r}^{DR}$	0.25	0.02	0.02	<0.01	<0.01	<0.01	<0.01
$J_{2,r}^{CR}$	0.12	0.03	0.02	0.01	0.01	<0.01	<0.01
$J_{2,r}^{A}$	9.30	1.02	1	0.14	0.15	0.06	0.03
$J_{3,r}^{DR}$	12.14	0.15	0.11	<0.01	<0.01	<0.01	<0.01
$J_{3,r}^{CR}$	10.34	0.08	0.06	0.01	<0.01	<0.01	<0.01
$J_{3,r}^{A}$	9.54	0.1	0.08	0.09	0.08	0.05	0.05
J_v^{DR}	2.73	0.33	0.35	0.15	0.14	0.14	0.12
J_v^{CR}	0.27	0.23	0.23	0.23	0.23	0.24	0.17
J_v^{A}	1.06	0.43	0.41	0.36	0.34	0.32	0.35
$J_{1,v}^{DR}$	6.61	0.47	0.48	0.27	0.26	0.25	0.21
$J_{1,v}^{CR}$	0.51	0.45	0.45	0.44	0.42	0.48	0.32
$J_{1,v}^{A}$	2.43	0.67	0.61	0.58	0.53	0.57	0.58
$J_{2,v}^{DR}$	0.56	0.33	0.37	0.07	0.05	0.05	0.05
$J_{2,v}^{CR}$	0.13	0.12	0.12	0.14	0.15	0.1	0.07
$J_{2,v}^{A}$	0.08	0.23	0.22	0.1	0.07	0.07	0.06
$J_{3,v}^{DR}$	0.13	0.12	0.13	0.1	0.11	0.11	0.1
$J_{3,v}^{CR}$	0.09	0.06	0.07	0.07	0.07	0.08	0.08
$J_{3,v}^{A}$	0.26	0.38	0.39	0.4	0.46	0.34	0.43
$\Delta E_{r,f}^{DR}$ [m]	91.1	12.82	11.41	2.79	3.03	2.62	2.91
$\Delta E_{r,f}^{CR}$ [m]	83.9	6.99	5.45	2.48	2.72	2.52	2.37
$\Delta E_{r,f}^{A}$ [m]	0.23	0.31	0.31	0.31	0.33	0.31	0.33

CHAPTER 6

Concept Demonstration Proposals

Though this research work is focused on the conceptual definition of ground based navigation infrastructures for extraterrestrial landing and the preliminary assessment of the achievable performance, some ideas are here proposed about how the developed concepts could be tested on ground, possibly with the usage of off-the-shelf hardware. The scope is therefore mainly to give some outlook for further studies, not to define requirements and design the test setup.
Different positioning systems have been developed in the last decade. This systems are able e.g.:

- to complement GNSS where satellite signals are not able to arrive or are too weak;
- to provide stand-alone positioning, either in indoor or outdoor environment.

Low-cost systems developed for indoor localization in recent years are able to determine position either using Bluetooth or the IEEE 802.11 WiFi's as beacons. The ranging is usually done either through TOA, RSS or phase measurements and literature reports that good accuracy can be obtained. A starting point for further studies could be to take into account the potential exploitation of one of these systems commercially available, tuning them to the tested scenario. At least any of such systems would enable the range measurement.
It could be also taken into account the use of the so called pseudo-satellites

(pseudolites), which are transmitters that provide GPS-like signals, which could be used for ranging and doppler. They are basically on-ground substitutes of navigation satellites, used either to complement GNSS or to test it or to work as an independent positioning system.
Different pseudolite systems have been proposed in literature. For example *Fraunhofer Institute for Integrated Circuits IIS* is studying, developing and testing different positioning systems, including pseudolites [27]: their pseudolite system could be used in different scenarios and may be tuned to the purpose of this research. It uses components from the mature *RedFIR* technology, a state-of-the-art wireless tracking technology, also developed by this institute.
Another possibility available off-the-shelf could be the technology *NAVIndoor* developed by *Space System Finland SSF* since the beginning of last decade, within the frame of ESA ARTES program [28]. NAVIndoor has found application, for example, in PLATFORM, an integrated robotic based validation test-bed designed by *GMV S.A.* to provide a large number of testing abilities, e.g. rendez-vous and docking, formation flying and planetary landing [29].

Figure 6.1: Pseudolite configuration [27]

CHAPTER 7

Conclusion

Moving from the hypothesis of a future lunar base on which multiple S/C will be possibly landing, the concept for a ground based infrastructure aiding the on-board navigation filter has been studied.
From the analysis of Earth based navigation architectures using radiometric measurement six possible configurations of this ground based infrastructure to be used in a lunar landing scenario have been proposed, and their performance assessed.
Observation models for the new measurements (range, range-rate and bearing) have been defined and complemented with the navigation filter (eEKF) and simulation models of the reference on-board navigation system (SINPLEX [6]).
Cost functions have been then defined to evaluate the performance of the proposed configurations, weighing worst case navigation solutions with relevant reference error profiles set as self-imposed requirement.
Monte Carlo analyses have been carried out to extract worst case results. Very good and promising results have been highlighted for all tested cases. Results have principally shown that:

- providing the navigation filter with measurements of range and range-rate from just one ground station (beacon) located on the surface near to the landing site, already improves significantly the navigation solution during the second half of the powered descent, with respect to the performance achieved by the reference navigation system;
- generally, the nearer these beacons to the landing site the better, being

the final phase of the landing the one requiring more improvements, with the aim of a precise landing relative to a predetermined spot;

- adding the bearing measurement brings some benefits, especially in the case of a single beacon, while its effect is less noticeable increasing the number of beacons;
- two beacons without bearing basically perform very similar to having the bearing enabled, and better than a single beacon with the bearing;
- the worst case navigation errors in presence of two beacons providing range and range-rate are smaller than the reference error profile, with final worst case errors lower than 3 m in the DR and CR, 0.5 m in altitude and 0.1 m/s in velocity; adding then a third and even a fourth beacon does not show to improve much more significantly the achieved performance.

Eventually sensitivity analyses have shown that:

- the uncertainty in beacon position affects mainly the final phase of the landing, when the S/C is nearer to the beacon;
- the increase in the frequency of the new measurement with respect to the nominal one used throughout the research (1 Hz), does not bring much more improvement, while the performance starts to get significantly worse decreasing the update frequency .

7.1 Future Outlook

It is opinion of the author that, once a lunar base is established, sooner or later a GBNS will provide navigation aid to approaching S/C and possibly also to users within the base. The preliminary results obtained in this work confirm that a concept like the ones studied here, would be a valuable help to the navigation of the landers, enabling precise state determination especially in the final phase of the approach, the most crucial for a precise landing.
The field of the radiometrics aided planetary landing is quite unexplored in literature at the time being, therefore the to-do list is quite long before a system could be validated. Here are outlined some possible guidelines for future work to further study and extend the concepts developed in this thesis:

- from the point of view of further performance analyses, a first step is to improve the observation models for range (pseudorange), range-rate and bearing measurements, considering biases, clock errors etc...

which in this work have not been modeled being it a preliminary performance assessment. This will require the extension of the navigation filter, since new state variables will have to be estimated. Together with the model refinement the noises would need to be checked, since in this work they have been intentionally taken larger than what could be expected. Then, since the sensitivity analysis on the uncertainty in beacon position revealed to have a noticeable influence, it would maybe be the case to deeply study this problem and include it in the performance analysis. Performance could be also evaluated with different baseline sensors suite, for example removing LA, with the aim of reducing the weight of the on-board system.

- From the point of view of the system level analysis, a feasibility study should be conducted to define requirements and for example estimate the cost of such a kind of infrastructure.
- With reference to the ideas proposed in this research, a test setup could be defined, designed and tests conducted to show the potentiality of the concept on-ground on a relevant scenario.
- As long as the radiometrics is concerned, eventually, it shall be defined how the system could be implemented and the measurements obtained; this would also allow in parallel to refine the measurement models, which could then take the radiometrics into account and simulate it.

Figure 7.1: Lunar base concept, courtesy of ESA

Acronyms

ADC	Analog to Digital Converter
ADF	Automatic Direction Finder
ALHAT	Autonomous Landing and Hazard Avoidance Technology
AOA	Angle Of Arrival
ATON	Autonomous Terrain based Optical Navigation
BC	Beacon
CN	Crater Navigation
CR	Cross-Range
DCA	Down-range Cross-range and Altitude frame
DME	Distance Measuring Equipment
DO	Descent Orbit
DOF	Degree Of Freedom
DOI	Descent Orbit Injection
DR	Down-Range
eEKF	error state Extended Kalman Filter
FOV	Field Of View
FT	Feature Tracking
GBNS	Ground Based Navigation System
GDOP	Geometric Dilution Of Precision
GNC	Guidance Navigation and Control
GNSS	Global Navigation Satellite System
GPS	Global Positioning System
GS	Ground Station

HG	High Gate
HPS	High Performance Satellite Dynamics Simulator
HR	High Rate
IMU	Inertial Measurement Unit
LA	Laser Altimeter
LCT	Lunar Communication Terminal
LH	Local Horizon
LOS	Line Of Sight
LR	Low Rate
LRS	Lunar Relay Satellite
LS	Landing Site
MCF	Moon Centered Fixed frame
MR	Medium Rate
NC	Navigation Camera
OTS	Off The Shelf
PD	Powered Descent
PDI	Powered Descent Initiation
PRN	Pseudo Random
RX	Receiver
S/C	Spacecraft
SINPLEX	Small Integrated Navigator for PLanetary EXploration
SLAM	Simultaneous Localization And Mapping
SR	Slant Range
ST	Star Tracker
TOA	Time Of Arrival
TDOA	Time Difference Of Arrival
UERE	User Equivalent Range Error
USB	Upper Side Band
VLBI	Very Long Baseline Interferometry
VOR	VHF Omni Directional Radio Range

Bibliography

[1] Zuber, Maria T., et al., *Constraints on the Volatile Distribution within Shackleton Crater at the Lunar South Pole*, Nature 486.7403: 378-381, 2012.

[2] Mazarico et al., *Illumination Conditions of the Lunar Polar Regions Using LOLA Topography*, Icarus 211.2: 1066-1081, 2011.

[3] E.N. Slyuta et al., *The Estimation of Helium-3 Probable Reserves in Lunar Regolith*, Lunar and Planetary Science XXXVIII, vol. 38, 2007.

[4] Jeffrey S. Parker, *Low-Energy Ballistic Lunar Transfer*, PhD Thesis, University of Colorado, 2007.

[5] Maria Isabel Ribeiro, *Kalman and Extended Kalman Filters: Concept, Derivation and Properties*, Institute for Systems and Robotics, Instituto Superior Tecnico, Lisbon, 2004.

[6] www.sinplex.eu (checked on 03-2015)

[7] Erik Laan et al., *Sinplex: A Small Integrated Navigation System for Planetary Exploration*, IAC, 2013

[8] Stephen R. Steffes, *Development and Analysis of SHEFEX-2 Hybrid Navigation System Experiment*, M.Sc Thesis, University of Bremen, 2013.

[9] D. Heise, S. Steffes, S. Theil, *Filter Design For Small Integrated Navigator for Planetary Exploration*, DLR, Institute of Space Systems, 2012.

[10] Striepe, Scott A., Chirold D. Epp, and Edward A. Robertson, *Autonomous Precision Landing and Hazard Avoidance Technology (ALHAT) Project Status as of May 2010*, International Planetary Probe Workshop, 2010.

[11] Ilir Fiqiri Progri, *An Assesment of Indoor Geolocation Systems*, PhD Thesis, Worcester Polytechnic Institute, 2003.

[12] Beggins, Andrew J., Lora M. Canney, and Anna Belle Dolezal, *Conceptual Development of a Ground-based Radio-beacon Navigation System for Use on the Surface of the Moon*, 1988.

[13] Chelmins, David T., et al., *A Kalman Approach to Lunar Surface Navigation Using Radiometric and Inertial Measurements*, NASA ,2009.

[14] Batista, Pedro, Carlos Silvestre, and Paulo Oliveira, *Single Beacon Navigation: Observability Analysis and Filter Sesign*, American Control Conference (ACC), 2010.

[15] Schier, James. *NASAâĂŹs Lunar Space Communication and Navigation Architecture*, American Institute of Aeronautics and Astronautics, 2007.

[16] D. Christensen, and D. Geller., *Terrain-Relative and Beacon-Relative Navigation for Lunar Powered Descent and Landing*, The Journal of the Astronautical Sciences 58.1: 121-151, 2011.

[17] D. Christensen, *Terrain-Relative and Beacon-Relative Navigation for Lunar Powered Descent and Landing*, M.Sc Thesis, Utah State University, 2009.

[18] S. Steffes et al., *Simulator And Sensor Model Description*, SINPLEX document SX-RYNR-TN-0401, 19/11/2012.

[19] S. Steffes et al., *Navigation and Image Processing Algorithms Description*, SINPLEX document SX-RYNR-TN-0406, 05/02/2013.

[20] F. Dellaert and M. Kaess, *Square Root SAM: Simultaneous Localization and Mapping via Square Root Information Smoothing*, Intl. Journal of Robotics Research, 2006

[21] *High Performance Satellite Dynamics Simulator (HPS)*, project from Zentrum fÃijr Angewandte Raumfahrttechnologie und Mikrogravitation (ZARM) and Deutsches Zentrum fÃijr Luft und Raumfahrt (DLR).

[22] Bradford W. Parkinson and James J. Spilker, *Global Positioning System: Theory and Applications, Volume I*: pp. 469-483, AIAA, 1996.

[23] Oliver Montenbruck, Takuji Ebinuma, E. Glenn Lightsey and Sunny Leung, *A real-time kinematic GPS sensor for spacecraft relative navigation*, Aerospace Science and Technology Journal (6): pp. 435-449, 2002.

[24] Unknown authors, *2001 Federal Radionavigation Systems*, Departments of Defense and Transport.

[25] Unknown authors, *NASAâĂŹs Recommendations to Space-Faring Entities: How to Protect and Preserve the Historic and Scientific Value of U.S. Government Lunar Artifacts*, NASA, 2011.

[26] Huang Yong et al., *Precise positioning of the ChangâĂŹE-3 lunar lander using a kinematic statistical method*, Astromechanics Vol. 57 No. 35: 4545-4551, 2012.

[27] A.Puengnim, L. Patino-Studencka, J. Thielecke, G. Rohmer, *Precise Positioning for Virtually Synchronized Pseudolite System*, International Conference of Indoor Positioning and Indoor Navigation (IPIN), 2013.

[28] Minna Väkevä, Kimmo Rautkoski, Mårten Ström, F. von Schoultz, *NAVIndoor 2: Final Report*, 2004.

[29] Alberto GarcÃŋa Casas, Angelo Tomassini, Fernando GandÃŋa, *PLATFORM: an Integrated Approach to Robotics and Space Navigation Validation. Designing and Testing the Robotic Test-Bed*, 8th International Symposium on Artifical Intelligence, Robotics and Automation in Space - iSAIRAS, 2005.